

COMPLEXES AND AGGREGATES OF CHLOROPHYLLS

CENTRALE LANDBOUWCATALOGUS



0000 0086 7180

BIBLIOTHEEK L.H.

0 2 APR. 1980

ONTV. TIJDSCHR. ADM

Promotor: dr. T. J. Schaafsma, hoogleraar in de molecuulfysica

R.P.H. Kooyman

Complexes and aggregates of chlorophylls

proefschrift

ter verkrijging van de graad
van doctor in de landbouwwetenschappen,
op gezag van de Rector Magnificus,
dr. H.C. van der Plas,
hoogleraar in de organische scheikunde,
in het openbaar te verdedigen
op vrijdag 11 april 1980
des namiddags te vier uur in de aula
van de Landbouwhogeschool te Wageningen

15N-106744-02

STELLINGEN

1

Niet-rationele overwegingen tegen de invoering van kernenergie moeten bij de "brede maatschappelijke diskussie" even ernstig worden genomen als rationele overwegingen.

2

De CNDO-methode is ongeschikt voor het interpreteren van foto-elektronspektra.

3

Bij het bestuderen van homogene energie-overdracht volgens het Förster-mechanisme in preparaten met een hoge optische dichtheid is meting van de fluorescentielevensduur te verkiezen boven meting van de fluorescentiedepolarisatie.

4

Er is voldoende aanleiding om de mogelijkheid te onderzoeken of het watervrije dimeer van chlorofyl a een goed modelsysteem is voor het reactiecentrum van fotosysteem 2.

5

Teneinde de ruimtelijke structuur van het chlorofyl a "speciale paar" dimeer verder te onderzoeken, verdient het aanbeveling de positie van de laagste aangeslagen triplettoestand van dit dimeer te bepalen.

dit proefschrift.

6

Het bestaan van uitgebreide wetenschappelijke programmabibliotheken in Fortran belemmert het gebruik van betere programmeertalen.

7

Bij het bepalen van de orde-parameters in uni-axiale vloeibare kristallen met behulp van laser Raman-spektroskopie dient de anisotropie van het lokale elektromagnetische stralingsveld bij de beschouwingen te worden betrokken.

S. Jen, N. A. Clark, P. S. Pershan, E. B. Priestley, Phys. Rev. Lett. 31 (1973) 1552.

V. F. Shabanov, E. M. Aver'yanov, P. V. Adomenas, V. P. Spiridonov, Sov. Phys. JETP 48 (1978) 970.

8

Het valt te verwachten dat met de komst van nog grotere en snellere computers de wiskunde zich zal ontwikkelen tot een deels empirische wetenschap.

9

Vergeleken met de Nederlandse universiteiten heeft de Landbouwhogeschool een uitstekende uitgangspositie om onderzoek te verrichten dat in een praktische relatie staat tot de maatschappij. Het onderwijs en onderzoek in de basisvakgroepen zouden meer van deze omstandigheid gebruik moeten maken.

aan mijn ouders
aan de Nederlandse belastingbetaler

Voorwoord

Het is niet verbazingwekkend als ik vertel dat dit boekje voor U ligt dankzij de medewerking van velen. Evenmin zult U opkijken bij de mededeling dat sommige mensen hier een grotere bijdrage aan hebben geleverd dan andere. Hier krijg ik de kans om deze met name te noemen.

In de eerste plaats wil ik Geertje Jansen en Tjeerd Schaafsma noemen. Tjeerd heeft mij grote vrijheid gegeven in de opzet en uitvoering van het onderzoek, hetgeen ik ten eerste heb gewaardeerd. Hij bleek een uitstekend gesprekspartner te zijn met vele waardevolle adviezen t.a.v. de interpretatie en het opschrijven van de resultaten. Geertje heeft mij zowel tijdens het uitvoeren en interpreteren van de experimenten als bij het schrijven van het boekje op alle mogelijke manieren terzijde gestaan. Zonder haar was dit proefschrift waarschijnlijk niet tot stand gekomen en was ik nu een ander mens geweest.

Joop Kleibeuker stond mij bij in mijn eerste aarzelende schreden op het fotosynthese/porfyrine gebied, waarvoor ik hem zeer erkentelijk ben.

Zowel Roelof Platenkamp als Jan van Rens waren een vraagbaak op theoretisch gebied. Jan was altijd bereid af te dalen tot mijn denkniveau, terwijl Roelof soms een meester was in het ondergraven van mijn ideeën. Van beiden heb ik veel geleerd. Roelof heeft nog de speciale verdienste gehad om mij te helpen een werkbare evenwicht te vinden tussen het relativeren en bedrijven van wetenschap.

Bij het uitvoeren van de experimenten heb ik veel steun ondervonden van Adrie de Jager, die mij hielp met apparatuurproblemen, Rob Koehorst, die mij voorzag van chlorofyl (en het omslagontwerp) en Herman Kramer, die een aantal experimenten heeft uitgevoerd.

Mevrouw Bos, Mevrouw Diraoui en Jannie Willebrand hebben de tekst getypt, terwijl de Heer Hoogeveen de tekeningen verzorgde. Aan allen, mijn hartelijke dank.

Tenslotte dank ik iedereen, die mij mijn regelmatige nukken en grillen kon vergeven. Al met al was het een prima tijd op Moleculaire Fysika.

I am grateful to the Pergamon Press and the North-Holland Publishing Company for their permission to copy articles which were previously published.

Contents

List of abbreviations and symbols	11
Chapter 1 INTRODUCTION AND SURVEY	13
1.1 GENERAL	13
1.2 IN VITRO STUDY OF CHLOROPHYLL COMPLEXES	15
1.3 EXPERIMENTAL METHODS	16
1.3.1 <i>Excited state studies</i>	16
1.3.2 <i>Ground state studies</i>	19
1.4 SURVEY	20
1.5 REFERENCES	21
Chapter 2 SOLVATION AND AGGREGATION OF CHLOROPHYLL	22
2.1 INTRODUCTION	22
2.2 CALCULATIONS ON PORPHYRINS	24
2.2.1 <i>π-type calculations</i>	24
2.2.2 <i>Ab-initio calculations</i>	26
2.3 CHLOROPHYLL COMPLEXES	27
2.3.1 <i>Chlorophyll-solvent interactions</i>	27
2.3.2 <i>Chlorophyll aggregates</i>	28
2.4 RELEVANCE TO PHOTOSYNTHESIS	33
2.5 REFERENCES	35
Chapter 3 A COMPARATIVE STUDY OF DIMERIZATION OF CHLOROPHYLLS AND PHEOPHYTINS BY FLUORESCENCE AND ODMR	37
3.1 INTRODUCTION	37
3.2 EXPERIMENTAL	38
3.2.1 <i>Sample preparation</i>	38
3.2.2 <i>Measurements</i>	38
3.3 RESULTS AND DISCUSSION	38
3.3.1 <i>Fluorescence and ODMR data</i>	38
3.3.2 <i>Bonding in Ph and Chl dimers; geometrical considerations</i>	38

3.4	ACKNOWLEDGEMENTS	41
3.5	REFERENCES	41
Chapter 4	SPECTROSCOPIC PROPERTIES OF CHLOROPHYLL <u>A</u> COMPLEXES	43
4.1	FLUORESCENCE SPECTRA AND ZERO-FIELD MAGNETIC RESONANCE OF CHLOROPHYLL <u>A</u> - WATER COMPLEXES	44
4.2	CHLOROPHYLL <u>A</u> - ETHANOL COMPLEXES	50
4.3	THE (CHLOROPHYLL <u>A</u>) ₂ DIMER	51
4.4	REFERENCES	53
Chapter 5	FLUORESCENCE AND ODMR OF CHLOROPHYLL <u>B</u> COMPLEXES	54
5.1	INTRODUCTION	54
5.2	EXPERIMENTAL	55
5.3	RESULTS	56
5.4	COMPLEXING PROPERTIES OF CHL <u>B</u> AND THE FOUR ORBITAL MODEL	60
5.5	DISCUSSION	62
5.5.1	<i>Monomeric Chl <u>b</u> species</i>	63
5.5.2	<i>Chl <u>b</u> aggregates</i>	67
5.6	CONCLUSIONS	70
5.7	REFERENCES	70
Chapter 6	NUCLEAR MAGNETIC RESONANCE OF CHL <u>A</u> COMPLEXES	71
6.1	INTRODUCTION	71
6.2	NUCLEAR SPIN RELAXATION AND MOLECULAR STRUCTURE	72
6.2.1	<i>Theory</i>	72
6.2.2	<i>Molecular structure of chlorophyll dimers from T₁-measurements</i>	76
6.2.3	<i>The choice of the molecular frame of reference</i>	77
6.3	PROTON CHEMICAL SHIFTS AND MOLECULAR STRUCTURE	77
6.3.1	<i>Ring current shifts in Chl <u>a</u> dimers</i>	78
6.3.2	<i>Calculations</i>	81
6.4	EXPERIMENTAL	81
6.4.1	<i>Sample preparation</i>	81
6.4.2	<i>NMR experiments</i>	82
6.4.3	<i>Data processing</i>	82
6.5	RESULTS	83
6.5.1	<i>Dimer geometries from T₁-data</i>	87
6.5.2	<i>Deuterium T₁-data and the diffusion axis system</i>	92

6.5.3	<i>Dimer geometries from ring current shifts</i>	92
6.6	DISCUSSION	94
6.6.1	<i>Validity of calculation procedures</i>	94
6.6.2	<i>Dimer geometries</i>	97
6.6.3	<i>Rotational diffusion constants</i>	98
6.7	CONCLUSIONS	99
6.8	REFERENCES	99
Chapter 7	A CHARGE RESONANCE - EXCITON DESCRIPTION OF CHLOROPHYLL AND PHEOPHYTIN DIMERS	102
7.1	INTRODUCTION	102
7.2	THEORY	104
7.2.1	<i>Singlet state properties</i>	105
7.2.2	<i>Triplet state properties</i>	106
7.2.3	<i>Calculation procedure</i>	108
7.3	APPLICATIONS	111
7.3.1	<i>The pheophytin dimer</i>	112
7.3.2	<i>The chlorophyll "special pair" dimer</i>	116
7.3.3	<i>The chlorophyll "pure" dimer</i>	117
7.4	DISCUSSION	119
7.4.1	<i>The model</i>	119
7.4.2	<i>The dimers</i>	120
7.5	CONCLUSIONS	122
7.6	REFERENCES	122
Summary		124
Samenvatting		126
Curriculum vitae		128

List of abbreviations and symbols

AO	atomic orbital
C_0	total concentration
CD	circular dichroism
Chl <u>a</u> , <u>b</u>	chlorophyll <u>a</u> , <u>b</u>
Chl.L	singly ligated Chl
Chl.L.H _a	singly ligated Chl, hydrogen bonded at aldehyde group
Chl.L.H _k	singly ligated Chl, hydrogen bonded at keto group
CI	configuration interaction
CNDO	complete neglect of differential overlap
CR	charge resonance
\vec{D}	zero field splitting tensor
\vec{D}_m	monomeric zero field splitting tensor
\vec{D}_R	rotational diffusion tensor
D_{Ri}	i th diagonal element of rotational diffusion tensor
ENDOR	electron-nuclear double resonance
EtOH	ethanol
FDMR	fluorescence detected magnetic resonance
H_0	static magnetic field
$H_1(t)$	time dependent magnetic field
HOMO	highest occupied molecular orbital
\vec{I}	moment-of-inertia tensor
INDO	intermediate neglect of differential overlap
IR	infrared
k	equilibrium constant
L	ligand
LUMO	lowest unoccupied molecular orbital
\vec{M}	magnetization (Ch. 6), transition moment (Ch. 7)
MO	molecular orbital
O.D.	optical density
Ph <u>a</u>	pheophytin <u>a</u>
Ph-Ph	covalently linked pheophorbide <u>a</u> dimer

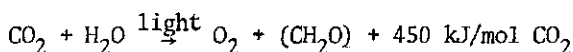
$(\text{Ph})_2$	pheophytin <u>a</u> dimer
PS	photosystem
Py	pyridine
\vec{r}_N	position vector of nucleus N
\vec{R}	transformation matrix
\vec{R}	rotation matrix
\vec{r}_μ	position vector of equivalent dipole μ
rf	radio frequent
SLR	spin-lattice relaxation
SP	special pair
$i.T_1^{(\mu)}$	nuclear spin-lattice relaxation time of nucleus i in molecule μ
T_2	nuclear spin-spin relaxation time
\vec{V}	translation vector
ZFS	zero field splitting
δ	ground state stabilization energy
$\delta(N)$	chemical shift of nucleus N
$\Delta\delta(N)$	ring current shift of nucleus N
ϵ	transition energy
η'	asymmetry-parameter
η	viscosity
$\{\mu\}$	set of dipoles
τ_c	rotational correlation time
τ_f	free rotor rotational time
$ \tau_i\rangle$	spin function
ω	frequency
$\vec{\Omega}$	set of Euler angles

1 Introduction and survey

1.1 GENERAL

This thesis deals with the geometrical and electronic structure of photosynthetic pigment-complexes *in vitro*. These complexes are known to be important in the process of photosynthesis where light-energy is converted into chemical energy. To indicate the importance of complexes and aggregates in photosynthesis, a brief description of this process is appropriate.

In its most simple form, (plant) photosynthesis can be written as the net reaction:



This reaction can be considered as a light-driven oxidation-reduction reaction in which four electrons are transferred from 2 H₂O to CO₂, oxidizing the former to O₂ and reducing the latter to carbohydrate.

Photosynthetic action can be divided into two main processes (see fig. 1):

(1) First, the so-called "primary events" take place [1]. Here light-quanta ($\lambda = 400 - 700 \text{ nm}$) are captured by photosynthetic "antenna" pigments. Via a system of energy-transferring molecules the harvested excitation energy is fed into a "reaction center" system, where it is used to produce a charge-separated state with low oxidation-reduction potential ($E_0 \approx -0.4 \text{ V}$).

(2) Subsequently, the reducing power of this state is utilized to drive a chain of redox reactions, finally yielding NADPH and ATP. These compounds can then be used to store the gained chemical energy in a carbohydrate (CH₂O). For more detailed discussions, we refer to [1-4].

Photosynthetic pigments, in our context defined as substituted porphyrins, are intimately involved in process (1); both in absorbing and transporting light-quanta as well as in the induction of a charge separation they can be considered as the "workers" of photosynthesis. In plants and algae chlorophyll a (Chl a) is the most important pigment (for the molecular structure of the chlorophylls, see fig. 1, Chapter 2); it serves both as a reaction center

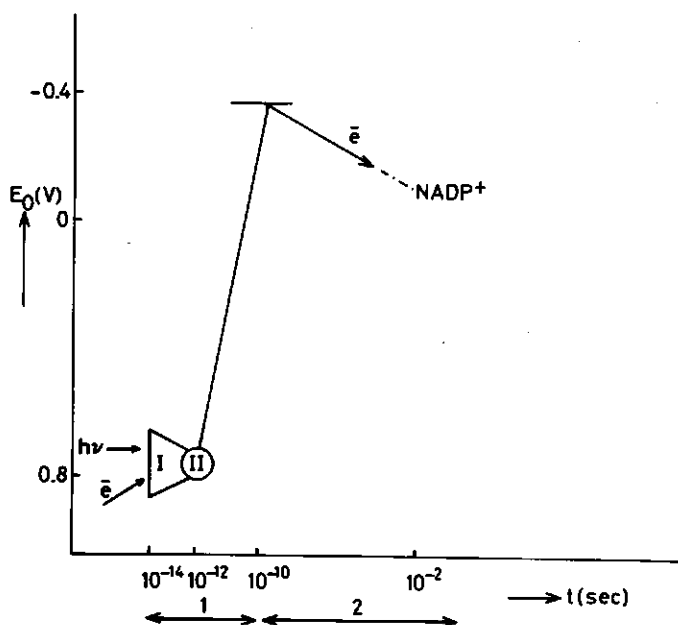


Fig. 1. The two main processes in photosynthesis

1. the era of "primary processes"

2. the era of "biochemistry".

Vertically the oxidation-reduction potential is indicated

I : antennapigment where photons are captured

II: reaction center which brings an electron to a low E_0 .

pigment and, together with chlorophyll b (Chl b) and other auxiliary pigments [1], as antenna pigment. Apparently, the Chl molecule can have various functional roles in the process of photosynthesis. Many observations, such as the finding that antenna and reaction center Chl can be spectroscopically distinguished [5] support a viewpoint that this functional differentiation (i.e. the antenna and reaction center function) is related to different local environments of Chl (for a review see Chapter 3 of ref. 1). The plant chloroplast, in which photosynthesis takes place, has a highly organized structure [6] allowing for such different local environments to be present. *In vitro* studies of the chlorophylls indicate [7] that their spectroscopic properties are strongly dependent on the nature and organization of their immediate surroundings, and the way of aggregation. For instance, in nonpolar solvents such as octane, benzene, carbon tetrachloride, Chl readily forms dimers and higher aggregates with molecular properties different from those of the monomolecular compound (see Chapter 2). By varying the composition of the solvent and the concentration of Chl molecules,

a series of Chl complexes with different molecular properties can be formed. Some of these complexes have properties quite similar to those found in *in vivo* systems (for some recent reviews, see refs. 7 and 8). Mainly because of these similarities it is generally believed that the different functions of Chl in photosynthesis are closely connected to different Chl complexes, which can form by various Chl-environment, or, more specifically, by Chl-Chl interactions.

From this hypothesis, a number of questions arise:

- (1) in which way is the *in vivo* environment of the pigment structured?
- (2) what is the structure of various Chl complexes, which are involved in different stages of the primary processes in photosynthesis?
- (3) which molecular properties make some Chl complexes so well suited for their particular role in photosynthesis?

Since the processes of capture, transfer and conversion of photons strongly depend on the geometrical and electronic properties of Chl complexes and aggregates, these properties will largely determine the specific role of different Chl complexes in photosynthesis. In the following the term "complex" will be used to denote a Chl molecule interacting with some other molecule(s), and the term "aggregate" whenever the other molecule(s) is (are) Chl; aggregates are a "subclass" of complexes.

1.2 IN VITRO STUDY OF CHLOROPHYLL COMPLEXES

The reasons for studying Chl complexes *in vitro* are obvious: it is possible to prepare a sample with controlled composition. This is in contrast to the *in vivo* situation where one often is puzzled by possible side-effects due to one or another of the many compounds present in an *in vitro* system. In an *in vitro* study, Chl complexes can be investigated *per se*, thereby providing the opportunity to focus on some particular complex and to study the properties of that complex alone. This can be of great value in answering the questions mentioned in Section 1.1.

However, it must be kept in mind that a sample of some Chl complex is far from being a photosynthetic system; conclusions about photosynthesis drawn from *in vitro* studies, should be regarded with caution, realizing the limitations of the *in vitro* system devoid of most of the compounds required for a functioning *in vivo* system.

In studying Chl and its complexes, much profit can be drawn from the experimental and theoretical results for the similar but simpler porphyrins and chlorins (see fig. 1, Chapter 2) which have been extensively studied for a long

time (for a short survey of these results, see Chapter 2). By now the mono-molecular properties of porphyrins are rather well understood, so it seems feasible to make a further step towards photosynthesis by studying porphyrin complexes, and in particular chlorophyll complexes. This thesis can be viewed as an attempt to make one such step.

1.3 EXPERIMENTAL METHODS

Using zero-field and high magnetic field triplet electron spin resonance, fluorescence measurements, and nuclear magnetic resonance, we have characterized a number of Chl complexes by their lower excited singlet and triplet state as well as their electronic ground state properties. These data can be used to study the molecular structure of these complexes.

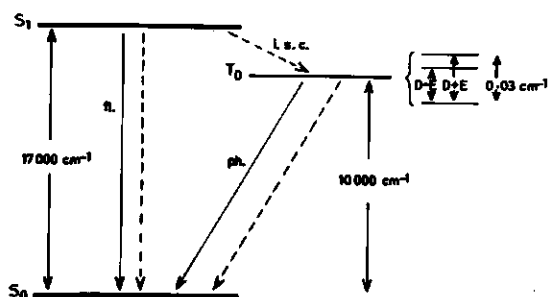
1.3.1 *Excited state studies*

Upon irradiation with light in the wavelength region 400 - 700 nm a molecule such as Chl can be brought into an excited singlet state S_1 (see fig. 2). From this state the molecule may decay radiatively to the ground state S_0 by emitting a photon (fluorescence) or non-radiatively by interconversion followed by vibrational relaxation. Another pathway is decay to the lower lying triplet state T_0 (intersystemcrossing) followed by radiative (phosphorescence) and non-radiative decay to the ground state.

Fluorescence spectra of various Chl complexes can easily be obtained, and they can be used to characterize the lowest excited singlet states of these complexes.

Fig. 2. Energy-level scheme of chlorophyll.

Solid lines : radiative decay
Dashed lines : non-radiative decay.



The position of the lowest excited triplet state T_0 is much harder to determine because of the low phosphorescence yield of the chlorophylls. T_0 can also be characterized in another way making use of the fact that this state carries two unpaired electron spins resulting in a net electron spin angular momentum S , with $S = 1$ (in units \hbar) [9]. Three spin sublevels are connected with this state, and because of dipole-dipole interactions between the two electrons spins described by a Hamiltonian \mathcal{H}_{dd} [9], these sublevels are in general non-degenerate, not even in zero magnetic field [9] (see fig. 2). \mathcal{H}_{dd} can be written as

$$\mathcal{H}_{dd} = \vec{S} \cdot \vec{D} \cdot \vec{S} \quad (1)$$

where \vec{D} is the zero-field-splitting (ZFS) tensor and \vec{S} is the spin-operator. In zero magnetic field this situation can be described with an effective spin Hamiltonian [9], relative to a frame of reference (x,y,z) in which \vec{D} is diagonal:

$$\mathcal{H}_S = - (XS_x^2 + YS_y^2 + ZS_z^2) \quad (2)$$

with eigenfunctions $|\tau_x\rangle$, $|\tau_y\rangle$, $|\tau_z\rangle$, corresponding to the three spin-substates, and eigenvalues X , Y , Z which are the expectation values of \vec{D} . The spin-operators S_k ($k=x,y,z$) have the properties:

$$\begin{aligned} S_x |\tau_x\rangle &= 0 \\ S_x |\tau_y\rangle &= i |\tau_z\rangle \quad \text{et cycl.} \end{aligned} \quad (3)$$

This last property gives the possibility to induce transitions between two sub-states by applying a radiofrequent magnetic field $\vec{H}_1(t) = \vec{H}_1 \cdot \cos \omega t$ which introduces an additional term $g\vec{H}_1(t) \cdot \vec{S}$ in eq. (2). If $\omega = X-Y$, $X-Z$, or $Y-Z$, then the resonance condition $\Delta E = \omega$ is fulfilled and power from the rf-source is absorbed. For chlorophylls, ω is in the range 200 - 1300 MHz.

The ZFS-tensor \vec{D} has the property that $\text{Trace}(\vec{D}) = 0$, so $X + Y + Z = 0$ and only two parameters are needed to specify the spin-Hamiltonian (2) completely. Commonly they are denoted by D and E [9] where

$$D = -\frac{3}{2} Z, \quad E = -\frac{1}{2} (X-Y)$$

D and E are the expectation-values of D, when integrated over the orbital part of the wavefunction:

$$D = \frac{3}{4} (g\beta)^2 \cdot \langle {}^3\Psi \left| \frac{r_{12}^2 - 3z_{12}^2}{r_{12}^5} \right| {}^3\Psi \rangle$$

$$E = \frac{3}{4} (g\beta)^2 \cdot \langle {}^3\Psi \left| \frac{x_{12}^2 - y_{12}^2}{r_{12}^5} \right| {}^3\Psi \rangle \quad (4)$$

where $\vec{r}_{12} = (x_{12}, y_{12}, z_{12})$ is the vector joining the two spins, and ${}^3\Psi$ is the orbital part of the wavefunction describing the triplet state. Eqs. (4) thus characterize the triplet state T_0 . They yield information concerning the electronic structure of T_0 . For a planar aromatic molecule ($z_{12} \ll x_{12}, y_{12}$), it can be seen that D is a measure of the average distance between the two unpaired electron spins, whereas E indicates the in-plane asymmetry of the charge distribution in the triplet state.

The ZFS-values can be determined in an elegant way by the technique of optically detected magnetic resonance (ODMR). Here a very short description will be given; for further details we refer to [10]. By inducing a transition between $|\tau_i\rangle$ and $|\tau_j\rangle$ ($i, j = x, y, z$), which in general have different population and decay rates to the ground state S_0 , these rates will be equalized which manifests itself as a changing population of S_0 . This can be monitored via the fluorescence intensity which is coupled to the ground state population. In this technique it is essential that the spin-lattice relaxation rate between the sublevels is small compared to the decay rates of the individual sublevels of T_0 . In order to fulfill this condition it is usually necessary that experiments are performed at low temperature ($T \lesssim 4$ K). The more classic method of high-field triplet electron spin resonance [9] where transitions are detected via absorption of microwave radiation, does not require this condition. However, for our purposes, where one deals with samples of randomly oriented molecules, zero-field is preferable over high-field esr:

- The fact that ODMR is an optical detection technique, makes it more sensitive than the conventional detection of micro-wave absorption.
- ODMR is a more selective technique, enabling one to select a particular fluorescence band, belonging to some species present in the sample, and to determine the triplet properties of that complex alone. This is valuable in the study of samples where an equilibrium mixture of species may be present.

- The spin-Hamiltonian in high magnetic field is not a simple dipolar Hamiltonian; anisotropic Zeeman-interaction and, especially for porphyrin-like materials where the orbital angular momentum is rather high ($L_z \sim 5 \hbar$ [12]), spin-orbit coupling should be included, complicating the interpretation of experimental data in unfavourable cases.

Because of these reasons, most electron spin resonance experiments, described in this thesis have been carried out using the zero-field ODMR technique.

1.3.2 *Ground state studies*

Another method to study molecular structures is the measurement of the nuclear spin-lattice relaxation (SLR) times T_1 , and the chemical shifts of magnetically inequivalent nuclei. Especially high-resolution spectra of small molecules in a low-viscosity solvent, where all magnetically inequivalent nuclei appear as distinct resonance lines, have proved to contain detailed information about the structure and the dynamical behaviour of the molecule under study. A short description of the SLR-processes, and the information which can be obtained from measurements of these parameters will be given here; more detailed discussions may be found in several textbooks [12-14].

A nucleus with nuclear spin angular momentum $I \neq 0$ in a static magnetic field \vec{H}_0 has an equilibrium magnetization \vec{M}_0 parallel to \vec{H}_0 . If this molecule is perturbed by some magnetic interaction $\mathcal{H}'(t) = \vec{H}'(t) \cdot \vec{M}_0$, \vec{M}_0 will shift to some non-equilibrium magnetization \vec{M}'_0 which is determined by the vector sum of \vec{H}_0 and $\vec{H}'(t)$. If the perturbing interaction is removed, \vec{M}'_0 will reach \vec{M}_0 after some characteristic time T_1 (by exchange of energy between the spin-system and the lattice), needed to relax to a Boltzmann equilibrium over the Zeeman-levels. In a molecule, all magnetically inequivalent nuclei i experience a different fluctuating field $\vec{H}'_i(t)$, arising from the random thermal motions of the molecule. This implies that for nucleus i $\mathcal{H}'(t) = \vec{H}'_i(t) \cdot \vec{M}_0$ is a fluctuating Hamiltonian (with vanishing expectation value) leading to a T_1 relaxation process for nucleus i . A T_1 measurement of nucleus i provides information about the time scale of the fluctuations, yielding insight into the dynamic behaviour of the molecule, and about the magnitude of the local fields \vec{H}'_i , which are dependent on the local structure around nucleus i .

The power of high resolution SLR studies is the possibility to selectively determine T_1 of different nuclei in the molecule, i.e. in principle one can extract as much parameters as are needed for a complete description of the molecular structure and motion [15].

Several perturbing fluctuating fields which give rise to a relaxation-process can be present in a molecule. The relative importance of these different bations is dependent on the molecule under study, the particular nuclei which are irradiated, and on some additional experimental conditions, such as the magnitude of H_0 , the frequency ω_0 of the irradiating rf-field, and the temperature. These relaxation processes are thoroughly treated in ref. 14 and we shall only discuss here the intramolecular dipolar relaxation process which is the main one for protons ($I = \frac{1}{2}$) in a small to medium-sized molecule ($M \lesssim 2000$).

For a molecule, T_1 due to dipole-dipole relaxation of nucleus j under the influence of nucleus i is given by $|16|$ (see also Chapter 6)

$$\frac{1}{T_1} = C \sum_{i \neq j} f(\vec{D}_R) \cdot \frac{1}{(\vec{r}_i - \vec{r}_j)^6} \quad (5)$$

where \vec{D}_R is the rotational diffusion tensor of the molecule, \vec{r}_i and \vec{r}_j are the position vectors of nucleus i and j , respectively. C is a constant depending on the nucleus studied. The function f contains the information about the structure and dynamical behaviour of the molecule. For a rigid molecule, the 3×3 tensor \vec{D}_R completely specifies the motional behaviour of the molecule in space.

If \vec{r}_i and \vec{r}_j are known (for instance from X-ray studies) and if n magnetically non-equivalent nuclei are present in the molecule, eq. (5) can be considered as a set of n equations with the (symmetric) tensor \vec{D}_R as the unknown. Thus, \vec{D}_R can be determined by measuring a number of T_1 -values. By introducing certain assumptions, which depend on the nature of the molecule studied, \vec{D}_R can be correlated to structural properties, such as size, geometry, rigidity. This is the basis of studying molecular geometries with NMR. The condition that all \vec{r}_i should be known, can in some cases somewhat be relaxed; as we will see in Chapter 6, this will be of importance in studying dimer geometries.

1.4 SURVEY

In Chapter 2, the chlorophyll molecules which form the subject of this thesis are introduced and the results of molecular orbital calculations for the monomers are shortly described. The different types of complexing and aggregation will be mentioned and discussed in view of their possible relevance for the photosynthetic system.

Chapter 3 contains the results of an experimental study on pheophytin dimers

These dimers are compared to chlorophyll dimers, and some conclusions are drawn with respect to the different dimerization behaviour of these two compounds.

In Chapters 4 and 5 some Chl a and Chl b complexes are characterized by their singlet and triplet state properties. Further, results of high-field ESR experiments on a Chl a dimer will be presented.

Chapter 6 reports the results of a nuclear magnetic resonance study on the Chl a monomer and dimer. A method will be outlined to study dimer geometries; resulting rotational correlation times will be discussed in relation to the geometry of the monomer and dimer.

Finally, Chapter 7 is an attempt to describe chlorophyll-like dimers in terms of a combined charge-resonance-exciton model. Results of this approach will be given for some representative examples.

1.5 REFERENCES

1. Bioenergetics of Photosynthesis, Ed. Govindjee (Acad. Press, New York, 1975).
2. Proceedings of the Symposium on Chlorophyll Organization and Energy Transfer in Photosynthesis, Ciba Foundation, Nr. 61. (Excerpta Medica, Amsterdam, 1979).
3. Photosynthesis I, Eds. A. Trebst, M. Avron (Springer, Berlin, 1977).
4. (a) Primary Processes of Photosynthesis, Vol. 2, Ed. J. Barber (Elsevier, Amsterdam, 1977).
(b) Primary Processes of Photosynthesis, Vol. 3, Ed. J. Barber (Elsevier, Amsterdam, 1979).
5. J.P. Thornber, J. Barber, in ref. 4b.
6. D. Branton, R.B. Park, J. Ultrastr. Res. 19 (1967) 283.
7. G.R. Seely, in ref. 4a.
8. J.J. Katz, J.R. Norris, L.L. Shipman, in Brookhaven Symposia in Biology, No. 28, Eds. J.M. Olson and G. Hind (U.S. Dep. of Commerce, Springfield, 1977).
9. S.P. McGlynn, T. Azumi, M. Kinoshita, Molecular Spectroscopy of the Triplet State (Prentice-Hall Inc., Englewood Cliffs, New Jersey, 1969).
10. W.G. van Dorp, Thesis (1975) Leiden University.
11. G.W. Canters, G. Jansen, M. Noort, J.H. van der Waals, J. Phys. Chem. 80 (1976) 2253.
12. C.P. Slichter, Principles of Magnetic Resonance (Springer, Berlin, 1978).
13. T.C. Farrar, E.D. Becker, Pulse and Fourier Transform NMR (Acad. Press, New York, 1971).
14. A. Abragam, The Principles of Nuclear Magnetism (Clarendon Press, Oxford, 1961).
15. K. Wüthrich, NMR in Biological Research: Peptides and Proteins (North-Holland, Amsterdam, 1976).
16. W.T. Huntress, J. Chem. Phys. 48 (1968) 3524.

2 Solvation and aggregation of chlorophyll

2.1 INTRODUCTION

In this Chapter we will discuss the properties of chlorophyll. Following a short description of the molecule and of the ways in which its spectroscopic properties can be theoretically described, we will give a survey of the interactions which are relevant for the complexing and aggregation behaviour of the chlorophylls. Finally, we will discuss the possible role of certain chlorophyll complexes in the photosynthetic system. Throughout this Chapter we will use the term "complex" to denote a chlorophyll molecule bonded to another as yet unspecified molecule, and the term "aggregate" when in this bonding other chlorophyll molecules are involved (chlorophyll dimers and polymers).

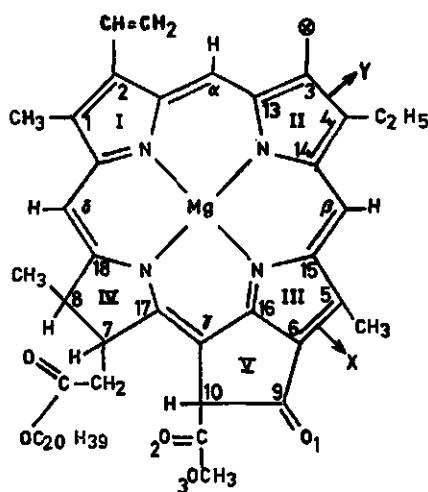


Fig. 1 (a) Molecular structure of chlorophylls; $X \equiv \text{CH}_3$ for Chl a, $X \equiv \text{CHO}$ for Chl b. In the corresponding pheophytins Mg has been replaced by 2 hydrogen atoms.

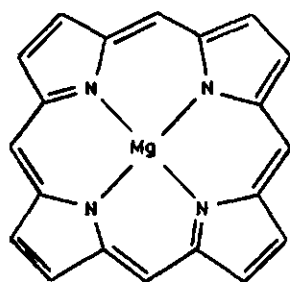


Fig. 1 (b) Molecular structure of porphyrin; by hydrogenating one pyrrole ring, one gets chlorin which is the basic skeleton for the chlorophylls.

Chlorophyll (Chl) a and b (see fig. 1a) are members of the class of molecules which are called *porphyrins* (fig. 1b). In Chl a and b one pyrrole ring is hydrogenated which makes Chl a and b belong to a subclass of the porphyrins, the dihydroporphyrins or *chlorins*. Further essential features of the chlorophylls are, as we shall see below, the presence of a Mg-atom in the center of the ring system, and the presence of a fifth ring containing a keto group. Another relevant feature is the presence of a long phytol tail, attached to ring IV (fig. 1a). This tail probably has a purely physiological function, i.e. it serves as an "anchor" to hold the Chl molecule in the lipid membrane of the chloroplast.

If the Mg-atom in the chlorophylls is replaced by two hydrogens, one forms the corresponding *pheophytins*. Apart from a possible role in photosynthesis [1,2], the study of these molecules is useful in investigating the effect of the presence of Mg on the spectroscopic properties of Chl and its complexes.

X-ray studies [3,4] have produced detailed information on the geometrical structure of the Chl molecule. It is found that the molecule is not completely planar (deviation ~ 0.1 Å), whereas the Mg-atom is situated at a distance ~ 0.4 Å from the "average" plane. However, the X-ray structure need not necessarily be the same as that for Chl in solution: X-ray structures were determined for a single crystal of Chl, implying that the molecule may be distorted by crystal field effects.

The absorption spectra ($\lambda = 350-900$ nm) of porphyrin-like compounds have been extensively studied (for a review see ref. 5). It is found that for these molecules two main absorption bands occur: the Q-bands in the region $\lambda = 500-900$ nm and the relatively intense Soret-bands in the region $\lambda = 350-450$ nm. For Chl a the Q-band is around 660 nm, whereas the Soret-band is situated at $\lambda \approx 430$ nm. A typical absorption spectrum of Chl a is presented in fig. 2. In order to describe these excited states of porphyrin-like compounds, much theoretical work has been done during the last three decades. In the next section, results of these theoretical considerations will be shortly discussed.

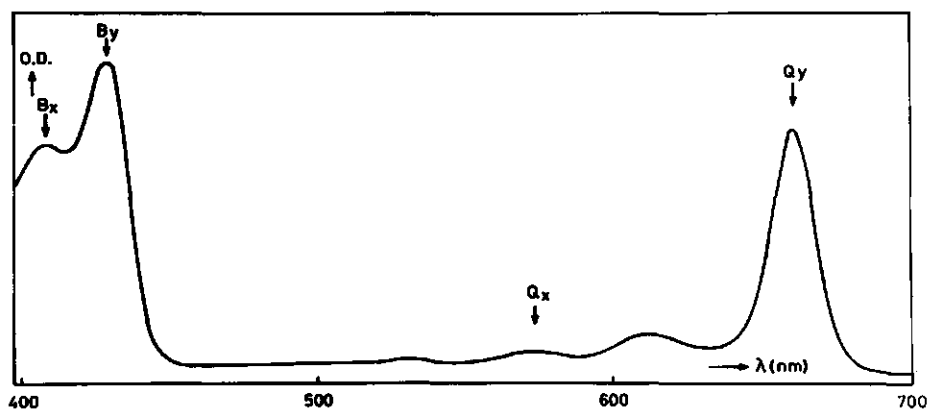


Fig. 2. Room temperature absorption spectrum of dilute Chl *a* in diethylether. Various transitions have been indicated by Q_x , Q_y and B_x , B_y (see text).

2.2 CALCULATIONS ON PORPHYRINS

2.2.1 π -type calculations

Simpson [6] was the first who supplied a qualitatively correct description of the lowest excited states of porphin. He assumed that in porphin (fig. 1b) 18 π -electrons move freely along a circular path confined to the innermost 16-membered ring. In this model the resulting molecular orbitals (MO's) can be expressed as $\psi_k = \exp(ik\phi)$ where the index k is associated with an angular momentum $L_z = k\hbar$ along the axis perpendicular to the molecular plane ($k = 0, \pm 1, \pm 2, \dots, \pm 4$). The MO's ψ_k and ψ_{-k} are degenerate. The lowest unoccupied MO's have an angular momentum $L_z = \pm 5\hbar$ associated with them. Considering one-electron promotions from the highest occupied MO (HOMO) to the lowest unoccupied MO (LUMO), two excited states are found with $L_z = \pm \hbar$ and $L_z = \pm 9\hbar$, respectively. Taking into consideration the optical selection rule $\Delta L_z = \pm \hbar$, it follows that a transition to the state with $L_z = \pm \hbar$ is allowed, whereas the transition to the state with $L_z = \pm 9\hbar$ is forbidden. Furthermore, by introducing in a somewhat artificial way electron-electron interactions, the state $L_z = 9\hbar$ was predicted to be the lowest in energy on the basis of Hund's rule. Simpson identified the Q-band with a transition to a state S_1 with $L_z = \pm 9\hbar$, and the Soret-band with the transition to a state S_2 with $L_z = \pm \hbar$. The unusual high orbital angular momentum for the state S_1 has been experimentally verified: for instance, for Zn-porphin a value of $L_z = 5.0\hbar$ has been determined [7].

In subsequent years, the LCAO-MO method was applied. Longuet-Higgins et al. [8] performed Hückel-type calculations on porphin and tetrahydroporphin. By properly parametrizing the semi-empirical constants reasonable quantitative agreement with the experimental results was obtained, with the important exception that the calculations failed to give the result that in porphin the Soret-band is much stronger than the Q-band. In contrast to the assumptions in Simpson's model, all 26 π -electrons were included in the calculation.

An important new concept arose with the introduction of the *four-orbital model*, developed by Gouterman [9]. Probably inspired by the abovementioned Hückel-calculations of Longuet-Higgins et al. [8], which exhibited relatively isolated positions of the 2 HOMO's and the 2 LUMO's (in porphin denoted by a_{1u} , a_{2u} and e_{gx} , e_{gy} , respectively), Gouterman assumed that excited state properties of porphyrins are mainly determined by the relative energies of these 4 MO's. For porphin, the two LUMO's e_{gx} and e_{gy} are degenerate, whereas he assumed that a_{1u} and a_{2u} are nearly degenerate. The excited states S_1 and S_2 are now calculated by considering the configuration interaction (CI) between states obtained by one-electron promotions from the HOMO to the LUMO. Because of symmetry restrictions, CI is limited to the configurations $a_{1u} \rightarrow e_{gy}$ with $a_{2u} \rightarrow e_{gx}$, and to $a_{1u} \rightarrow e_{gx}$ with $a_{2u} \rightarrow e_{gy}$. Thus, as a result of CI four states are obtained, distinguished from each other by their polarization (x and y) and their energy. For porphin, the x and y states are degenerate, resulting in two states with different energy. From this model it follows quite naturally that the lower energy transition is forbidden, whereas the higher energy transition is strongly allowed.

More refined π -calculations (SCF-PPP) prove that the assumptions underlying the four-orbital model are basically correct [10,14]. Extensive CI results in lowest excited state energies, which are only slightly different from those calculated when CI is restricted to the two LUMO's and two HOMO's: it is found that after extensive CI the lowest excited state consists of more than 95% four-orbital configurations.

The use of the four-orbital model is not restricted to porphin. For many porphyrins, the experimental spectroscopic properties were compared to the predictions of the four-orbital model and found to agree [11]. Furthermore, the effects of substitutions of side groups and central metal atoms on the spectroscopic properties of porphyrins have been investigated [10a,11] and most effects could be described in the framework of this model. From SCF-PPP calculations on Chl it was concluded [12] that the four-orbital model provides a good description for the Q-bands; for the Soret-bands, however, the model fails, possibly because of the presence of ring V containing carbonyl groups. To account for these effects

adequately, it is appropriate to perform MO calculations including σ - and n -electrons. Furthermore, these calculations are inherently capable to describe the interaction of the central metal atom with the surrounding porphyrin electrons, which is very important for the study of the complexing and aggregation behaviour of the chlorophylls. Some results of these calculations will be summarized in the next section.

2.2.2 *Ab-initio calculations*

Ab-initio calculations have been carried out on the ground state of porphin, chlorin, ethyl pheophorbide a (i.e. pheophytin a without a phytolchain) and their Mg-analogs [13,14]. Also, the lower excited singlet and triplet state of these molecules were studied [15-17] using a limited CI approach on the basis of the MO's determined in the ground state calculations. In these excited state calculations an accurate computation of transition energies was not obtained, probably since the basis set which was employed was still too small. However, other spectral features, such as relative oscillator strengths, Q_x - Q_y splittings, Soret-Q splittings, were found to be in reasonable agreement with experiment, especially when the different molecules were compared to each other. From these calculations it was concluded that Simpson's intuitive idea [6] that Mg-porphin and Mg-chlorin can be viewed upon as macrocycles with 18 π -electrons moving along the innermost ring, is essentially correct; the other π -electrons form localized C-C bonds. Furthermore, the following results are relevant for our purposes:

(1) For all molecules studied, the four-orbital model is qualitatively correct in the description of the Q-bands. For the Soret-bands, the situation is much more complex; generally, these bands are composed of many configurations, implying that the four-orbital model fails in the description of the Soret-bands.

(2) Comparing chlorin (where ring IV is hydrogenated at C7 and C8) to porphin, it is found that the energies of those MO's which have electron density at the centers C7 and C8 (see fig. 1) are changed, whereas the charge distributions associated with those MO's remain virtually unchanged, except in the regions C7 and C8. Other MO's are hardly affected upon hydrogenation of ring IV. The same trends are found for Mg-porphin and Mg-chlorin.

(3) The introduction of Mg in any of the three molecules has little effect on the electron distributions in the higher occupied and lower unoccupied MO's, which is a consequence of the finding that Mg-orbitals do not substantially participate in the π -type MO's, which are involved in the visible transitions. The main effect is that some π -electron redistribution occurs at the 4 nitrogen

atoms, so that Mg indirectly influences the π -system.

(4) Upon introduction of ring V with its keto and carbomethoxygroup, it is found that the C9-O1 group (see fig, 1a) substantially participates in the HOMO and LUMO of ethyl-pheophorbide a and ethyl-chlorophyllide a, whereas the C10a-O2 group only yields a minor contribution.

(5) From electrostatic isopotential maps which were constructed for ethyl-chlorophyllide a, it can be concluded that the Mg-atom has a strong tendency to attract negative charges. Thus the generally accepted view that nucleophilic molecules easily ligate to Mg (see below) is confirmed.

2.3 CHLOROPHYLL COMPLEXES

In the following, only main features of Chl complexes will be described; for more detailed discussions we refer to ref. 18-20.

2.3.1 Chlorophyll-solvent interactions

Katz et al. [21] were the first to recognize the important role of the central Mg-atom in assessing complexing properties of Chl. Mg has usually a coordination number of four in a tetrahedral environment [22]. The ground state configuration of Mg^{2+} is $1s^2 2s^2 2p^6$; four-coordination can be qualitatively understood by assuming sp^3 hybridization of the Mg^{2+} orbitals, resulting in a tetrahedral coordination. If, however, Mg^{2+} is forced to coordinate to four nearly coplanar atoms, such as in the case for Chl where Mg^{2+} is coordinated to the nitrogen atoms, then d orbitals of Mg^{2+} will be involved: four coplanar hybrid orbitals can be constructed from linear combinations of s, p_x , p_y and $d_{x^2-y^2}$ orbitals (sp^2d hybridization). The p_z orbital which is not used in the hybridization, can be employed to form a fifth bond with a ligand. Alternatively, another d-orbital (d_z^2) can further be used to form a sixth coordination bond.

Thus, in Chl Mg prefers five or six coordination. Six coordination of Mg has been observed in numerous Mg-complexes [23,24] and also in Mg-porphyrins [24,25]. Extrapolating these considerations to Chl, Katz assumed that in principle the central Mg-atom in Chl has two axial positions available to obtain six-coordination by accepting lone pair electrons from a nucleophile. However, due to the fact that Mg is ~ 0.4 Å displaced from the macrocycle plane, the Mg-atom is easily accessible only from one face of the macrocycle, resulting in a preferential coordination number of five; six-ligation occurs only under forcing conditions, such as the presence of a strong electron donor, or at low temperature.

Thus by the presence of its Mg-atom Chl acts as an *electron accepting* compound. Simultaneously, Chl can act as an *electron donating* compound via its carbonyl groups, for instance in forming hydrogen bonds. These two properties are of crucial importance in forming Chl dimers and higher aggregates (see section 2.3.2). When Chl is dissolved in a polar electron donating solvent (e.g. ethanol, ether, pyridine), a solvent molecule can ligate to the Mg-atom, thus forming the monoligated complex Chl.L. In a strong electron donating solvent, such as pyridine, the biligated complex Chl.L₂ is formed. The Mg-atom in Chl is a very strong electrophile: for the equilibrium $\text{Chl} + \text{L} \xrightleftharpoons{k_1} \text{Chl.L}$, the equilibrium-constant k_1 is estimated to be of the order 10^9 l/mol [26], implying that nonligated Chl is absent in polar solvents. This should be compared with $\text{Chl.L} + \text{L} \xrightleftharpoons{k_2} \text{Chl.L}_2$, where $k_2 \sim 10 \text{ l/mol}$ [27]. In nonpolar solvents, the ligation demand of Mg will be satisfied in another way, as will be discussed in section 2.3.2.

In Chl a, three carbonyl groups are present which can have a donor function (see fig. 1a). From NMR [28] and IR [19,21,29] measurements strong evidence was provided that the donor function of Chl a is mainly exerted by the ring V keto group C9-O1. Results based on ab-initio calculations [28] point into the same direction. For Chl b the situation is less clear: of the relative donor strength of the ring II aldehyde group no experimental and theoretical data are available; there is some reason to suspect that this group is a relatively strong donor [21,30].

2.3.2 Chlorophyll aggregates

Chlorophyll aggregation has been mainly studied employing IR [19,21,29,31,34], NMR [28,32], and visible spectroscopy [19,32-34] methods. For some representative examples of the effect of association on the Q_y-band of the visible spectrum of Chl a, we refer to table I. For comparison, also some monomeric Chl a forms have been included.

Chl molecules can aggregate in three ways:

- (1) by interaction of the phytol chains
- (2) by π - π interaction of the Chl macrocycles
- (3) by interaction of the Mg-atom of one Chl molecule with an electron donating group of another Chl molecule. This can either be
 - (a) direct C=O...Mg interaction, or
 - (b) a C=OL....Mg interaction where the carbonylgroup and the Mg-atom interact via an interstitial ligand (see below).

Table I. Chl a species

Solvent	Species	Conc (M/l)	Temp (K)	λ_{Q_y} (nm)	ref.
ether	Chl.L	10^{-5}	300	661	63
ethanol	Chl.L	10^{-5}	300	663	35
pyridine	Chl.L ₂	10^{-5}	300	669	41
ethanol	(Chl.L ₂) ₂ ¹⁾	10^{-2}	300	665	35
CCl ₄	(Chl) ₂ ²⁾	10^{-4}	300	678	41
n-octane	(Chl ₂) _n	10^{-4}	300	678	41
dodecane/film	(Chl.H ₂ O) _n	10^{-4}	300	743	41
ethanol	Chl.L	10^{-5}	77	672	19
toluene/ethanol	(Chl.L) ₂ ³⁾	10^{-1}	120	700	19
pentane/ methylcyclohexane	(Chl.H ₂ O) ₂	10^{-4}	120	702	43

¹⁾ aggregate via phytyl-phytyl interaction

²⁾ dimer via Mg-keto interaction

³⁾ dimer via Mg-solvent-keto interaction ("special pair").

Interaction (1) occurs in polar solvents at high concentrations. This type of aggregation has been observed in concentrated solutions ($\sim 10^{-2}$ M/l) in pyridine or ethanol at low temperatures [35].

Interaction (2) is presumably not very important in Chl, since the binding energy is relatively low: for pheophytin a dimers, the binding energy arising from π - π interactions has been estimated at ~ 18 kJ/mol [36], and is expected to be similar for Chl. Furthermore, in polar solvents the dimer geometry needed for optimum π - π interaction will be sterically hindered by ligation of a solvent molecule to the Mg-atom, which is, as already mentioned, a very strong interaction. In nonpolar solvents the third mechanism prevails.

Mechanism (3a) occurs if in a Chl solution no electron donating molecules are present, as is the case in very dry nonpolar solvents, such as benzene, carbon tetrachloride and octane; then the ligation demand of the central Mg atom of one Chl molecule is satisfied by the donor function of the ring V keto group of another Chl molecule. The binding energy of this type of interaction is about 40 kJ/mol [33].

Experimental evidence for this last type of aggregation was provided by the above-mentioned NMR and IR observations. Furthermore, it was found that in solvents such as benzene and CCl_4 , Chl a mainly forms dimers, $(\text{Chl } \underline{a})_2$, whereas in dry aliphatic hydrocarbons (octane) much larger aggregates were found, $(\text{Chl } \underline{a}_2)_n$ with $n > 5$. This last type of aggregates is composed of a repeating chain of $(\text{Chl } \underline{a})_2$ dimers. In the visible spectrum aggregation manifests itself as a redshift of the Q_y band relative to the monomer (see table I) which has been described in terms of exciton interaction [37]. As can be concluded from a comparison of NMR and optical (IR and visible spectrum) data, the dimer equilibrium $2 \text{ Chl} \rightleftharpoons \text{Chl}_2$ is fast on the NMR time-scale (~ 1 msec) and slow on the optical timescale. Thus NMR sees an "average" dimer, whereas optical techniques can discern between "donor" and "acceptor". A further interesting feature of $(\text{Chl } \underline{a})_2$ is the complete absence of fluorescence [38]. From NMR experiments, making use of ring current induced shifts when going from monomer to dimer, Katz *et al.* [18,31a] have proposed a dimer structure, in which both chlorin planes are $\sim 45^\circ$ tilted with respect to each other. Houssier and Sauer [39] suggest on the basis of circular dichroism experiments that $(\text{Chl } \underline{a})_2$ is formed not only by ring V keto-Mg interactions, but also by a ring IV ester-Mg interaction. This would result in ligation at the Mg-atoms of both molecules, whereas also in their structure both planes make an angle of $\sim 45^\circ$. However, IR [34] and ^{13}C NMR data [28] do not indicate that the ring IV ester-group is involved in bonding. Also, the tilted structure proposed by Katz *et al.* is somewhat difficult to conceive: in order to obtain optimum overlap between the ring V keto lone pair orbitals and the Mg-orbitals, and to avoid sterical hindrance when both macrocycles approach each other, one should rather expect a dimer geometry in which both molecular planes are approximately perpendicular to each other (see fig. 6 in Chapter 7).

Finally, aggregates of type (3b) can be generated by dissolving Chl a in a nonpolar solvent in the presence of molecules which can serve as bifunctional ligands, i.e. molecules which have both electron donating and -accepting properties. Examples of this type of molecules are ethanol and in particular water, which can both ligate to the Mg atom by their oxygen lone pair electrons and can form a hydrogen bond with a Chl carbonylgroup. In this way, bifunctional ligands can form a link between two Chl molecules. It has long been known [40] that upon addition of water to a nonpolar solution of Chl a the visible absorption band shifts to ~ 743 nm (see table I). The polymeric nature of the Chl species associated with this band was established from the narrow ESR linewidth which was found when this species was oxidized, indicating that the unpaired spin was delocalized over the whole aggregate [41]. The structure of this

aggregate remained unclear, until Strouse determined the crystal structure of (ethylchlorophyllide a. $2\text{H}_2\text{O}$)_n with X-ray diffraction [3]. In this structure linear arrays of $-\text{Chl} \cdot \text{H}_2\text{O} \cdot \text{Chl}-$ are crosslinked by a second water molecule to form a two-dimensional sheet; these sheets are then stacked to form a three-dimensional crystal (see fig. 3 for a picture of such a sheet). All chlorin planes are parallel to each other. By removing the crosslinking water molecule a film $(\text{Chl} \cdot \text{H}_2\text{O})_n$ is formed in which the linear chain arrangement is maintained; this film has an absorption maximum at 743 nm [40]. It is generally accepted that the Chl-water aggregate absorbing at 743 nm consists of such a linear arrangement of $(\text{Chl} \cdot \text{H}_2\text{O})$ units.

The X-ray structure determination of (ethylchlorophyllide a. $2\text{H}_2\text{O}$)_n provided important hints considering the structure of still another Chl a form, the so-called "special pair" dimer [19,42]. By adding an equimolar amount of ethanol to a concentrated (≈ 0.1 M/l) solution of Chl a in dry toluene, the Q_y absorption band shifts at low temperature to ≈ 700 nm [19] (see table I). The same effect is found in a dilute ($\approx 10^{-5}$ M/l) solution of Chl a in dry methylcyclohexane [43]. The latter authors estimate that in their solutions an equimolar amount of water was present. The IR spectrum of the toluene solution indicates that at low temperatures the ring V keto group is bound and is either ligated to Mg or is strongly hydrogen bonded. Upon oxidizing this 700 nm absorbing chlorophyll aggregate, it was found that the $g = 2$ ESR line had a line width which was smaller by a factor $\sqrt{2}$ than that of the monomer, indicating that the unpaired electron spin is equally delocalized over two molecules [19]. Furthermore, the

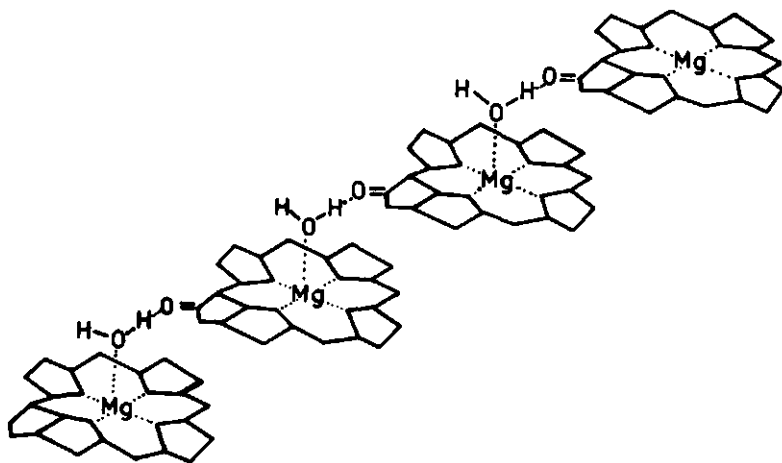


Fig. 3. The structure of $(\text{Chl} \cdot \text{H}_2\text{O})_n$ according to Chow et al. [3]. All macrocycles are plane-parallel.

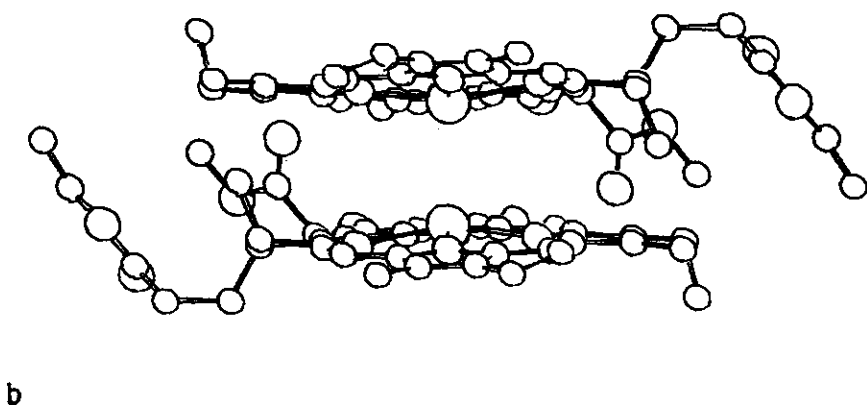
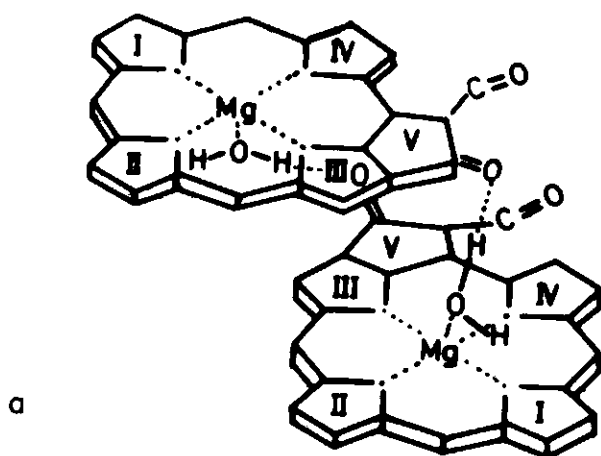


Fig. 4 (a) Structure of "special pair" according to Shipman *et al.* [42].
 (b) Computer drawing of "special pair" viewed along an axis parallel to the macrocycle planes. (Both interstitial ligands have been omitted).

results of an ethanol titration on Chl a /toluene solution, monitoring the Q_y bands, can be described in terms of the equilibrium $(\text{Chl } \underline{a})_2 + 2 \text{ ethanol} \rightleftharpoons (\text{Chl } \underline{a}.\text{ethanol})_2$ [19]. The free enthalpy of forming the Chl a.ethanol aggregate was estimated at $\approx 25 \text{ kJ/mol}$ [19]. Based on these experimental observations, on Strouzes X-ray results [3], and on exciton calculations [44], it has been proposed that this dimer has a structure as depicted in fig. 4. The dimer is composed of two plane-parallel Chl a molecules, which are linked via two bifunctional molecules (for instance ethanol) each forming a hydrogen bond with the ring V keto group of one molecule and ligating to the Mg atom of the other molecule in such a way that the dimer has an overall C_2 symmetry. Fong [45], who actually was the first to propose a C_2 dimer linked via two bifunctional ligands, suggests a slightly different structure in which the two ester carbonylgroups C10-O2 are hydrogen bonded. It cannot be excluded that both dimer structures can exist depending on the preparation conditions [46]. It must be realized, however, that both "special pair" structures are rather speculative; only few experimental data are available confirming one or another structure. The only firmly established facts seem to be the stoichiometry of the complex, i.e. $(\text{Chl } \underline{a}.\text{ligand})_2$, and the importance of hydrogen bonds in forming the dimer. In further investigating the "special pair" structure the approach of synthesizing covalently linked Chl-dimers with properties similar to Chl a "special pair" [47-49] seems to become a fruitful route. In principle, it should be possible to synthesize a dimer with predetermined structure, and the properties of such a dimer can be compared with those of Chl a "special pair". By a trial-and-error procedure a dimer might be synthesized which closely mimics Chl a "special pair".

2.4 RELEVANCE TO PHOTOSYNTHESIS

An important reason for the great interest in Chl aggregates is the notion that these are present in the photosynthetic system [50]. For both the reaction center of photosystem (PS) 1 and the antenna system *in vitro* models have been proposed. ESR [41], ENDOR [51] and optical (CD) [52] measurements on *in vivo* systems indicate the dimeric nature of the PS 1 reaction center. For this reaction center, the most promising model up to now seems to be the 700 nm absorbing "special pair" Chl a dimer with a structure as proposed by Shipman et al. [42] (see fig. 4). This dimer has the same optical and ESR properties as the PS 1 reaction center [53]. Furthermore, the *in vitro* "special pair" can be photo-oxidized in the presence of a suitable electron acceptor, yielding an ESR signal

which is practically indistinguishable from that in photo-oxidized *in vivo* systems [42]. Redox properties of the *in vitro* "special pair" dimer have not yet been determined; it would be interesting to compare these to those of *in vivo* systems. For a detailed and lucid discussion on the Chl "special pair" we refer to Katz et al. [53].

Models of antenna Chl are even more speculative. Katz et al. [26] have proposed that antenna Chl consists of anhydrous Chl oligomers, $(\text{Chl})_n$, with a structure analogous to that of *in vitro* oligomers in aliphatic hydrocarbon solutions. The only experimental basis for this suggestion is the correspondence in absorption maximum (678 nm) between *in vitro* oligomers and *in vivo* antenna Chl a [54]. Apart from the serious objections which can be raised against this speculation, namely the complete absence of fluorescence in *in vitro* $(\text{Chl } \underline{a})_n$, whereas antenna chlorophyll is known to fluoresce [54], and the strictly apolar environment which is required in forming $(\text{Chl } \underline{a})_n$, the *in vivo* measurements clearly point into a different direction. There is a wealth of evidence [55-58] that *in vivo* many Chl a forms are present. Litvin et al. [58] conclude even that at least ten different Chl a forms exist in the plant photosynthetic system, in absorption maximum varying from 664 to 735 nm. From resonance Raman spectroscopy, Lutz [59] inferred that at least six major forms of *in vivo* Chl a can be discerned. In none of these forms he found ring V keto C = O vibrations characteristic of $(\text{Chl } \underline{a})_n$ oligomers indicating that the presence of $(\text{Chl } \underline{a})_n$ is unlikely. Moreover, no evidence was found for Chl a forms in which the Mg and the ring V keto group are linked via water molecules, thus falsifying another model [60] for antenna Chl, which was based on the Strouse X-ray structure.

Thus, it is rather uncertain how Chl molecules are arranged to form antenna Chl. A further complicating factor in the study of *in vivo* absorption spectra is the presence of Chl b in the antenna system. This makes an unambiguous assignment of the various absorption bands to different Chl a forms very difficult, in particular because the *in vitro* complexing properties of Chl b are much less well known than those for Chl a. Undoubtedly, Chl aggregates must be present in the antenna system, in view of the long-wavelength absorption maxima and the very high local Chl concentration (0.1 M/l). It can be expected that these aggregates are formed by Chl-protein interactions in which the carbonyl groups and the Mg-atom of Chl are involved. This type of interaction is strongly suggested by the results of an X-ray study of a bacteriochlorophyll-protein complex [61] which is *in vivo* associated with the bacterial antenna system. From this study it can also be concluded that the chromophoric groups are close enough to each other for

having appreciable interaction resulting in a significant absorption redshift. Although this bacteriochlorophyll-protein complex is probably much simpler than the plant antenna system and is not really an antenna system, the latter might well have a structure analogous to that of the bacteriochlorophyll-protein complex in view of the similar environment [62] and similar interactions [59] present in the plant antenna system. A combination of *in vivo* (X-ray, resonant Raman) and *in vitro* (IR, visible, absorption, exciton calculations) studies are probably the most direct way to an elucidation of the structure of the plant antenna system.

2.5 REFERENCES

1. H.J. van Gorkum, Thesis, Leiden (1978).
2. J.A. van Best, L.N.M. Duysens, Biochim. Biophys. Acta, 459 (1977) 187.
3. H.C. Chow, R. Serlin, C.E. Strouse, J. Am. Chem. Soc. 97 (1975) 7230.
4. C. Kratky, Thesis, ETH Zürich (1976).
5. G.P. Gurinovich, A.N. Sevchenko, K.N. Solov'ev, "Spectroscopy of Chlorophyll and Related Compounds" (Minsk, 1968) distributed by NTIS, Springfield Va. 22151, USA.
6. W.T. Simpson, J. Chem. Phys., 17 (1949) 1218.
7. G.W. Canters, G. Jansen, M. Noort, J.H. van der Waals, J. Phys. Chem. 80 (1976) 2253.
8. H.C. Longuet-Higgins, C.W. Rector, J.R. Platt, J. Chem. Phys. 18 (1950) 1174.
9. (a) M. Gouterman, J. Mol. Spectr. 6 (1961) 138.
(b) M. Gouterman, G. Wagnière, J. Mol. Spectr., 11 (1963) 108.
10. (a) C. Weiss, H. Kobayashi, M. Gouterman, J. Mol. Spectr. 16 (1965) 415.
(b) A. McHugh, M. Gouterman, C. Weiss, Theor. Chim. Acta, 24 (1972) 346.
11. M. Gouterman, in "Excited States of Matter", (Ed. C.W. Choppes), Grad. Studies Texas Tech. Univ. (1973).
12. C. Weiss, J. Mol. Spectr. 44 (1972) 37.
13. D. Spangler, G.M. Maggiora, L.L. Shipman, R.E. Christoffersen, J. Am. Chem. Soc. 99 (1977) 7470.
14. D. Spangler, G.M. Maggiora, L.L. Shipman, R.E. Christoffersen, J. Am. Chem. Soc. 99 (1977) 7478.
15. J.D. Petke, G.M. Maggiora, L.L. Shipman, R.E. Christoffersen, J. Mol. Spectr. 71 (1978) 64.
16. J.D. Petke, G.M. Maggiora, L.L. Shipman, R.E. Christoffersen, J. Mol. Spectr. 73 (1978) 311.
17. J.D. Petke, G.M. Maggiora, L.L. Shipman, R.E. Christoffersen, J. Mol. Spectr. in press.
18. J.J. Katz, J.R. Norris, in "Current Topics in Bio-energetics" (Eds. D.R. Sanadi and L. Packer), Vol. 5, pp. 41-75, Acad. Press, New York (1973).
19. T.M. Cotton, Thesis, Evanston, Ill. (1977).
20. G.R. Seely, in "Primary processes of Photosynthesis" (Ed. J. Barber), Ch.1, Elsevier Publ. Comp, Amsterdam (1977).
21. J.J. Katz, G.L. Closs, F.C. Pennington, M.R. Thoma, H.H. Strain, J. Am. Chem. Soc. 85 (1963) 3801.
22. R.W. Parr in "the Chemistry of Coordination Compounds" (Ed. J.C. Bailar), Reinhold Publishing Corp., New York (1956).
23. N.V. Sidgwick, "the Chemical Elements", Vol. 1, Oxford Press, Oxford (1950).
24. P.E. Wei, A.H. Corwin, R. Arellano, J. Org. Chem. 27 (1962) 3344.
25. J.R. Miller, G.D. Dorough, J. Am. Chem. Soc. 74 (1952) 3977.

26. J.J. Katz, J.R. Norris, L.L. Shipman, Brookhaven Symposia in Biology, 28 (1976) 17.
27. T.A. Evans, J.J. Katz, Biochim. Biophys. Acta, 396 (1975) 414.
28. L.L. Shipman, T.R. Janson, G.J. Ray, J.J. Katz, Proc. Natl. Acad. Sci. USA 72 (1975) 2873.
29. M. Henry, J.P. Leicknam, Colloque Intern. du C.N.R.S. 191 (1970) 317.
30. Chapter 5 of this thesis.
31. (a) J.J. Katz, R.C. Dougherty, L.J. Boucher in "the Chlorophylls", Chapter 7 (Eds. L.P. Vernon and G.R. Seely) Acad. Press, New York (1966).
(b) S.G. Boxer, G.L. Closs, J.J. Katz, J. Am. Chem. Soc. 96 (1974) 7058.
32. K. Sauer, J.R. Lindsay Smith, A.J. Schultz, J. Am. Chem. Soc. 88 (1966) 2681.
33. J.P. Leicknam, M. Henry, J. Kléo, J. Chim. Phys. 75 (1978) 529, 535.
34. T.M. Cotton, P.A. Loach, J.J. Katz, K. Ballschmiter, Photochem. Photobiol. 27 (1978) 735.
35. S.B. Broyde, S.S. Broyde, Biophys. J. 8 (1968) 1511.
36. R.P.H. Kooyman, T.J. Schaafsma, G. Jansen, R.H. Clarke, D.R. Hobart, W.R. Leenstra, Chem. Phys. Lett., 68 (1979) 65; Chapter 3 of this thesis.
37. L.L. Shipman, T.M. Cotton, J.R. Norris, J.J. Katz, J. Am. Chem. Soc. 98 (1976) 8222.
38. R. Livingston, W.F. Watson, J. McArdle, J. Am. Chem. Soc. 71 (1949) 1542.
39. C. Houssier, K. Sauer, J. Am. Chem. Soc. 92 (1970) 779.
40. E.E. Jacobs, A.E. Vatter, A.S. Holt, Arch. Biochem. Biophys. 53 (1954) 228.
41. J.R. Norris, H. Scheer, J.J. Katz, Ann. N.Y. Acad. Sci. 244 (1975) 260.
42. L.L. Shipman, T.M. Cotton, J.R. Norris, J.J. Katz, Proc. Natl. Acad. Sci. USA, 73 (1976) 1791.
43. F.K. Fong, V.J. Koester, Biochem. Biophys. Acta, 423 (1976) 52.
44. L.L. Shipman, J. Phys. Chem. 81 (1977) 2180.
45. (a) F.K. Fong, Appl. Phys. 6 (1975) 151.
(b) F.K. Fong, "Theory of Molecular Relaxation: Applications in Chemistry and Biology", Chapter 9, Wiley-Interscience, N.Y. (1975).
46. F.K. Fong, V.J. Koester, L. Galloway, J. Am. Chem. Soc. 99 (1977) 2372.
47. M.R. Wasielewski, M.H. Studier, J.J. Katz, Proc. Natl. Acad. Sci. USA, 73 (1976) 4282.
48. N. Periasamy, H. Linschitz, G.L. Closs, S.G. Boxer, Proc. Natl. Acad. Sci. USA, 75 (1978) 2563.
49. S.G. Boxer, R.R. Bucks, J. Am. Chem. Soc. 101 (1979) 1883.
50. K. Sauer in "Bioenergetics of Photosynthesis", Chapter 3 and references therein (Ed. Govindjee) Acad. Press, New York (1975).
51. J.R. Norris, H. Scheer, M. Druyan, J.J. Katz, Proc. Natl. Acad. Sci. USA, 71 (1974) 4897.
52. K.D. Philipson, K. Sauer, Biochemistry 11 (1972) 1880.
53. J.J. Katz, L.L. Shipman, J.R. Norris in "Chlorophyll Organization and Energy Transfer in Photosynthesis", Ciba Foundation 61 (new series) Excerpta Medica, Amsterdam (1979).
54. (a) Govindjee, R. Govindjee in ref. 50, Chapter 1 and references therein.
(b) J.C. Goedheer, Photosynthetica 10 (1976) 411.
55. C.N. Cederstrand, E. Rabinowitch, Govindjee, Biochim. Biophys. Acta, 126 (1966) 1.
56. C.S. French, J.S. Brown, M.C. Lawrence, Plant Physiol. 49 (1972) 421.
57. G. Papageorgiou in ref. 50, Chapter 6.
58. F.F. Litvin, V.A. Seneschekov in ref. 50, Chapter 12.
59. M. Lutz, Biochim. Biophys. Acta, 460 (1977) 408.
60. C.E. Strouse, Proc. Natl. Acad. Sci. USA, 71 (1974) 325.
61. (a) R.E. Fenna, B.W. Matthews, Nature 258 (1975) 573.
(b) R.E. Fenna, B.W. Matthews in ref. 26, pp. 170-182.
62. J.P. Thornber, Annu. Rev. Plant Physiol. 26 (1975) 127.
63. G.S. Singhal, W.P. Williams, E. Rabinowitch, J. Phys. Chem. 72 (1968) 3941.

3 A comparative study of dimerization of chlorophylls and pheophytins by fluorescence and ODMR

R.P.H. KOOYMAN, T.J. SCHAAFSMA, G. JANSEN

*Laboratory of Molecular Physics, Agricultural University,
6703 BC Wageningen, The Netherlands*

and

Richard H. CLARKE, David R. HOBART and Willem R. LEENSTRA
Department of Chemistry, Boston University, Boston, Massachusetts 02215, USA

Received 3 September 1979

Optical and ODMR data for dimers of pheophytin a and b and chlorophyll a and b are presented. It is proposed that pheophytin a forms a parallel dimer arising from π - π interaction, binding being essentially different from that in the corresponding chlorophyll dimer. The dimer of pheophytin a is less stable ($K \approx 10^4$ l/mol) than that of chlorophyll a ($K \approx 10^6$ l/mol).

1. Introduction

The capability of the chlorophyll (Chl) molecule (fig. 1) to form aggregate structures has long been considered an important physical property in its role in photosynthesis [1,2]. The consideration of models for antenna and reaction center Chl have utilized this physical feature in the development of ligand-stabilized dimer structures, as well as higher order aggregates [3-5]. Magnetic and dynamic properties of the photo-excited triplet state can be used to study the structure of such aggregates and the interactions which stabilize them [6-8].

The pheophytins (fig. 1) provide another useful system to investigate properties of pigment aggregation, since their ability to form ligand-bound dimers is restricted by the absence of a metal center within their chlorin ring structure. Therefore, they provide an opportunity to determine the effect and importance of ring substituents in aggregation processes and the possible role of ligand attachment to these ring substituents in stabilizing dimer structures. We present data on pheophytin a (Ph a), pheophytin b (Ph b), chlorophyll b (Chl b), their concentration dimers (Ph a)₂, (Ph b)₂, (Chl b)₂, and a covalently linked dimer of

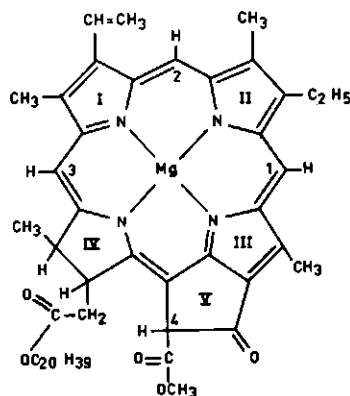


Fig. 1. Molecular structure of chlorophyll a; in pheophytin a the Mg atom is replaced by two hydrogen atoms.

pheophorbide a (Ph-Pb) in hydrocarbon solution in the presence and absence of hydrogen bonding ligands. Fluorescence data and triplet state zero field splittings (ZFS) for these systems are discussed with regard to possible dimer structures for pheophytins and are compared with structures measured for the parent chloro-

phylls; specific binding interactions in these two types of molecules are discussed.

2. Experimental

2.1. Sample preparation

Chl **a** and **b** were obtained from Sigma, Ph **a** and **b** were prepared according to standard procedures [9]. Pheophorbide **a** covalently linked dimer was prepared from chlorophyllide **a** covalently linked dimer, which was a gift from Professor G.L. Closs. Demetalization was checked via the room-temperature absorption spectrum. All solvents were analytical grade. Dried samples were prepared as follows: Ph **a** films were pumped at 10^{-5} Torr during more than 12 h, with slight heating at $\approx 70^\circ$ C. Solvents were dried on CaH_2 . Utilizing this drying procedure a substantial amount of ligand-free Chl dimer, absorbing at 678 nm [10] in non-polar solvents (such as toluene) can be produced. The requirements for drying pheophytins are expected to be not as severe as for the chlorophylls, because of the absence of the Mg atom, which is able to hold one or two polar ligands, such as water [3]. Therefore we feel confident in using the procedure described above, which is less laborious than that described by Cotton [10].

2.2. Measurements

Concentration-dependent fluorescence spectra were taken at 77 K; Ph **a** spectra were obtained using surface-excitation in order to avoid self-absorption in the determination of the equilibrium constant for dimerization. ODMR experiments [11] were carried out at 4.2 K for Ph **a**, 2 K in other cases, using broad-band optical excitation in the 400–500 nm region. For further instrumental details we refer to previous work: ref. [11] for Ph **a** and ref. [12] for Ph **b**, Chl **b** and Ph–Ph.

3. Results and discussion

3.1. Fluorescence and ODMR data

Fig. 2 represents the concentration dependence of the fluorescence of Ph **a** in *n*-octane at 77 K. It is seen,

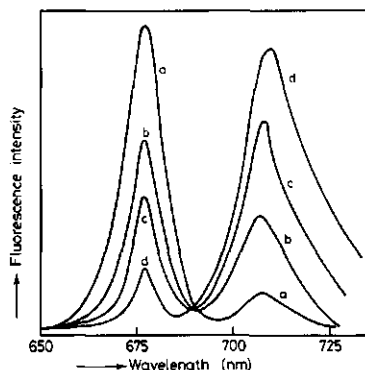


Fig. 2. Concentration dependence of the fluorescence spectrum of Ph **a** at 77 K. (a) 10^{-6} M; (b) 5×10^{-5} M; (c) 10^{-4} M; (d) 10^{-3} M. For various concentrations, the spectra have been normalized to equal integrated intensity.

that by gradually increasing the Ph **a** concentration, a new band appears at 712 nm whereas the 675 nm band simultaneously decreases. Dried samples exhibit the same behaviour as those containing various amounts of electron-donating compounds. At higher concentration, the long-wavelength band shifts up to 5 nm to the red. The appearance of two bands is similar to that observed for Chl **a** in hydrocarbon solution, a spectrum that is interpreted as arising from monomeric and ligand-bound dimeric Chl **a** [13]. The same features are found for Ph **b** (660 nm and 704 nm) and for Chl **b** (650 nm and 700 nm).

The ODMR spectra for Ph **a** and Ph **b** also indicate the presence of new species in solution when detecting on the red-shifted fluorescence peak, with different ZFS than observed on the monomer fluorescence peak. In fact, the ODMR spectra of frozen *n*-octane solutions, containing (Ph **a**)₂ are rather complicated, indicating the presence of at least two different species. By double resonance we sorted out one pair of two mutually associated resonances, yielding the ZFS splittings given in table 1. Also for Chl **a** in solution a difference in ODMR transition frequencies has been observed when detecting on the monomeric and dimeric fluorescence peaks [7,8]. A comparison of the ODMR frequencies for the chlorophylls and the pheophytins may be seen in table 1.

The concentration effect on Ph **a** fluorescence spec-

Table 1
ZFS parameters of monomers and dimers of chlorophylls and pheophytins

Species	Solvent	Detection wavelength (nm)	$10^4 D$ (cm^{-1})	$10^4 E$ (cm^{-1})	Reference
pheophytin a monomer	<i>n</i> -octane	675	350 (± 2)	20 (± 1)	this work
pheophytin a dimer	<i>n</i> -octane	713	324 (± 3)	16 (± 4)	this work
pheophytin b monomer	<i>n</i> -octane	660	376 (± 5)	40 (± 5)	this work
pheophytin b dimer	<i>n</i> -octane	704	323 (± 5)	15 (± 5)	this work
chlorophyll a monomer	<i>n</i> -octane	687	291 (± 5)	38 (± 4)	[8]
chlorophyll a dimer	methylcyclohexane/pentane (1:1)	720	272 (± 5)	36 (± 4)	[7,8]
chlorophyll b monomer	methylcyclohexane/pentane (1:1)	650	296 (± 3)	40 (± 3)	this work
chlorophyll b dimer	methylcyclohexane/pentane (1:1)	700	281 (± 3)	31 (± 3)	this work

tra can be described with a monomer-dimer equilibrium constant for which $\log K = 4 \pm 0.5$. This value was obtained from a log-log plot of $[\text{dimer}]/[\text{monomer}]$ versus total pheophytin concentration. The insensitivity of Ph a fluorescence to the amount of hydrogen-bonding molecules present is in contrast with the titration behaviour of Chl fluorescence [10,13], where it was observed that aggregate fluorescence intensity increased with addition of hydrogen-bonding component. Therefore, it is inferred that in pheophytins dimerization via ligation by hydrogen-bonding molecules is not important. The titration results with methanol, which is an electron-donating compound with hydrogen-bonding capability, indicates that in forming Ph dimers no ligand molecules are required at all. This is in contrast with the results for chlorophyll, where the presence of ligand molecules determines the structure of the dimer. Both in the covalently linked dimer [14] and in the equilibrium chlorophyll-ethanol adduct [4], formation of a parallel dimer occurs by a magnesium-ringing V keto bond via two interstitial bifunctional ligands. Results obtained from experiments with covalently linked dimers point to the same direction. It is known that the covalently linked Chl dimer exists in two forms, depending on the nature of the solvent: in a non-electron-donating solvent the dimer exists in its unfolded form, whereas in the presence of bifunc-

tional ligands the dimer can fold in such a way that a sandwich-like parallel dimer is formed, in which both parts have appreciable mutual interaction [14].

However, a thoroughly dried sample of the Ph-Ph dimer in toluene at 77 K exhibited a fluorescence spectrum (fig. 3) consisting essentially of unfolded dimer regardless of the cooling rate. An added amount of methanol varying from 1% to as much as 50% did not

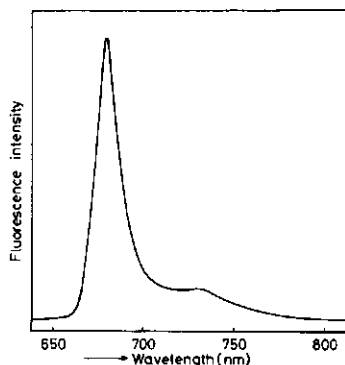


Fig. 3. Fluorescence spectrum of Ph-Ph dimer in toluene. Addition of up to 50 vol % methanol does not affect the spectrum; $T = 77$ K.

affect the fluorescence spectrum. This result contrasts with that for the Mg- or Zn-substituted covalently linked dimer, in which a 1% addition of methanol produced essentially all folded dimer [7]. This finding thus provides additional support for the non-hydrogen bonding nature of the pheophytin dimerization.

3.2. Bonding in Ph and Chl dimers; geometrical considerations

For substituted aromatic hydrocarbons, two main intermolecular interactions can be distinguished: hydrogen-bonding and π - π interaction. Bonding in the Chl dimer occurs via two interstitial bifunctional ligands [13]. For Ph, as our optical data for the covalent and concentration dimer indicate, no hydrogen bonds are involved in bonding of both monomers. A similar distinction between dimerization of chlorophylls and pheophytins has been noted by Katz et al. [15,16] in their early IR and NMR study of aggregation of these compounds in solution. We can thus conclude that dimerization in Ph occurs via the common phenomenon [17] of π - π overlap of the two chlorin macrocycles. π - π complexes of aromatic hydrocarbons almost exclusively form parallel dimers in accordance with optimum overlap requirements.

Measured ZFS values (table 1) of pheophytin dimers are indeed consistent with a parallel structure. As is evident from table 1, the D value of the dimers is not far below that of the monomer. Application of a pure triplet exciton model [7,18] to a parallel dimer predicts equal D values for monomer and dimer. Preliminary results from a calculation including charge-resonance (CR) contributions [19] due to $\text{Ph}^+\text{Ph}^- \leftrightarrow \text{Ph}^-\text{Ph}^+$ structures indicate that the lowering of the D value of the dimer with regard to that of the monomer can be accounted for with a contribution of <10% CR in the dimer wavefunction of $(\text{Ph a})_2$.

From the fluorescence data of the Ph-Ph dimer and the ZFS values of the $(\text{Ph})_2$ concentration dimer, we can draw some preliminary conclusions with regard to the configuration of the latter. The striking difference between the folding of the covalent Chl dimer resulting from addition of hydrogen-bonding components to solutions of chlorophyll in non-polar solvents and the absence of this folding in the corresponding Ph-Ph compound cannot be explained by different values of the dissociation enthalpy, since Ph readily forms $(\text{Ph})_2$

concentration dimers. The effect of reduction of the dissociation entropy in the Ph-Ph dimer by the presence of the connecting chain is counteracted by steric hindrance as can be demonstrated by building molecular models. Maximum π - π overlap between both parts of the Ph-Ph dimer is prevented in two ways: it turns out to be rather difficult to construct a Ph-Ph dimer in which both chlorin macrocycles are on top of each other. Furthermore, only a very restricted set of configurations, obtained by mutual in-plane rotations of the sub-units, is possible. This is in contrast with the situation in the Chl a covalent dimer which is isomorphous with the "special pair" [20], where virtually no π - π overlap is present (fig. 4); only rings III and V may have some overlap. In this case, the association enthalpy due to hydrogen bonding is able to overcome the steric hindrance which is smaller for the proposed structure [14] anyway.

For the $(\text{Ph})_2$ dimer, we should seek for configurations with maximum overlap. Intuitively, it is expected that the unsaturated parts of both molecules should be as much as possible on top of each other. Surprisingly, calculations for the $(\text{Ph a})_2$ dimer including charge-resonance contributions to the stabilization energy [19] show that for dimers with *displaced* projections of

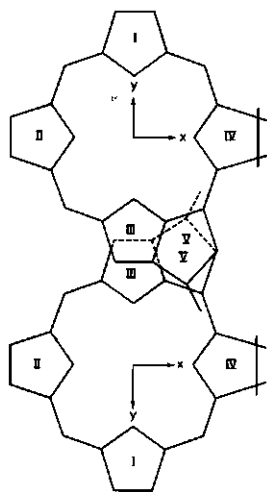


Fig. 4. In-plane projection of the "special pair" chlorophyll dimer (after ref. [3]).

monomer centers, the dimeric ground state is stabilized with regard to that of the monomer, whereas the intermolecular overlap integrals and the attractive Coulomb forces are not much smaller than for undisplaced monomeric centers. For the latter almost no stabilization occurs. From aggregation maps (obtained from NMR shifts) for Ph a, a sandwich-type structure has been derived, in which the projections of the molecular centers are indeed somewhat displaced from each other [15,16]. We have calculated two $(\text{Ph a})_2$ dimer configurations:

(I) Both porphyrin macrocycles are mutually rotated over $\approx 180^\circ$, so that rings IV are on opposite sites of the dimer and outside the $\pi-\pi$ interaction region. In this dimer (I) both monomers are translationally inequivalent.

(II) Both monomers within the dimer are translationally equivalent.

The experimental dimer S_1 energy (≈ 1.73 eV) is very close to the calculated value for dimer I (1.75 eV) and quite different from that for dimer II (1.56 eV), favouring the former as the most likely configuration. This provides a simple explanation for the non-folding of the covalent Ph-Ph dimer, since the dimer I configuration then cannot be formed due to the limited length of the ten-atom chain connecting rings IV, as can be demonstrated by molecular models.

In both configurations, the $(\text{Ph a})_2$ dimer should have a virtually unchanged E value with regard to that of the monomer, as is consistent with experiment (table 1).

In summary, comparison of Chl and Ph dimer structures indicates that the binding mechanism in both complexes is quite different. In addition, thermodynamic arguments are consistent with the conclusions from our spectroscopic data. From the fact that the $(\text{Ph a})_2$ concentration dimer does not form in 10^{-3} M Ph a *n*-octane solution at room temperature, as judged from the fluorescence spectrum, whereas the dimer is the dominant species at the freezing point of *n*-octane (-60°C), and the magnitude of ΔS of ≈ 80 kJ/K mol generally found in forming $\pi-\pi$ complexes [17], the dissociation enthalpy can be estimated at ≈ 18 kJ/mol, i.e. distinctly lower than the dissociation enthalpy for the Chl dimer, which has been estimated at ≈ 28 kJ/mol [10]. The large value of ΔS of $\pi-\pi$ dimers [17], such as pheophytins, indicates a rather rigid configuration of the dimer, once formed. Also, the equilibrium

constants for both complexes indicate that $(\text{Ph a})_2$ is a weaker complex than the Chl dimer: $K \approx 10^4$ l/mol for pheophytin as compared to $\approx 10^6$ l/mol for chlorophyll [10]. This then adds justification for the important role of ligand complexing in chlorophylls as compared to $\pi-\pi$ stacking interactions, interactions which are necessarily dominant in the case of pheophytin aggregation, in agreement with previous conclusions from NMR work by Katz' group [15,16].

Acknowledgement

This investigation was supported by the Netherlands Foundation for Chemical Research (S.O.N.), with financial aid from the Netherlands Organization for the Advancement of Pure Research (Z.W.O.) and in part by the EC Solar Energy Program, under contract nr. 547-78 ESN, the U.S. Department of Energy under contract nr. EY-76-S02-2570 and by the donors of the Petroleum Research Fund, administered by the American Chemical Society. The authors gratefully acknowledge technical assistance by Mr. R.B.M. Koehorst.

References

- [1] J.S. Brown and C.S. French, *Plant Physiol.* 34 (1959) 305.
- [2] K. Sauer, in: *Bioenergetics of photosynthesis*, ed. Govindjee (Academic Press, New York, 1975), and references therein.
- [3] J.J. Katz, J.R. Norris and L.L. Shipman, *Brookhaven Symp. Biol.* 28 (1976) 16.
- [4] F.K. Fong, *Appl. Phys.* 6 (1975) 151.
- [5] H. Chow, R. Serlin and C.E. Strouse, *J. Am. Chem. Soc.* 97 (1975) 7230.
- [6] W. Hägele, D. Schmid and H.C. Wolf, *Z. Naturforsch.* 33a (1978) 94.
- [7] R.H. Clarke, D.R. Hobart and W.R. Leenstra, *J. Am. Chem. Soc.* 101 (1979) 2416.
- [8] R.P.H. Kooyman, T.J. Schaafsma and J.F. Kleibeuken, *Photochem. Photobiol.* 26 (1977) 235.
- [9] J.H.C. Smith and A. Benitez, in: *Moderne Methoden der Pflanzenanalyse*, eds. K. Paech and M.V. Tracey (Springer, Berlin, 1955) pp. 151-154.
- [10] T.M. Cotton, Thesis, Northwestern University, Evanston, Illinois (1976).
- [11] S.J. van der Bent, P.A. de Jager and T.J. Schaafsma, *Rev. Sci. Instr.* 47 (1976) 117.

- [12] R.H. Clarke and R.H. Hofeldt, *J. Chem. Phys.* 61 (1974) 4582.
- [13] T.M. Cotton, P.A. Loach, J.J. Katz and K. Ballschmiter, *Photochem. Photobiol.* 27 (1978) 735.
- [14] S.G. Boxer and G.L. Closs, *J. Am. Chem. Soc.* 98 (1976) 5406.
- [15] G.L. Closs, J.J. Katz, F.C. Pennington, M.R. Thomas and H.H. Strain, *J. Am. Chem. Soc.* 85 (1963) 3809.
- [16] J.J. Katz, R.C. Dougherty and L.J. Boucher, in: *The chlorophylls*, eds. L.P. Vernon and G.R. Seely (Academic Press, New York, 1966) ch. 7.
- [17] Th. Förster, *Angew. Chem.* 81 (1969) 364.
- [18] H. Sternlicht and H.M. McConnell, *J. Chem. Phys.* 35 (1961) 1793.
- [19] R.P.H. Kooyman and T.J. Schaafsma, *J. Mol. Struct.*, to be published.
- [20] M.R. Wasielewski, M.H. Studier and J.J. Katz, *Proc. Natl. Acad. Sci. US* 73 (1976) 4282.

4 Spectroscopic properties of chlorophyll *a* complexes

4.1 FLUORESCENCE SPECTRA AND ZERO-FIELD MAGNETIC RESONANCE OF CHLOROPHYLL α -WATER COMPLEXES

R. P. H. KOOYMAN, TJEERD J. SCHAAFSMA and JOOP F. KLEIBEUKER

Agricultural University, Department of Molecular Physics, De Dreijen 6, Wageningen, The Netherlands

(Received 3 February 1977; accepted 5 May 1977)

Abstract—Fluorescence detected magnetic resonance (FDMR) and fluorimetry have been used to study chlorophyll-water complexes at $T = 4.2$ K. By combining these methods, zero-field splitting (ZFS)-parameters can be assigned to the triplet state of the various species. It is found that these parameters decrease upon aggregation and/or complexation. These results can be rationalized by using a simple free-electron model for chlorophyll including excitonic interaction. Evidence is presented favouring a structure recently proposed by Shipman and Katz for a chlorophyll-dimer involving hydrogen-bonded water, present in non-polar solutions at low temperature with spectral properties similar to those of chlorophyll *in vivo*.

INTRODUCTION

Monitoring fluorescence emission has been widely used as a means to follow photosynthetic processes in bacteria and green plants (Olson *et al.*, 1966; Papa-georgiou, 1975). Since an understanding of the fluorescence properties of chlorophyll α (Chl α) *in vitro* is essential for a reliable assignment of the various emission bands of *in vivo* systems, its *in vitro* spectral properties have been extensively studied, especially at low temperatures (Cotton, 1976; Amster, 1969; Broyde *et al.*, 1967; Fernandez *et al.*, 1959; Vacek, 1976).

Different fluorescence bands of Chl α *in vitro* have been ascribed to various ligated and/or aggregated forms, i.e. dimers, polymers, or solute-solvent complexes (Amster, 1969; Broyde *et al.*, 1967; Fernandez *et al.*, 1959; Balny *et al.*, 1969).

Since low-temperature emission spectra of Chl α usually contain overlapping bands due to perturbation of electronic transitions by environmental electric fields, the identification of the various species is rather difficult and published assignments are often contradictory (Amster, 1969; Fong *et al.*, 1976; Broyde *et al.*, 1967). An additional complication arises from the strong temperature dependence of emission and absorption spectra (Cotton, 1976; Balny *et al.*, 1969).

Using NMR and IR methods, which are inherently not very sensitive to the effects of the environmental electric fields on the overall electronic distributions because these methods focus on local interactions, Katz has found evidence for the important role of the central magnesium-atom and the carbonyl-oxygens for the aggregation- and complexing behaviour of the chlorophylls (Katz *et al.*, 1973). Because zero-field splitting (ZFS) parameters of the triplet state are sensitive to local interactions due to their dependence on the average distance between triplet spins along the molecular axes, we have studied these parameters (denoted by D and E) of Chl α in a non-

polar solvent containing a small amount of ligand, by fluorescence-detected magnetic resonance in zero-field (FDMR). The principles of this method, suggested some time ago by Harris (Harris *et al.*, 1972), first applied to porphyrin free base (Van Dorp *et al.*, 1973), and also to chlorophylls (Clarke *et al.*, 1974a; 1974b) can be outlined as follows:

Referring to Fig. 1, zero-field spin levels $|\tau_x\rangle$, $|\tau_y\rangle$ and $|\tau_z\rangle$ have energies corresponding to the eigenvalues X , Y and Z of the zero-field spin-Hamiltonian

$$\mathcal{H} = -(XS_x^2 + YS_y^2 + ZS_z^2) \quad (1)$$

where S_x , S_y and S_z are spin-operators, such that the eigenvalue of $S^2 = S_x^2 + S_y^2 + S_z^2$ equals $S(S+1) = 2$ in units \hbar^2 , for each of the zero-field levels, and $S_i|\tau_i\rangle = 0$ ($i = x, y, z$) (Weissbluth, 1965). Transitions between spin-levels can occur when microwaves with frequency ν satisfy the resonance condition $\Delta E = \nu/c$ (in cm^{-1}), where $\Delta E = |X-Y|$, $|X-Z|$, or $|Y-Z|$, and c is the velocity of light in cm s^{-1} (See Fig. 1). Absorption of microwave radiation is detected through its effect on the total number of molecules returning from all three triplet spin levels to the ground state. The resulting small change in ground state population can be detected by an accompanying change in fluorescence intensity. For further details, we refer to previous and more detailed papers on this subject (Van Dorp *et al.*, 1973; Clarke *et al.*, 1974a,b; Van der Bent *et al.*, 1975). Noting that

$$X + Y + Z = 0 \quad (2)$$

due to the purely dipolar nature of the spin-Hamiltonian (1), ZFS parameters are usually defined as

$$D \equiv \frac{1}{2}(X + Y) - Z = -\frac{3}{2}Z \quad (3a)$$

$$E \equiv \frac{1}{2}(X - Y) \quad (3b)$$

in accordance with Fig. 1.

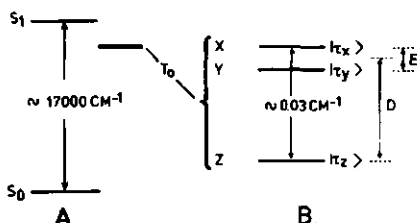


Figure 1. Energy level diagram of Chl *a* (A). The triplet state spinlevels have been magnified in the right hand side of this Figure (B). Symbols are defined in text. S_0 , S_1 define the singlet ground and first excited state, respectively; T_0 defines the lowest excited triplet state.

Then, transitions can occur at $\nu = 2E/c$, $(D - E)/c$ and $(D + E)/c$, if D and E are expressed in cm^{-1} . For porphyrin-like molecules in their lowest triplet state, $D = 0.025\text{--}0.045 \text{ cm}^{-1}$ and $E = 0\text{--}0.01 \text{ cm}^{-1}$, and ν is in the range 100–1500 MHz. The advantage of this method is that it allows simultaneous measurements of two parameters, both of which can provide information on the nature of the detected species. In this study, these parameters are the position and relative intensity of the fluorescence band maximum on one hand, and the triplet ZFS-parameters D and E on the other hand of one and the same species. In this way, one is able to obtain a more reliable assignment of fluorescence bands to various species, making use of their ZFS parameters.

MATERIALS AND METHODS

Chlorophyll *a* was purchased from Sigma and was sufficiently free from contaminants such as Chl *b* as shown by thin-layer chromatography and absorption spectra. *n*-Octane (Baker), purified by chromatography (Murray, 1969), was used as solvent. Preparations of the samples were done in the following way: a concentrated stock solution of Chl *a* in *n*-octane was made ($\sim 1 \text{ mM}$). Aliquots of this solution were diluted to the desired concentration, which was determined spectrophotometrically.

Preparation conditions were not strictly anhydrous, the amount of water in the sample was $< 1 \text{ mM}$ (i.e. the maximum solubility of water in *n*-octane). About 0.5 ml of sample was mounted onto a quartz rod and was quickly cooled down, first to 77 K, and then to 4.2 K. The FDMR-spectrometer is essentially the same as previously described (Van der Bent *et al.*, 1976). Surface-excited fluorescence using properly filtered blue light ($\lambda = 400\text{--}460 \text{ nm}$) from a super high pressure 900 W Xe arc for excitation was detected by a 0.25 m Spex monochromator and a RCA C 31034 photomultiplier which was cooled to -35°C . Fluorescence spectra were not corrected for photomultiplier sensitivity: the RCA 31034 has a rather flat spectral response in the interval 500–800 nm. By monitoring the various fluorescence bands, ZFS-parameters were determined. In a typical experiment, $\sim 2^{12}$ spectra were accumulated ($\sim 0.5 \text{ h}$); microwave power was $\sim 50 \text{ mW}$, and microwave-induced changes in fluorescence intensity varied between 0.01 and 0.001% for various fluorescence bands. All measurements were carried out at 4.2 K. As shown by a control absorption spectrum, no degradation of samples occurred during the experiments.

RESULTS

Figures 2 a–d represent the concentration dependence of Chl *a* fluorescence at $T = 4.2 \text{ K}$. At a Chl

a concentration $C_0 = 1 \mu\text{M}$, an intense band occurs at 669 nm, with a shoulder at 687 nm. At $C_0 = 10 \mu\text{M}$, the 687 nm band has disappeared; new bands occur at 725 nm and 675 nm. At $C_0 = 100 \mu\text{M}$, these effects become more dominant, whereas the 669 nm band has a relatively lower intensity. In the most concentrated solution ($C_0 = 1 \text{ mM}$), only two dominant bands at about 750 nm and 675 nm are present, while the 725 nm band has almost completely disappeared.

The shape of the fluorescence spectra, shown in Figs. 2 a–d, is a function of the cooling procedure to some extent and the amount of water present in the stock solution. Typically, the largest variation in the intensity ratio of any pair of bands in a series of experiments amounted to less than 20%. Apart from these variations in fluorescence spectra obtained in different series of experiments, the general trends as discussed in the next section are quite reproducible.

Figure 3 shows the effect of adding pyridine (5 mM) to a $10 \mu\text{M}$ solution of Chl *a* in *n*-octane. In the pyridine-sample, only one relatively sharp band at 686 nm appears, almost coinciding with the 687 nm band observed for a sample without pyridine. The spectrum agrees with results reported earlier (Cotton, 1976). A control experiment with pheophytin *a*, in

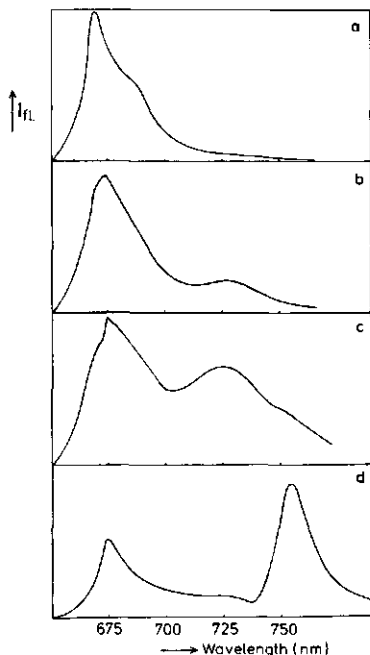


Figure 2. Concentration dependence of Chl *a* fluorescence spectrum in *n*-octane. $T = 4.2 \text{ K}$; fluorescence intensity is given in arbitrary units and vertical scale is different for curves a–d; Chl concentrations: a, $1 \mu\text{M}$; b, $10 \mu\text{M}$; c, $100 \mu\text{M}$; d, 1 mM .

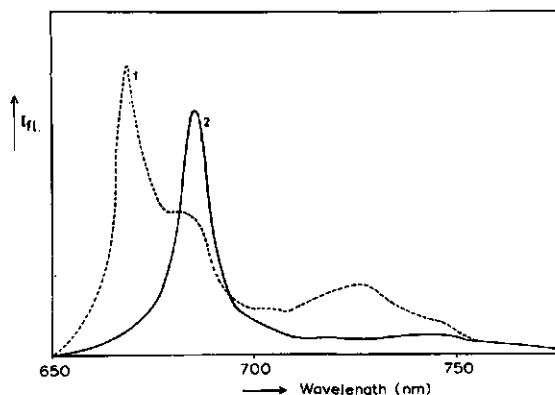


Figure 3. Effect of pyridine on the fluorescence of Chl *a* ($T = 4.2$ K). 1 $\sim 20 \mu\text{M}$ Chl *a* in *n*-octane. 2 $\sim 20 \mu\text{M}$ Chl *a* + 5 mM pyridine in *n*-octane.

which the central magnesium-atom is missing, did not show this effect.

Curves *a-d* in Fig. 4 depict surface-excited Soret-band fluorescence excitation spectra of a 0.5 mM Chl *a*/*n*-octane solution at 4.2 K, obtained by monitoring the emission at 669, 687, 725 and 746 nm, respectively, using detection- and excitation widths of 5 and 10 nm, respectively. Detecting at 669 nm yields a partially resolved excitation profile in the Soret region with maxima at ~ 410 and 430 nm (see Fig. 4, curve *a*), corresponding to the Chl *a* absorption spectrum in

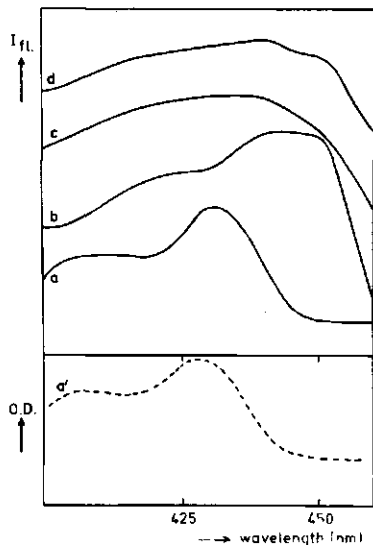


Figure 4. Soret band fluorescence-excitation spectra of ~ 0.1 mM Chl *a* in *n*-octane ($T = 4.2$ K). (a) $\lambda_{em} = 669$ nm; (b) $\lambda_{em} = 685$ nm; (c) $\lambda_{em} = 726$ nm; (d) $\lambda_{em} = 746$ nm. Excitation slitwidth: 10 nm. Detection slitwidth: 5 nm. (a') Room temperature absorption spectrum of $10 \mu\text{M}$ Chl *a* in diethylether.

a polar solvent at room temperature (Fig. 4, curve *a'*). Red-shifting the detection wavelength to ~ 687 nm results in a broadening and a red-shift of the two main Soret transitions to ~ 420 and ~ 445 nm (Fig. 4, curve *b*). This has also been found in low temperature absorption spectra of Chl *a* in polar glasses (Kleibeker, unpublished results). Using detection at still longer wavelength leads to further broadening of the Soret region, obscuring any shifts. The excitation-difference spectrum, obtained by subtraction of excitation spectra recorded at fluorescence detection wavelengths of 726 and 746 nm, exhibits a maximum around 700 nm.

From FDMR spectra obtained by detecting at 669, 687, 725, and 750 nm, ZFS-parameters were determined, as collected in Table 1. For low Chl *a* concentrations, using 675 nm detection, ZFS-parameters could not be determined with sufficient accuracy, probably due to the vicinity of intense FDMR transitions associated with the strong 669 nm fluorescence bands. As the ZFS-parameters are all different for the various fluorescence bands, we may conclude that there are at least four different species present in the samples, and that the observed concentration-effects on fluorescence spectra are not due to a change of the relative intensity of vibrational bands of a single species. With regard to ZFS-parameters, it is found that *D*-values continuously decrease when the fluorescence-wavelengths increase; the *D*-value corresponding to the 669 nm species is distinctly larger than those, reported previously (Clarke *et al.*, 1974b; Kleibeker *et al.*, 1974; Levanon *et al.*, 1975; Norris *et al.*, 1975) and agrees with the *D*-value recently reported for Chl *a* in polymethylmethacrylate (Hägele *et al.*, 1976). ZFS-parameters obtained in the sample containing pyridine are in accordance with previous reports using high field EPR techniques (Norris *et al.*, 1975; Kleibeker *et al.*, 1976). All FDMR signals, except the 669 nm signal, correspond to an increase in fluorescence intensity.

Table 1. ZFS-parameters as a function of fluorescence detection wavelength. T = 4.2 K

Solvent	Species assigned as	$\lambda_0(\text{nm})^\dagger$	$C_0(M)$	$D(\times 10^4 \text{ cm}^{-1})^*$	$E(\times 10^4 \text{ cm}^{-1})^*$	Method
n-octane	Chl·H ₂ O	669	10^{-6}	309 ± 4	42 ± 4	FDMR
n-octane	Chl·2H ₂ O	687	10^{-5}	291 ± 5	38 ± 4	FDMR
n-octane	(Chl·H ₂ O) ₂	725	10^{-4}	286 ± 5	31 ± 5	FDMR
n-octane	(Chl·H ₂ O) _n §	750	10^{-3}	275 ± 5	38 ± 6	FDMR
n-octane + excess pyridine	Chl·2 Pyr.	686	10^{-5}	283 ± 5	40 ± 5	FDMR
Toluene + pyridine	Chl·2 Pyr.		10^{-4}	$280 \pm 3^\ddagger$	$40 \pm 3^\ddagger$	EPR

*The errors quoted in Table 1 do not reflect that the relative ordering of ZFS values from top to bottom as presented in this Table was invariably found for one experimental run. For different runs, using different samples, systematic variations were found in these parameters, not affecting the relative ordering. This error is included however in the figures quoted in Table 1, resulting in a conservative estimate of total error.

λ_0 is detection wavelength of fluorescence band maximum.

‡ Kleibecker *et al.* (1976).

§ Tentative assignment.

DISCUSSION

The experiments on Chl *a* and pheophytin *a* in n-octane/pyridine indicate that ligand-interaction of pyridine and Chl *a* primarily occurs with the central magnesium-atom. It has been previously shown that adding excess pyridine to a solution of Chl *a* in a non-polar solvent gives rise to one dominant species in the solution, the biligated Chl *a* monomer, in which two pyridine molecules are coordinated to the central magnesium atom (Evans *et al.*, 1975). Therefore, we conclude from our pyridine-experiment that the 686 nm fluorescence band arises from the biligated Chl *a* monomer; extrapolating this assignment to the fluorescence spectrum shown in Fig. 2a, we ascribe the 687 nm shoulder to Chl *a*, biligated with water. This assignment can be used as a starting point for the analysis of the remaining fluorescence bands, correlating the observed ZFS-parameters to particular ligated or aggregated forms of Chl *a* involving water.

Identifying the 687 nm fluorescence band with Chl *a*·2H₂O, the ZFS-parameters of this species are found to be $D = (0.0291 \pm 0.0005) \text{ cm}^{-1}$, $E = (0.0038 \pm 0.0005) \text{ cm}^{-1}$ (Table 1). These values agree with those obtained from high-field EPR experiments on Chl *a* in polar glasses (Kleibecker *et al.*, 1974). Interestingly, this correspondence suggests that published ZFS data on the triplet state of Chl *a* in polar solvents in fact are those of the complex of the pigment with two solvent molecules.

The Mg²⁺-ion in porphyrin-like compounds in solution, such as chlorophyll, is known to have a coordination number of 5 or 6, implying that at least one extra ligand is bound to Mg²⁺, which is already bound to the four porphyrin-nitrogens (Katz *et al.*, 1973). Thus, the main fluorescence band of very dilute Chl-solutions (such that aggregation is suppressed) at room temperature in the absence of an excess of polar ligands should be characteristic for monoligated Chl-monomers.

Turning to Fig. 4, we note that the Soret absorption band of Chl *a* in ether almost coincides with the 4.2 K excitation spectrum, monitoring the 669 nm emission, indicating that the species giving rise to this low temperature emission corresponds to the dominant complex in dilute solutions at room temperature.

Furthermore, monoligated monomeric Chl *a* is expected to have a zero or very small Stokes' shift, since its environment largely consists of frozen non-polar solvent molecules, providing almost no opportunity for Stokes' losses through reorientation of the polar solvent molecules, close to Chl *a*. Indeed, it is observed that the low temperature 669 nm fluorescence maximum almost coincides with the room-temperature absorption-maximum of 663 nm which previously has been assigned to monomeric monoligated Chl *a* (Livingston *et al.*, 1949). Based on these spectral data, and in accordance with previous assignments, we conclude that the 669 nm fluorescence originates from the Chl *a*·H₂O complex; its ZFS-parameters are given by $D = (0.0309 \pm 0.0004) \text{ cm}^{-1}$, $E = (0.0042 \pm 0.0004) \text{ cm}^{-1}$ (see Table 1).

Since conventional high-field EPR does not distinguish between various ligated Chl triplet species with different ZFS parameters, the occurrence of differently ligated complexes in non-polar solvents which have not been carefully freed from polar impurities (such as small amounts of water) can result in broadening of $\Delta m = 1$ and $\Delta m = 2$ transitions. A triplet ESR spectrum of a solid solution containing, for example, a 1:1 ratio of mono- and biligated forms of triplet Chl would exhibit a typical increase in line-width of $(309-291) \times 10^{-4} = 18 \times 10^{-4} \text{ cm}^{-1}$, corresponding to $\sim 20 \text{ G}$, as compared with the case where only one species is present. Such a broadening corresponds to at least a doubling of the linewidth and a decrease of signal-to-noise ratio of at least a factor of 4. This can possibly explain why we could

not observe $\Delta m = 1$ high-field ESR signals of the triplet state of these Chl-water complexes.

Before we turn now to a discussion of the assignment of the other fluorescence bands and their corresponding ZFS-parameters, it is necessary to find a model relating the fluorescence redshift to a change in ZFS-parameters. For this purpose, we note that attaching an electron-donating ligand to Mg in Chl *a* is equivalent to the replacement of Mg by a less electronegative metal. For porphyrins, it has been shown that this results in a lowering of the energy of the first excited singlet state $E(S_1)$, if the effect of configuration interaction (CI) between the two lowest unoccupied and two highest occupied MO's is taken into account (Gouterman, 1959, 1961). Analogously, the observed fluorescence red shift of Chl *a* upon Mg^{2+} ligation can be understood by increased CI.

The magnitude of the ZFS parameter D is determined by the average dipole-dipole interaction between both triplet spins in the lowest triplet state T_0 and depends on the value of $\langle r_{12}^{-3} \rangle$, where r_{12} measures the distance between the spins. For a reliable calculation of D , one should also include CI; only a limited number of calculations of this type has been reported (van Dorp *et al.*, 1974; Langhoff *et al.*, 1975) and does not allow unambiguous predictions for the effect of Mg^{2+} ligation on the magnitude of D .

Qualitatively, however, one can also understand the observed fluorescence red-shift and the decrease of D on the basis of the free electron model for cyclic polyenes (Platt, 1956) by realising that Mg^{2+} ligation in chlorophyll effectively causes a net electron displacement towards the molecular periphery thus reducing $\langle r_{12}^{-3} \rangle$ and lowering $E(S_1)$ at the same time.

The free electron model can only be applied as long as lateral solvent-solute interactions are weak (e.g. hydrogen-bonding); it is invalid for side-chain substitution involving a strong anisotropic perturbation of the π -electron distribution.

So far, we have only considered solute-solvent interactions in constructing the model outlined before. According to Fig. 2 for non-dilute solutions of Chl *a* in non-polar solvents the intensity of fluorescence bands attributed to monomers has decreased, whereas new emissions appear at ~ 725 and ~ 750 nm. These bands have been ascribed to the $(Chl \cdot H_2O)_2$ and $(Chl \cdot H_2O)_n$ species (Cotton, 1976; Fong *et al.*, 1976). These authors have shown that the 725 nm emission corresponds to a 700 nm absorption maximum. Our results indicate a similar correspondence between the 725 nm fluorescence and a maximum at ~ 700 nm in the excitation difference spectrum, recorded at 725 and 746 nm. Thus, we feel confident to assign the 725 nm fluorescence to $(Chl \cdot H_2O)_2$ —the so-called "special pair"—, in which the redshift relative to the monomer partly arises due to excitonic coupling (Shipman, 1976). If excitonic coupling is the main mechanism responsible for a further redshift relative to the monomer, and if charge-transfer interaction

does not strongly contribute to this red shift, then the proposed geometry of this $(Chl \cdot H_2O)_2$ complex (Shipman *et al.*, 1976a; Fong, 1975) can be verified on the basis of experimental ZFS-parameters. Both the Fong model (Fong, 1975) and the Katz-Shipman model (Shipman *et al.*, 1976a) have parallel structures; in the Fong model, hydrogen bonding occurs at the ester carbonyl group, in the Katz-Shipman model the keto carbonyl is involved in hydrogen bonding. An exciton description (strong coupling limit) of both models predicts that D that does not change with respect to the D -value of the monoligated monomer (Clarke *et al.*, 1976). Experimentally, we find $D = (0.0286 \pm 0.0005) \text{ cm}^{-1}$, $E = (0.0031 \pm 0.0005) \text{ cm}^{-1}$ i.e. $ZFS(\text{dimer}) < ZFS(\text{monomer})$ (see Table 1). Taking into consideration recent results of ab-initio calculations on ethyl-chlorophyllide *a*, in which it was shown that the ring V keto group participates in the π -electron macrocycle (Spangler *et al.*, 1975), then the reduction of ZFS(dimer) relative to ZFS(monoligated monomer) can be understood in our free-electron model if hydrogen bonding occurs at the ring V keto group. Additional evidence for this conclusion arises from results previously reported for ZFS-parameters in Chl *a*/ethanol (Kleibekker *et al.*, 1976). Therefore, in view of these observations, the Katz-Shipman structure seems more probable. Furthermore, it is interesting that the exciton description predicts for Fong's model $E \sim 0$, whereas for the Katz-Shipman structure one expects $E \sim E(\text{monomer})$, when it is assumed that the principal magnetic inplane axes of porphyrine-like compounds are located near the $N-N$ -axes (Van Dorp *et al.*, 1974). Experimentally, we find $E(\text{dimer}) \neq 0$ and not much different from $E(\text{monomer})$. This may be considered as additional evidence for the Katz-Shipman structure.

The origin of the 750 nm band (see Fig. 1d) is obscure. Presumably it is a $(Chl \cdot H_2O)_n$ complex, as suggested by the concentration dependence of its emission. Our results do not allow conclusions with respect to the geometry of this species.

CONCLUSIONS

As demonstrated by our results, simultaneous measurement of ZFS- and fluorescence parameters is useful for the study of the structure of Chl-water-complexes. In this way, fluorescence bands and ZFS-parameters have been assigned to mono- and biligated Chl monomer, whereas our triplet state data of a species previously described as a Chl dimer ("special pair") are in favour of the Katz-Shipman model. However, static ZFS-parameters alone do not yield all information needed for an unambiguous structure assignment of all species, observed in low-temperature, non-polar solutions. For example, only qualitative conclusions with respect to the structure of the so-called 725 and 750 nm species can be drawn from our measurements due to the lack of detailed knowledge about the effect of aggregation on fluorescence

and ZFS-parameters. Of course, kinetic triplet-state parameters could provide additional keys to a more definitive structural assignment as already suggested by Norris (Norris *et al.*, 1975) and illustrated by Clarke (Clarke *et al.*, 1976).

Acknowledgements—This investigation was supported by the Netherlands Foundation for Chemical Research (S.O.N.) with financial aid from the Netherlands Organization for the Advancement of Pure Research (Z.W.O.).

REFERENCES

- Amster, R. L. (1969) *Photochem. Photobiol.* **9**, 331–338.
- Balny, C., S. S. Brody and G. H. Bon Hoa (1969) *Photochem. Photobiol.* **9**, 445–454.
- Brody, S. B. and S. S. Brody (1967) *J. Chem. Phys.* **46**, 3334–3340.
- Clarke, R. H. and R. H. Hofeldt (1974a) *J. Am. Chem. Soc.* **96**, 3005.
- Clarke, R. H. and R. H. Hofeldt (1974b) *J. Chem. Phys.* **61**, 4582–4587.
- Clarke, R. H., R. E. Connors and H. A. Frank (1976) *Biochem. Biophys. Res. Commun.* **71**, 671–675.
- Cotton, T. M. (1976) Thesis, Northwestern Univ., Evanston, IL.
- Evans, T. A. and J. J. Katz (1975) *Biochim. Biophys. Acta* **396**, 414–426.
- Fernandez, J. and R. S. Becker (1959) *J. Chem. Phys.* **31**, 467–472.
- Fong, F. K. (1975) *Appl. Phys.* **6**, 151–166.
- Fong, F. K. and V. Koester (1976) *Biochim. Biophys. Acta* **423**, 52–64.
- Goedheer, J. C. (1966) In *The Chlorophylls*, Chapter 6 (Edited by L. P. Vernon and G. R. Seely) Academic Press, New York.
- Gouterman, M. (1959) *J. Chem. Phys.* **30**, 1139–1161.
- Gouterman, M. (1961) *J. Mol. Spectrosc.* **6**, 138–163.
- Hägele, W., F. Driessler, D. Schmid and H. C. Wolf (1976) In *The Proceedings of the International Seminar on Energy Transfer in Condensed Matter*, Prague, to be published.
- Harris, C. B. and R. J. Hoover (1972) *J. Chem. Phys.* **56**, 2199–2206.
- Katz, J. J. and J. R. Norris (1973) In *Current Topics in Bioenergetics* (Edited by D. R. Sanadi and L. Packer), Vol. 5, pp. 41–75. Academic Press, New York.
- Kleibeuker, J. F. and T. J. Schaafsma (1974) *Chem. Phys. Lett.* **29**, 116–122.
- Kleibeuker, J. F., S. J. van der Bent and T. J. Schaafsma (1976) In *The Proceedings of the International Seminar on Energy Transfer in Condensed Matter*, Prague, to be published.
- Langhoff, S. R., E. R. Davidson, M. Gouterman, W. R. Leenstra and A. L. Kwiram (1975) *J. Chem. Phys.* **62**, 169–176.
- Levanon, H. and A. Scherz (1975) *Chem. Phys. Lett.* **31**, 119–124.
- Livingstone, R., W. F. Watson and J. McArdle (1949) *J. Am. Chem. Soc.* **96**, 1942–1955.
- Murry, E. C. and R. N. Keller (1969) *J. Org. Chem.* **34**, 2234–2235.
- Norris, J. R., R. A. Uphaus and J. J. Katz (1975) *Chem. Phys. Lett.* **31**, 157–161.
- Olson, J. M. and E. K. Stanton (1966) In *The Chlorophylls* (Edited by L. P. Vernon and G. P. Seely), Chapter 12. Academic Press, New York.
- Papageorgiou, G. (1975) In *Bioenergetics of Photosynthesis* (Edited by Govindjee), Chapter 6. Academic Press, New York.
- Platt, J. F. (1956) In *Radiation Biology* (Edited by A. Hollaender), Vol. III, Chapter 2. McGraw-Hill, New York.
- Shipman, L. L., T. M. Cotton, J. R. Norris and J. J. Katz (1976a) *Proc. Natl. Acad. Sci. U.S.A.* **73**, 1791–1794.
- Shipman, L. L., J. R. Norris and J. J. Katz (1976b) *J. Phys. Chem.* **80**, 877–882.
- Spangler, D., R. McKinney, R. E. Christoffersen, G. M. Maggiora and L. L. Shipman (1975) *Chem. Phys. Lett.* **36**, 427–431.
- Vacek, K. (1976) In *The Proceedings of the International Seminar on Energy Transfer in Condensed Matter*, Prague, to be published.
- Van der Bent, S. J. and T. J. Schaafsma (1975) *Chem. Phys. Lett.* **35**, 45–50.
- Van der Bent, S. J., P. A. de Jager and T. J. Schaafsma (1976) *Rev. Sci. Instrum.* **47**, 117–121.
- Van Dorp, W. G., T. J. Schaafsma, M. Soma and J. H. van der Waals (1973) *Chem. Phys. Lett.* **21**, 221–225.
- Van Dorp, W. G., M. Soma, J. A. Kooter and J. H. van der Waals (1974) *Mol. Phys.* **28**, 1551–1568.
- Weissbluth, M. (1965) In *Molecular Biophysics* (Edited by B. Pullman and M. Weissbluth), pp. 205–239. Academic Press, New York.

4.2 CHLOROPHYLL A - ETHANOL COMPLEXES [†]

In fig. 5 the fluorescence spectrum of dried Chl a in n-octane with varying amounts of added ethanol is depicted. The spectrum consists of three bands located at 670, 680 and 720 nm, respectively; the 680 and 720 nm band intensities increase upon addition of ethanol. At each of the three fluorescence bands ODMR experiments were carried out. For the 670 and 720 nm bands ODMR spectra agreed with those mentioned in Section 4.1; monitoring the 680 nm band no ODMR signals could be detected.

Cotton [1] has described a dimer fluorescing at ~ 720 nm which is formed by Chl a - ethanol interactions (the "special pair"). Also in Section 4.1 it was concluded that the species fluorescing at ~ 725 nm corresponds to the "special pair". In view of the similar excited state properties of the present 720 nm band

[†] These experiments were carried out by G.H. van Brakel and R. Avarmaa.

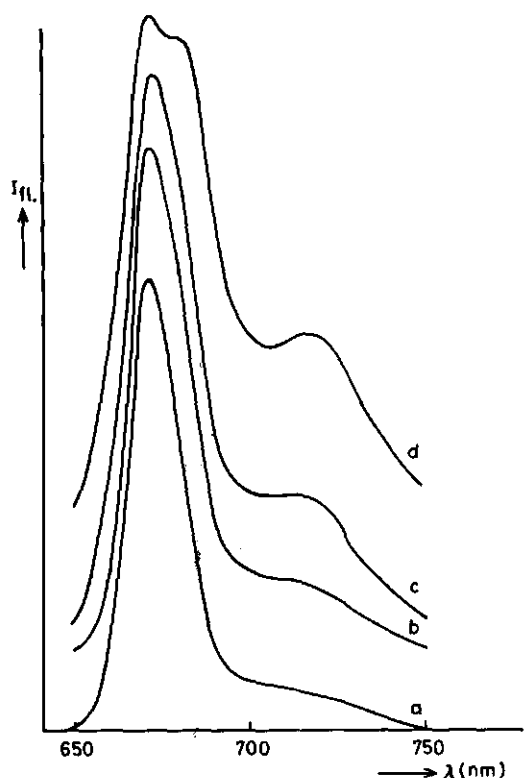


Fig. 5. Fluorescence spectrum of 10^{-5} M Chl a in n-octane. $T = 4.2$ K.
(a) no ethanol
(b) 2×10^{-5} M ethanol
(c) 10^{-4} M ethanol
(d) 5×10^{-4} M ethanol

and the 725 nm band in Section 4.1, we ascribe the 720 nm band to the "special pair" ($\text{Chl } \underline{a.L}_2$). Further, in view of the results mentioned in Section 4.1, the 670 nm band corresponds to $\text{Chl } \underline{a.L}$. Thus, only the 680 nm band remains to be assigned.

It has been shown in Section 4.1 that biligated $\text{Chl } \underline{a.L}_2$ has its fluorescence maximum at 687 nm, irrespective whether water or pyridine is ligated to the Mg-atom. Biligation occurs only if a large excess of an electron-donating molecule is added or if a strong electron-donating compound such as pyridine is added (see Chapter 2). Pyridine and ethanol differ in two respects: first, pyridine is a stronger electron-donating compound than is ethanol, second, ethanol (as a bi-functional ligand) is able to act as an electron-acceptor as well, whereas pyridine is not. From the last property ethanol derives the possibility to form hydrogen bonds with a Chl keto group. Thus, ethanol will not easily form biligated $\text{Chl } \underline{a}$, but it may form monoligated $\text{Chl } \underline{a}$ with an additional ethanol molecule solvated to the ring V keto group. Since hydrogen bonding at the ring V keto group is known to result in a Q_y redshift [2-4], the fluorescence maxima agree with this assignment: monoligated $\text{Chl } \underline{a}$ has its fluorescence maximum at 670 nm and the monoligated $\text{Chl } \underline{a}$ hydrogen bonded at the ring V keto group at 680 nm.

4.3 THE ($\text{CHLOROPHYLL } \underline{A}$)₂ DIMER

It is known (see Chapter 2) that $\text{Chl } \underline{a}$, when dissolved in nonpolar solvents forms dimers and higher aggregates; in toluene $\text{Chl } \underline{a}$ mainly forms dimers ($\text{Chl } \underline{a}$)₂ which are non-fluorescent [1]. ($\text{Chl } \underline{a}$)₂ has an absorption maximum at 678 nm. In order to further characterize this dimer, we have determined the ZFS values of ($\text{Chl } \underline{a}$)₂. Knowledge of singlet and triplet state properties gives the possibility to consider the electronic and geometrical structure of this dimer (see Chapter 7).

$\text{Chl } \underline{a}$, dried by the CCl_4 codestillation method described by Cotton [1] was dissolved in p.a. toluene which was dried over 4 Å molecular sieves (Union Carbide). The solution ($\sim 10^{-3}$ M) was transferred *in vacuo* to a 3 mm quartz tube and after degassing sealed at $\sim 10^{-5}$ torr (77 K).

Because of the absence of dimer fluorescence, ODMR is not well suited to determine ZFS values of ($\text{Chl } \underline{a}$)₂; therefore, we have carried out conventional high field ESR experiments at $T \sim 5$ K.

The sample was optically excited either by a 150 W Xe-lamp or by a dye-laser in the region 650 - 680 nm. Both methods yielded similar results. ESR spectra were recorded using continuous or modulated optical excitation. The detection of signals obtained by phase-sensitive detection on the modulated optical excitation generally

results in a better signal-to-noise ratio. This method, however, has an important disadvantage: the information concerning the electron spin polarization $|4|$, which is a measure of the relative population of the three triplet sublevels, is lost $|5|$. Therefore, we also performed experiments under continuous illumination.

The $\Delta m_S = 1$ ESR spectra exhibit two species, A and B; species A is characterized by $D = (270 \pm 4) \times 10^{-4} \text{ cm}^{-1}$, $E = (40 \pm 2) \times 10^{-4} \text{ cm}^{-1}$, whereas species B, which was weakly present in the ESR spectrum, has $D = (298 \pm 8) \times 10^{-4} \text{ cm}^{-1}$, $E = 40 \times 10^{-4} \text{ cm}^{-1}$. Both species exhibit different electron spin polarization patterns, implying that for species A the populations of $|\tau_x\rangle$ and $|\tau_z\rangle$ are large compared to that of $|\tau_y\rangle$, whereas for species B the population of $|\tau_x\rangle$ is large compared to $|\tau_y\rangle$ and $|\tau_z\rangle$.

D-values around $300 \times 10^{-4} \text{ cm}^{-1}$ have been reported earlier for Chl a $|6,7|$; it was concluded that monomeric Chl a, either singly ligated $|6|$ or non-ligated $|7|$ corresponds to this D-value. Furthermore, the electron spin polarization pattern found for species B is the same as that found for monomeric Chl a $|5|$. Based on these considerations, and in view of the weak signal intensity, we assign this signal to residual monomeric Chl a present in the Chl a / toluene sample. The species A signal must be ascribed to the presence of $(\text{Chl } \underline{a})_2$: signal A is relatively intense, and the spin polarization pattern, indicative for a relatively large population of $|\tau_x\rangle$ and $|\tau_z\rangle$ is clearly different from that of the monomer. In fact, the finding that in contrast to the monomer $|\tau_z\rangle$ of species A is now populated provides a hint on the structure of $(\text{Chl } \underline{a})_2$. It can be shown $|8|$ that for pure $\pi\pi^*$ states, where the π MO's can be described by p_z AO's (z-axis perpendicular to the molecular plane), there is virtually no spin-orbit coupling between the singlet states and $|\tau_z\rangle$, implying that this spin level is only weakly involved in radiationless processes which depopulate the excited singlet state. This situation applies roughly for monomeric Chl a. If we now consider a dimer consisting of two *non-parallel* macrocycles, then the excited states can no longer be described with p_z AO's (perpendicular to one molecular plane) only, but p_x and p_y AO's need to be included. This has the effect that $|\tau_z\rangle$ may become active in the inter-system crossing process.

In view of these results, we conclude that $(\text{Chl } \underline{a})_2$ has $D = 270 \times 10^{-4} \text{ cm}^{-1}$. Norris *et al.* $|9|$ who have carried out similar experiments on deuterated Chl a, report a significantly higher D-value ($D = 288 \times 10^{-4} \text{ cm}^{-1}$) which they ascribe to $(\text{Chl } \underline{a})_2$. However, data on the spin polarization pattern were lacking. The reason of this indiscrepancy is presently unclear. The D-value found by Norris *et al.* seems to point to a biligated monomeric Chl a species.

We will postpone the discussion on the geometry of $(\text{Chl } \underline{a})_2$ until Chapters 6 and

4.4 REFERENCES

1. T.M. Cotton, Thesis (1976), Northwestern Univ. Evanston, Ill.
2. A.A. Krasnovskii jr., N.N. Lebedev, F.F.Litvin, Dokl. Akad. Nauk SSSR, 216 (1974) 1406.
3. G.R. Seely, R.G. Jensen, Spectrochim. Acta, 21 (1965) 1835.
4. J.F. Kleibeuker, Thesis (1977), Agricultural University, Wageningen.
5. J.F. Kleibeuker, R.J. Platenkamp, T.J. Schaafsma, Chem. Phys. Lett., 41 (1976) 557.
6. R.P.H. Kooyman, T.J. Schaafsma, J.F. Kleibeuker, Photochem. Photobiol., 26 (1977) 235.
7. W. Hägele, D. Schmid, H.C. Wolf, Z. Naturforsch. A, 33 (1978) 94.
8. F. Metz, S. Friedrich, G. Hohlneicher, Chem. Phys. Lett., 16 (1972) 353.
9. J.R. Norris, R.A. Uphaus, J.J. Katz, Chem. Phys. Lett., 31 (1975) 157.

5 Fluorescence and ODMR of chlorophyll *b* complexes

5.1 INTRODUCTION

Chlorophyll *b* (Chl *b*) differs from Chl *a* by the presence of an aldehyde group at one of the pyrrole rings (see fig. 1a of Chapter 2). This group has electron donating properties analogous to the ring V keto group, i.e. in a hydrogen bonding solvent, such as ethanol or water, Chl *b* may be solvated by interaction between the solvent and the aldehyde group. Furthermore, analogous complexing properties as for Chl *a* hold, such as hydrogen bonding at the ring V keto group and, in the presence of electron donating molecules (e.g. pyridine), ligation at the central Mg atom (see Chapter 2). Thus, it can be suspected that Chl *b* complexing and aggregation properties are more complicated than those for Chl *a*: in particular, formation of Chl *b* dimers and higher aggregates may be much more complex than in Chl *a* because of the additional aggregation possibility via the aldehyde group. Katz *et al.* [1] have found evidence that the Chl *b* aggregation behaviour is different from that of Chl *a*, indicating that indeed the aldehyde group plays an important role in aggregation.

Chl *b* has received less attention than Chl *a* in studies of photosynthesis; this and the complicated aggregation behaviour might be two of the reasons why only a few optical studies have been published on Chl *b* solvation and aggregation properties [2-5]. Here we wish to investigate the effects of such solvation and aggregation on the optical (fluorescence) properties of Chl *b*. It will be demonstrated that measurement of the triplet zero field splitting (ZFS) parameters, selectively determined for the various fluorescence bands of Chl *b* by ODMR can assist in the assignment of these bands to different Chl *b* species.

We will discriminate between ligation at the Mg atom of some electron donating ligand L (Chl *b*.L), hydrogen bonding of a compound H at the ring V keto group (Chl *b*.H_k) and hydrogen bonding at the ring II aldehyde group (Chl *b*.H_a). We will also consider such complexes as Chl *b*.2L, Chl *b*.L.H_a and Chl *b*.L.H_a.H_k. Finally, we will make some speculations about the structure of Chl *b* dimers.

5.2 EXPERIMENTAL

Chl b was purchased from Sigma. Contaminants could not be detected in absorption spectra ($\lambda = 400 - 700$ nm), whereas thin layer chromatography revealed a weak spot due to the presence of Chl a. This impurity could not be detected in the fluorescence spectra; therefore, we decided not to further purify the Chl b samples. n-Octane was purified by column chromatography on alumina (Merck), and dried over 4 Å molecular sieves (Union Carbide). Chl b was dried by pumping a film during ~ 12 hours at 10^{-3} torr. Ethanol and pyridine (p.a.) were used without further purification.

The effect of drying on the room temperature absorption spectrum can be seen in fig. 1. The drying procedure causes a new absorption band to appear at ~ 665 nm, which, analogously to the situation in Chl a, can be ascribed to an aggregate of Chl b, presumably $(\text{Chl } \underline{b})_2$. Further, the Soret-band of dried samples is broadened with respect to that of undried samples. Although the drying procedure is sufficiently thorough to produce aggregates, we do not claim that the dried samples are completely free of electron donating molecules such as traces of water.

Concentration-dependent fluorescence spectra were obtained from samples that were prepared in the following way: a concentrated (10^{-3} M) stock-solution of Chl b in n-octane was prepared by adding 10^{-2} M ethanol to the Chl b/ n-octane mixture. Adding ethanol has the purpose of increasing the solubility of Chl b. From this stock-solution more dilute samples were prepared by adding appropriate

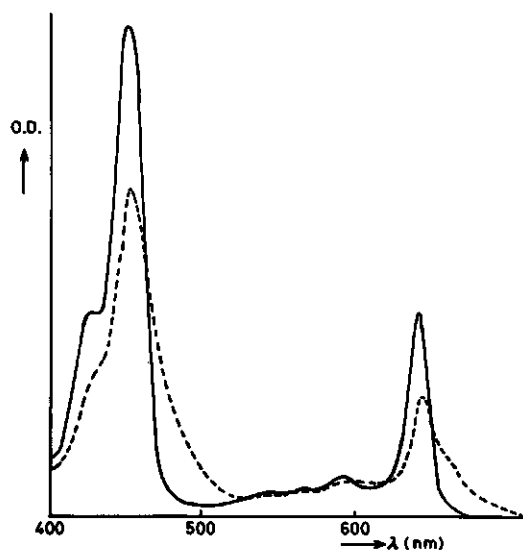


Fig. 1. Room temperature absorption spectrum of 10^{-5} M Chl b in n-octane.
— undried sample,
--- dried sample.

quantities of n-octane.

In the titration experiments, which were carried out with ethanol and pyridine, the stock-solution consisted of Chl b in neat n-octane. To this stock-solution appropriate amounts of pyridine or ethanol were added.

Fluorescence and ODMR spectra were determined using an experimental set-up which has been described previously [6].

5.3 RESULTS

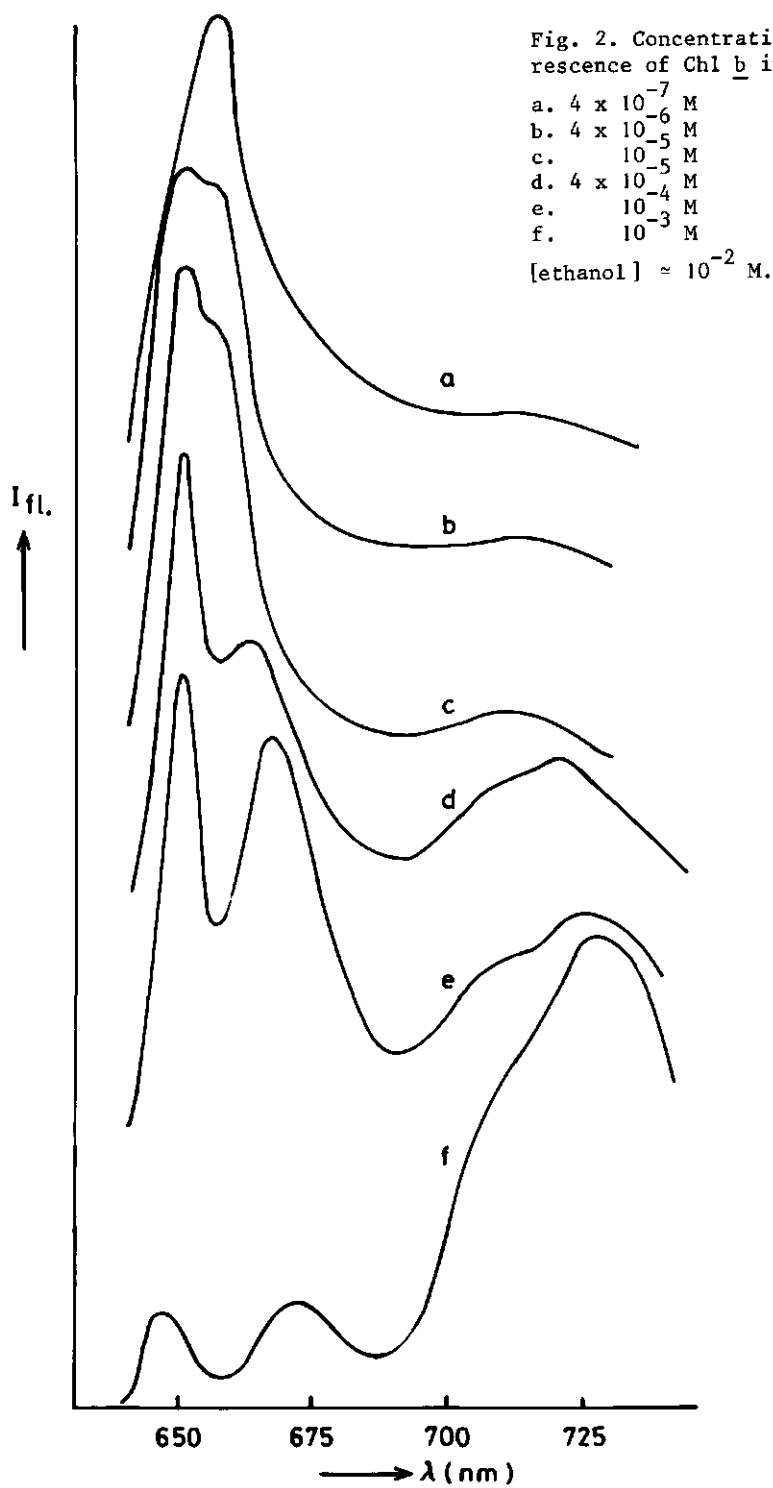
Figures 2 a-f represent the concentration dependence of the Chl b fluorescence spectrum at $T = 4.2$ K starting from a $\sim 10^{-3}$ M Chl b stock-solution in n-octane + 10^{-2} M ethanol. At a Chl b concentration $C_0 = 4 \times 10^{-7}$ M, the main band is centered at $\lambda = 656$ nm, with a shoulder at $\lambda = 648$ nm. By increasing the Chl b concentration, the 648 nm band becomes more apparent, whereas the relative intensity of the 656 nm band simultaneously decreases, and somewhat shifts to the red. (The band at ~ 664 nm at $C_0 = 4 \times 10^{-5}$ M may be the result of overlap of the red-shifted 656 nm band and the 669 nm band, both with comparable intensities). At $C_0 \approx 10^{-4}$ M a band at $\lambda \approx 669$ nm appears, whereas the 656 nm band has disappeared. Simultaneously, fluorescence at $\lambda > 700$ nm gains in intensity. By comparison of spectra a-f in the region $\lambda > 700$ nm two bands can be distinguished, with maxima at ~ 710 nm and ~ 725 nm. Going to still higher concentration, it is seen that the 648 nm band decreases relatively to the 669 nm band; furthermore, almost all fluorescence is now situated at $\lambda > 700$ nm.

For the various fluorescence bands, ZFS parameters have been determined by ODMR. All ODMR signals, except those detected at $\lambda > 700$ nm, correspond to a decrease in fluorescence intensity. The ODMR results are summarized in Table I.

Table I. ZFS parameters as a function of fluorescence detection wave length.
Solvent: n-octane + ethanol. $T = 4.2$ K

C_0 (M)	λ_{det} (nm)	D (10^{-4} cm^{-1})	E (10^{-4} cm^{-1})	sign [†]
10^{-6}	644	332 ± 2	33 ± 2	-
5×10^{-5}	648	319 ± 2	38 ± 2	-
5×10^{-6}	656	317 ± 2	27 ± 2	-
5×10^{-5}	669	297 ± 2	40 ± 2	-
5×10^{-4}	708	320 ± 3	37 ± 3	+
5×10^{-4}	725	277 ± 4	29 ± 4	+

[†] "-" corresponds to a decrease in fluorescence intensity, "+" to an increase.



At low concentration ($C_0 = 4 \times 10^{-7}$ M) ODMR experiments reveal a band at $\lambda = 644$ nm, which can be hardly observed in the fluorescence spectra. Its presence has been confirmed by dye-laser excited fluorescence spectra [7]. This band can be distinguished from the other bands by its clearly different D value (see Table I). At $C_0 > 10^{-6}$ M the ODMR signals corresponding to $\lambda = 644$ nm have disappeared, indicating that the species corresponding to the 644 nm band was not present at these Chl b concentrations.

Summarizing up to now, the concentration dependent fluorescence spectra

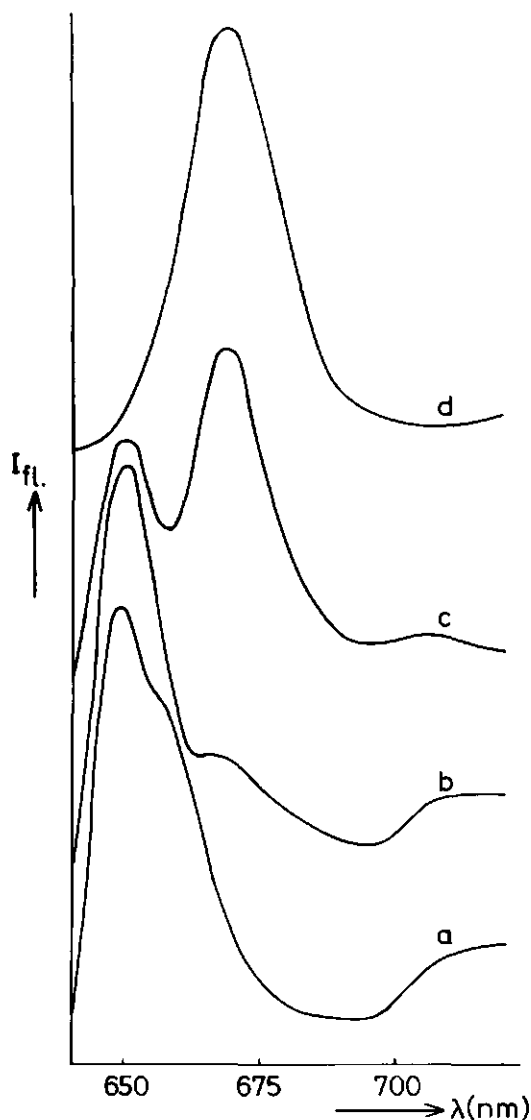


exhibit 4 bands at $\lambda < 700$ nm, and 2 bands at ~ 710 and ~ 725 nm, forming a broad, nearly structureless band at $\lambda > 700$ nm; the relative intensities of all bands vary with the Chl b concentration. For an interpretation of this rather complicated fluorescence behaviour, it should be realized that different complexing and aggregation processes may occur in Chl b solutions simultaneously. Firstly, various monomeric Chl b complexes exist at low Chl b concentrations, and secondly, at higher concentrations Chl b dimers and higher aggregates will form. For the moment we shall focus on monomeric Chl b complexes. As already noted in Section 5.1, three different complexing possibilities should be considered

Fig. 3. Fluorescence of Chl b/n-octane as a function of $R \equiv [\text{Py}]/[\text{Chl } \underline{b}]$.

a. $R = 0$

b. $R = 10^2$

c. $R = 10^3$

d. $R = 1.6 \times 10^4$

$[\text{Chl } \underline{b}] = 3 \times 10^{-5}$ M

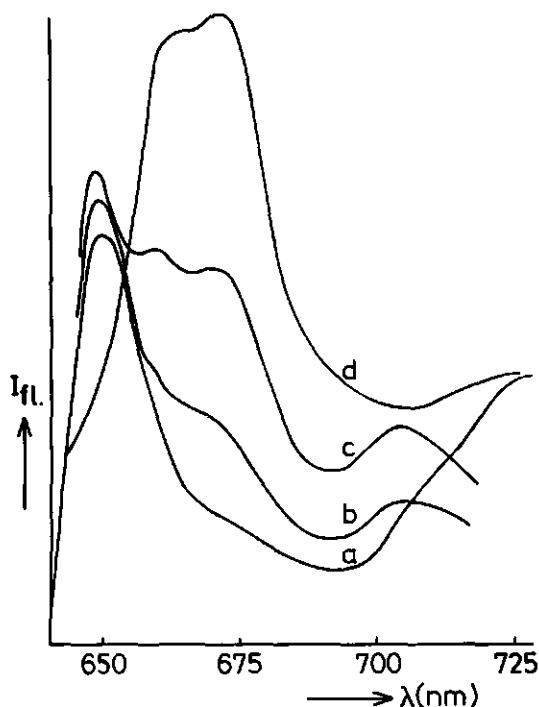
$T = 4.2$ K

These are:

- (1) ligation to the central Mg atom with one or two electron donating compounds.
- (2) hydrogen bonding to the ring V keto group of a molecule which can act as acceptor in a hydrogen bond.
- (3) hydrogen bonding to the ring II aldehyde group.

The other two carbonyl groups present in Chl b, are not expected to have an appreciable effect on the optical properties of Chl b, so these will not be considered here.

In order to discriminate between effect (1) on one hand, and effects (2) and (3) on the other hand, titration experiments were carried out, using pyridine and ethanol, respectively. Pyridine is a relatively strong electron donor, whereas ethanol is an electron donor with acceptor capability in hydrogen bonding. In fig. 3 the effect of adding various amounts of pyridine on the low temperature fluorescence spectrum of Chl b in *n*-octane is depicted. It can be seen that by increasing the pyridine concentration the 656 nm and 648 nm bands diminish, with a simultaneous increase of a 669 nm band. Simultaneously, the long-wavelength fluorescence diminishes in intensity. At 10^4 -fold excess of pyridine only the 669 nm band is present. This can be contrasted with the results, found when various amounts of ethanol are added (see fig. 4). Here the 656 nm band does not disappear,



not even at very high ethanol concentrations. Moreover, the fluorescence intensity at $\lambda > 700$ nm does not disappear in a simple manner on adding increasing amounts of ethanol: at intermediate ethanol concentration (curves b and c of fig. 4) a band at ~ 713 nm appears, which is absent again at higher ethanol concentration (curve d). Its relative intensity is also low in the absence of ethanol (curve a).

Fig. 4. Fluorescence of Chl b/n-octane as a function of $R \equiv [\text{ethanol}]/[\text{Chl } \underline{b}]$.

a. $R = 0$

b. $R = 4 \times 10^2$

c. $R = 3 \times 10^3$

d. $R = 5 \times 10^4$

$[\text{Chl } \underline{b}] = 5 \times 10^{-5} \text{ M}$, $T = 4.2 \text{ K}$

5.4 COMPLEXING PROPERTIES OF CHL B AND THE FOUR-ORBITAL MODEL

Before discussing the experimental results, it is appropriate to outline in which way ligation at the Mg atom and hydrogen bonding at the ring V keto and the ring II aldehyde group may affect the spectral properties and ZFS value D of Chl B. E values will not be discussed because they are very sensitive to small perturbations of the in-plane molecular symmetry due to solvent-solute interactions.

Ab-initio calculations [8] indicate that of the three carbonyl groups in Chl a only the ring V keto group participates in the π system of the chlorin macrocycle. Moreover, from a comparison of the absorption spectra of Chl a and b it can be inferred that in Chl b also the aldehyde group is part of the π -electron system: the so-called Q_y -band of Chl b, corresponding to the lowest-energy electronic transition, is blue-shifted by ~ 12 nm relative to that of Chl a. Hydrogen bonding at the keto and aldehyde groups, involving the n -electrons of oxygen, can be considered as a first-order perturbation of the oxygen core-Hamiltonian (the "a" in Hückel terminology). This perturbation results in a change of the (π) MO energies of those MO's which contain the carbonyl π -orbitals. From first order perturbation theory it follows that hydrogen bonding results in a larger core-attraction energy, thus stabilizing the corresponding π MO's.

The effect of ligation at the Mg atom of chlorophylls on their spectral properties was discussed by Kleibeuker [9], who demonstrated that the four-orbital model, developed by Gouterman [10], could also be successfully applied to a qualitative description of the effects of ligation. Furthermore, this model proved to be valuable in considering the spectroscopic effects of side group substituents, such as the keto and aldehyde group in Chl b [9]. Because we will use the four-orbital model in a discussion of the experimental results, Kleibeuker's analysis is shortly summarized below.

In the four-orbital model, the interaction between the highest occupied MO's (HOMO's), denoted by b_1 and b_2 , and the lowest unoccupied MO's (LUMO's), labeled c_1 and c_2 , determines the spectroscopic properties of the system [10]. Since we are concerned with fluorescence, originating from the lowest excited singlet state, we will focus our discussion on the lowest energy transition, conventionally denoted by Q_y . For this Q_y transition, it is sufficient to consider the configuration interaction (CI) between the states $|b_1c_1\rangle$ and $|b_2c_2\rangle$. The extent of mixing of these two states depends on the energy difference $\delta \equiv E_{b_1c_1} - E_{b_2c_2}$. It is found that an increase in δ , resulting in a decrease of CI, produces a red shift in Q_y , and simultaneously a decrease of the triplet D value [9]. Then, by considering the π charge distributions of b_1, b_2 and c_1, c_2 , it is found [9]

that:

- (1) introduction of the ring V keto group results in a Q_y red shift.
- (2) introduction of the ring II aldehyde group in Chl b produces a Q_y blue shift.
- (3) ligation at the Mg atom results in a Q_y red shift.
- (4) any Q_y red shift parallels a decrease of the D value.

These predictions have been shown to be in agreement with experimental results [9]. For instance, the experimentally found blue shift of the Chl b Q_y band with respect to that of Chl a follows directly from the second statement cited above.

For the effect of hydrogen bonding at the aldehyde and keto groups of Chl b, we may follow the same reasoning as that used by Kleibeuker [9]. Formation of hydrogen bonds at these groups results in a stabilization of those MO's which contain the keto and aldehyde π -orbitals. By application of statements (1) and (2) it is predicted that hydrogen bonding at the keto and aldehyde groups results in a red and a blue shift of the Q_y band, respectively. It should be realized, however, that this result applies to the Q_y *absorption* band only. For *fluorescence*, a red shift may result from a reorganization of the immediate environment of the excited molecule during the life time of its excited state. For Chl b in solid octane, an extensive solvent reorientation, such as may occur in liquid solution, must be excluded. However, the electron donating properties of the aldehyde and keto groups are expected to be different from those in the ground state, resulting in a re-adjustment of the hydrogen bond lengths in the excited state. Analogously to what is observed for $n\pi^*$ -transitions [15] in liquid solution, such a readjustment causes a lowering of the first excited singlet state during its life time. In addition, by emitting a photon the molecule will at first return to an electronic ground state where the hydrogen bond lengths are not yet adapted to the energetically most favourable position in the ground state: this "unrelaxed" ground state has a higher energy than the "relaxed" ground state. Thus, the "environmental" effect of hydrogen bonding is a red shift of the fluorescence.

Summarizing, the net-shift of the fluorescence of Chl b due to hydrogen bonding at the aldehyde group of ring II is the result of a blue "orbital"-shift and a red "environmental"-shift, the sum of which cannot be easily predicted in a quantitative way, but still can be a net red shift. For hydrogen bonding at the keto group of ring V, both types of shifts act in the same direction, which leads us to the conclusion that we may expect the fluorescence red shift due to hydrogen bonding at the Chl b aldehyde group to be appreciably smaller than that due to similar bonding at the keto group.

Assuming the red shifts of various types of ligation and hydrogen bonding to be additive in first approximation, an increase of the number of solvent molecules

interacting with a single Chl b molecule is predicted to cause a red shift of the fluorescence band. This working-hypothesis has been combined with a comparison of band shifts for Chl b with those of Chl a for an assignment of the various fluorescence bands to different Chl b species.

5.5 DISCUSSION

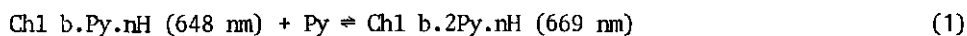
From fluorescence spectra and the ZFS parameters it is apparent that at least 5 Chl b species are present in n-octane solutions at low temperature. For an assignment of the fluorescence bands to various Chl b complexes we note that the relative amounts of these complexes present in solid solution can be expected to reflect those present in liquid solution prior to freezing (for n-octane -56°C). In fact, the equilibria between the various complexes and the ligands involved, are probably frozen at an effective temperature which may be higher than the solidifying temperature of the solvent mixture, since we have employed rapid freezing of samples with a small volume by insertion into liquid helium. Since for all experiments we have used an identical freezing procedure, the results of various experiments can be mutually compared, assuming the same freezing temperature for all equilibria involved in Chl b complexing. The composition of the solutions containing Chl complexes at room temperature cannot simply be derived from the low temperature fluorescence spectra, however, because we do not accurately know the effective temperature at which the equilibria are frozen. In addition, the fluorescence yield of the various complexes is not known. Therefore, the following discussion will be limited to an assignment of the fluorescence bands to various complexes, based on a qualitative analysis of the equilibria between Chl b complexes, including aggregates.

For the analysis of the results presented in figs. 2-4 we make the following assumptions:

- (a) Ligation and solvation equilibria of Chl b can be treated similarly to those of Chl a, except for the ring II aldehyde group.
- (b) The change in relative amounts of various complexes and their constituents is reflected by the change of their respective fluorescence band intensities.
- (c) Displacement of equilibria between various complexes and their constituents by changing the concentration of reactants (e.g. by dilution with an inert solvent, or addition of ligand) obeys the law of mass action for chemical equilibria.

5.5.1 Monomeric Chl b species

As in ref. 6, we use the pyridine titration results (fig. 3) as a starting point for an assignment of the various fluorescence bands. In view of the predominance of the 669 nm band at high pyridine concentration ($[Py]$) and the correspondence between measured ZFS parameters for this band (see Table I) and those obtained by Kleibeuken in toluene-pyridine mixtures [9], we assign the 669 nm band to the biligated monomeric species Chl b.2L.nH, where $n = 0, 1$, or 2 , and H is a molecule hydrogen bonded at the keto and/or aldehyde group. Complexing of Chl b with Py at the ring V keto or ring II aldehyde group can be excluded, since pyridine does not form hydrogen bonds with carbonyl groups. The increase of the 669 nm band intensity at the expense of the 648 nm band upon adding Py, can be understood by assuming an equilibrium:



between both species; again, $n = 0, 1$, or 2 .

Analogously to Chl a complexes, the presence of non-ligated Chl b in solution is extremely unlikely, since for chlorophylls the equilibrium



is far to the right-hand side, even at room temperature [11]. Therefore, we may assume that the 648 nm complex contains at least one ligand attached to Mg.

Apart from the main effect of increasing $[Py]$ on the above-mentioned bands, there are also noteworthy changes in other spectral regions of fig. 3. The shoulder at 656 nm, present in n-octane solution without Py (fig. 3a), has disappeared in fig. 3b, whereas a broad band in the 700-725 nm region gradually decreases in intensity when $[Py]$ increases (fig. 3a-d). These results can be understood by realizing that none of the solvents, as well as Chl b, are completely free from polar impurities (in particular water) capable of forming ligand or hydrogen bonds. In the sequence of experiments presented in figs. 3a-d, we may safely assume that the concentration ratio of polar impurities vs. Chl b remains constant. Although Py cannot act as an acceptor in hydrogen bonding, it is a relatively strong donor [12]. Thus an increase of $[Py]/[Chl]$ will cause an increasing fraction of hydrogen bonding impurity to be involved in complexing with Py. This explains the disappearance of the 656 nm band, which must be assigned to a Chl b species containing at least one hydrogen bonded molecule (presumably water). No other complexes

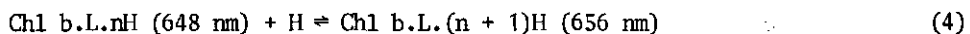
with ligands attached to Mg are possible in addition to those with bands at 648 and 669 nm, since Mg has a maximum coordination number of six.

Turning to fig. 4, it can be seen that the intensity ratio of the 656 and 669 nm bands does not change appreciably over a wide range of ethanol concentrations (cf. figs. 4b-d, taking into account the sloping "baseline" of figs. 4b and c, onto which the 656 and 669 bands are superimposed).

This independence of ethanol concentration can be understood in the following way. An equilibrium of the type



where S is a hydrogen bonding or ligating solvent, will be displaced to the right hand side by adding S. Noting that the intensity ratio of the 656 and 669 nm species is almost constant for a 120-fold increase of the ethanol concentration, we conclude that both species must have the same stoichiometry. It is easily seen that this implies that the 656 nm species should be written as $\text{Chl } \underline{b}\text{.L.}(n + 1)\text{H}$, formed by

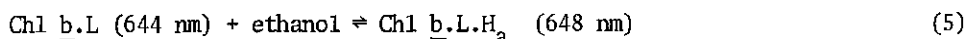


where L and H both represent ethanol. Since the maximum number of hydrogen bonded molecules (H) in the 656 nm species with an appreciable effect on the fluorescence wave length equals two, it follows from eq. (4) that the 648 nm species contains 0 or 1 H. Correspondingly, the 656 nm species contains 1 or 2 H's, whereas the above-mentioned results for the 669 nm species imply that it contains 0 or 1 H.

Under forcing conditions, such as in fig. 4d, it is likely that both carbonyl groups are hydrogen bonded to ethanol. Therefore, we assign the 656 nm band to $\text{Chl } \underline{b}\text{.L.H}_a\text{.H}_k$, i.e. a monoligated species hydrogen bonded to ethanol at the keto and aldehyde groups. Then, the 669 nm species must be either $\text{Chl } \underline{b}\text{.2L.H}_a$ or $\text{Chl } \underline{b}\text{.2L.H}_k$ and the 648 nm species either $\text{Chl } \underline{b}\text{.L.H}_a$ or $\text{Chl } \underline{b}\text{.L.H}_k$. In $\text{Chl } \underline{b}$, the aldehyde group is expected to form hydrogen bonds more readily than the keto group, due to the fact that the hydrogen atom in the aldehyde group is electro-positive compared to the ring V C-atom adjacent to the keto group. This is confirmed by the observation [7], that the 656 nm species of $\text{Chl } \underline{b}$ is invariably observed in n-octane containing traces of water, whereas a corresponding band at 680 nm in n-octane solutions of $\text{Chl } \underline{a}$ (see Section 4.2) or protochlorophyll [7], which both lack an aldehyde group, is only observed by adding an excess of hydrogen bonding solvent, such as ethanol. The different behaviour of both types of

compounds with respect to hydrogen bonding is another indication that the 656 nm species contains a solvent molecule which is hydrogen bonded at the aldehyde group.

The blue side of the 648 nm shoulder in fig. 2a contains a species with a weak unresolved emission at 644 nm which can be distinguished from the other species by its quite different ZFS values (Table I). In view of the foregoing results, and noting that the occurrence of completely unligated Chl b is extremely unlikely, this species may be described as Chl b.L. This assignment is confirmed by the rapid disappearance of its ODMR signals at higher concentration (figs. 2b-f), which can be understood by the displacement of the equilibrium



to the right-hand side by increasing the ethanol or Chl b concentration.

A further confirmation for assigning the 644 and 648 nm bands to monoligated species comes from the excitation spectra obtained at both wave lengths. In these spectra, the Soret region coincides with the room temperature absorption spectrum of dilute solutions of Chl b in ether. Previously, it has been shown [13], that biligation at the Mg atom at room temperature only occurs under forcing conditions, such as a large excess of a strong electron donating compound. Consequently, it is generally accepted, that in dilute ether solutions Chl is present as a monoligated species [14]. In view of these results, the 644 and 648 nm are considered to be monoligated.

A summary of the above-mentioned assignments is presented in Table II (A). The crucial presumption for the set of assignments A is that nonligated Chl b is

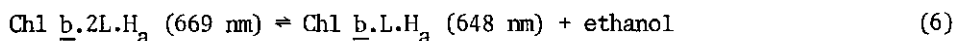
Table II. Assignment of fluorescence bands of Chl b complexes and aggregates. For comparison Chl a data [6] have been included.

Chl <u>b</u>				Chl <u>a</u>		
Species		λ_f (nm)	Δf (cm ⁻¹)	Species	λ_f (nm)	Δf (cm ⁻¹)
A	B					
Chl <u>b</u> .L	?	644		Chl <u>a</u> .L	669	
Chl <u>b</u> .L.H _a	Chl <u>b</u> .L	648	100			240
Chl <u>b</u> .L.H _a .H _k	Chl <u>b</u> .L.H _a	656	190	Chl <u>a</u> .L.H _k	680	
Chl <u>b</u> .2L.H _a	Chl <u>b</u> .2L	669	300	Chl <u>a</u> .2L	687	150
(Chl <u>b</u> .L) ₂ or			1400	(Chl <u>a</u> .L) ₂	720	1060
(Chl <u>b</u> .L.H _a) ₂		707				

[†] Bandshift in wave numbers. The error is estimated to be $\pm 25 \text{ cm}^{-1}$, approximately corresponding to $\pm 0.5 \text{ nm}$.

absent in solution. If this assumption is released, then the assignments B in Table II are also possible. As already noted, the concentration of nonligated Chl a molecules in solution has been shown to be vanishingly small [11,14]; it is only a very small step to extrapolate this result to Chl b. Furthermore, the Chl b solutions, which we have used, were not completely free from electron donating molecules. Therefore, we prefer the set of assignments A.

We will now discuss the concentration dependence of the fluorescence (fig. 2) in view of the afore-mentioned assignments. It should be kept in mind that the compounds which we used in our experiments (n-octane, Chl b, pyridine, ethanol) were not completely free from electron donating or accepting impurities, in particular water (cf. Section 5.2). Assuming that the impurity concentration is approximately constant over the Chl b concentration range in fig. 2, the concentration ratio of impurity vs. Chl b increases with decreasing Chl b concentration. This explains the presence of large amounts of Chl b.L.H_a.H_k (656 nm) at low concentration. Further, the 656 nm species may be directly involved in forming the 725 nm aggregate (see Section 5.5.2), thus providing a mechanism explaining the disappearance of this species when going to higher concentration. For the 669 nm species present in a large excess of electron donating solvent (fig. 4d) ZFS values are the same as those found for a sample with a composition corresponding to fig. 2e (detected at the same wave length), confirming that the 669 nm band in figs. 2 and 4 arise from the same biligated species. The 669 nm species Chl b.2L.H_a remains present, even at high concentrations, since it cannot form ethanol-linked Chl b oligomers or aggregates involving Mg...ethanol bonds (cf. Section 5.5.2). Having assigned the 669 nm band to Chl b.2L.H_a, and the band at 648 nm to Chl b.L.H_a, it is now understood why the intensity of the latter increases relative to the former upon decreasing the Chl b concentration, i.e. going from fig. 2e to 2d. We note that the equilibrium



is displaced to the right-hand side if an inert solvent, such as n-octane is added, because in this way the number of molecules in solution increases according to the law for chemical equilibrium.

Up to now we have not considered the predictions which were formulated in Section 5.4. These predictions are in general agreement with the afore-mentioned assignments:

- (1) The D values for the 644 and 648 nm species are larger than that for the biligated species (669 nm) (see Table I), confirming that they have to be asso-

ciated with monoligated species (statement (4) of four-orbital model).

- (2) The 656, 648, and 644 nm bands (monoligated) are blue shifted w.r.t. the 669 nm band (biligated) in accordance with statement (3) of four-orbital model.
- (3) The small red shift of 100 cm^{-1} as a result of hydrogen bonding at the aldehyde group as compared to the 190 cm^{-1} red shift for hydrogen bonding at the keto group agrees with the predictions made in Section 5.4.

5.5.2 Chl b aggregates

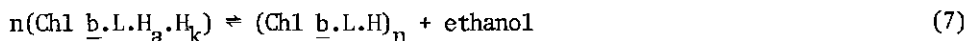
Turning to the emission bands at $\lambda > 700\text{ nm}$, it is evident from the concentration dependence of the spectra presented in fig. 2, that these bands must arise from aggregates. In view of the fact, that excitation spectra taken at fluorescence wavelengths $\lambda < 700\text{ nm}$ are different from those detected at $\lambda > 700\text{ nm}$, it can be concluded that the long wavelength emissions cannot be vibrational bands of the $\lambda < 700\text{ nm}$ bands. This can also be inferred from the sign reversal of the ODMR transitions which is found for the $\lambda > 700\text{ nm}$ bands. Moreover, this finding indicates that the population and depopulation kinetics of aggregates is different from that of the monomeric species.

Analogously to what has been found for Chl a aggregates [6,14], it is very likely that these Chl b aggregates are composed of monomeric units linked *via* bifunctional ligands.

The gradual diminishing of the bands at $\lambda > 700\text{ nm}$ upon adding pyridine (fig. 3) indicates that the interaction of pyridine with Chl b monomers is able to break hydrogen bonds between these monomers in polymeric aggregates, which is not surprising in view of the high equilibrium constant for binding of pyridine to the Mg atom of chlorophylls [14]. A careful comparison of the $\lambda > 700\text{ nm}$ bands in figs. 3a-d reveals that they contain at least two components, one at $\lambda > 720\text{ nm}$ and a second at $\sim 707\text{ nm}$, most clearly observed in fig. 3c. Addition of pyridine causes the former band to disappear more rapidly than the latter, suggesting that the $\lambda > 720\text{ nm}$ band is due to $(\text{Chl } \underline{b} \cdot \text{xS})_n$ aggregates where n is large and S is a polar impurity, probably water. By analogy with the results for Chl a [6], the 707 nm band can be ascribed to water linked Chl b oligomers. In contrast to Chl a, both the aldehyde and keto group of Chl b can participate in aggregate formation by coordination to the central Mg atom. Katz *et al.* [1] have found evidence for aggregation at both the aldehyde and keto group. Moreover, aggregation can occur by linking bifunctional ligands, such as has been demonstrated for Chl a. It has been demonstrated [1] that at high concentrations Chl b forms trimers, whereas under identical experimental conditions Chl a forms dimers.

Apparently, the presence of the aldehyde group causes the Chl b aggregation behaviour to be much more complicated than that of Chl a. Our experimental data on Chl b do not permit to draw detailed conclusions about the structure of the aggregates associated with the long wave length emission bands. However, from a comparison of figs. 3 and 4, one can draw some qualitative conclusions about the origin of the 707 nm band (fig. 4c). For Chl a it has been demonstrated that by adding small quantities of ethanol to a nonpolar solution of Chl a, a dimer is formed consisting of two plane-parallel Chl a molecules, linked via two ethanol molecules [11,14]. By further increasing the ethanol concentration relative to that of Chl a the dimer dissociates into its monomer components. This behaviour is the same as that observed for the 707 nm band in fig. 4, whereas the $\lambda > 700$ nm region of fig. 3 merely reflects a continuous dissociation upon addition of Py. Although we cannot draw the conclusion, that the 707 nm band corresponds to a plane-parallel Chl b dimer, these findings make it probable that this band corresponds to an ethanol-linked oligomer.

Interestingly, ZFS parameters determined at the 707 nm band are equal to those detected at 648 nm, within the error limits of the experiment (Table I). The similarity between ZFS parameters detected for both species also indicates that the 707 nm band corresponds to an ethanol-linked oligomer. It has been shown [16] that in the presence of intermolecular overlap between the monomer parts the D value of a dimer is smaller than that of the corresponding monomer, even if the dimer consists of two plane-parallel monomers. Assuming some overlap and extending the argument to oligomers, this implies that Chl b.L, Chl b.L.H_a, or Chl b.L.H_a.H_k can be the monomeric units forming the 707 nm oligomer, whereas Chl b.2L.H_a can be excluded (Table I). The Chl b.L.H_a.H_k species is unlikely to be the "building block" for the 707 nm oligomer, since both carbonyl groups, of which at least one is needed for constructing an oligomer linked via two Mg...EtOH...O=C bonds, are hydrogen bonded to ethanol in the 656 nm species. Aggregation of this species according to



($n \geq 2$, but small), can be excluded, since the equilibrium would be displaced to the right upon diluting Chl b/ ethanol/ octane solutions with octane, contrary to experimental results (cf. figs. 2f and 2a). These results provide evidence that the 707 nm oligomer contains at least the same number of ethanol molecules per chlorophyll, as compared to the monomer from which it is formed.

Thus, only Chl b.L (644 nm) and/or Chl b.L.H_a (648 nm) can be the building

blocks for the 707 nm aggregate. If Chl $\underline{b.L.H_a}$ is the building block, then the stoichiometry of the 707 nm species can be further defined, assuming it is built from Chl \underline{b} molecules linked via two Mg...EtOH...O=C bonds as in the ethanol-linked Chl \underline{a} dimer [14]. According to this architecture, the oligomer can only be dimeric, since no carbonyl groups are available for attaching more chlorophylls following the double-link principle. (Of course, we cannot exclude oligomers with a fundamentally different structure, e.g. involving linking of more than two chlorophylls via single ethanol bridges). We conclude then that the composition of the 707 nm species is given by $(\text{Chl } \underline{b.L.H_a})_2$. Here, each Chl \underline{b} molecule is connected to the other one through a Mg...EtOH...O=C (keto) bond, so that the dimer is composed of two molecules each having the spectroscopic properties of Chl $\underline{b.L.H_a.H_k}$.

On the other hand, if Chl $\underline{b.L}$ is the building block for the 707 nm species, then the oligomer need not be dimeric, since now two carbonyl groups are available in forming the aggregate. However, from another point of view, the dimeric nature of the 707 nm species is still probable in view of the moderate red shift ($\sim 1400 \text{ cm}^{-1}$) which is found relative to the 644 nm band. (Compare the red shift of $\sim 1100 \text{ cm}^{-1}$ for Chl \underline{a} dimer relative to the monomer). Thus, if Chl $\underline{b.L}$ is the building block, then the 707 nm band may be $(\text{Chl } \underline{b.L})_2$. Here, both chlorophylls are linked by two Mg...EtOH...O=C (aldehyde) bonds and the properties of each Chl \underline{b} unit are similar to those of Chl $\underline{b.L.H_a}$. On the basis of available data we cannot eliminate one of these species. If the 648 nm species is the building block then the ZFS results indicate that the 707 nm species is a parallel dimer without any intermolecular overlap; this is a situation which is unlikely in view of the Chl \underline{a} results of ref. 16, where it was shown that even a very small amount of intermolecular overlap results in a measurable decrease of the D value. On the other hand, the concentration dependence of Chl \underline{b} fluorescence provides some evidence for the 648 nm species as the building block: it is seen that a decrease of the 648 nm band parallels an increase of the 707 nm band. Furthermore, the 644 nm band is already nearly absent at very low concentration which makes it unlikely that this band is involved in forming the 707 nm band.

The 725 nm band can only tentatively be assigned to higher aggregates possibly akin to the large aggregates $(\text{Chl } \underline{a})_n.L_m$ ($m, n \geq 3$) which have been previously reported [17]. The rather large difference between the D values of the 707 and 725 nm species reflects the different modes of aggregation in both species: the 725 nm aggregate cannot be considered to be composed of weakly interacting dimers.

5.6 CONCLUSIONS

It has been demonstrated that due to the presence of the aldehyde group, the complexing and aggregation behaviour of Chl b is much more complicated than that of Chl a. On the basis of the concentration and titration behaviour of Chl b in n-octane various fluorescence bands are assigned to different species (see Tables I and II). These assignments agree with the predictions based on the four-orbital model [9,10]. Some evidence is presented that the aggregate corresponding to the 707 nm band may be stoichiometrically equivalent to the Chl a "special pair". However, the geometrical structure of this aggregate may be rather different due to the fact that in the Chl b aggregate hydrogen bonding preferentially occurs at the aldehyde group.

5.7 REFERENCES

1. J.J. Katz, R.C. Dougherty, L.J. Boucher in "the Chlorophylls", Eds. L.P. Vernon and G.R. Seely (Acad. Press, New York, 1966) Chapter 7.
2. S. Freed, K.M. Sancier, J. Am. Chem. Soc., 76 (1954) 198.
3. J. Fernandez, R.S. Becker, J. Chem. Phys., 31 (1959) 467.
4. P.S. Stensby, J.L. Rosenberg, J. Phys. Chem., 65 (1961) 906.
5. R.L. Amster, Photochem. Photobiol., 9 (1969) 331.
6. R.P.H. Kooyman, T.J. Schaafsma, J.F. Kleibeuker, Photochem. Photobiol., 26 (1977) 235, (Chapter 4.1 of this thesis).
7. R. Avarmaa, private communication.
8. D. Spangler, G.M. Maggiora, L.L. Shipman, R.E. Christoffersen, J. Am. Chem. Soc., 99 (1977) 7478.
9. J.F. Kleibeuker, Thesis (1977), Wageningen.
10. M. Gouterman, J. Mol. Spectr. 6 (1961) 138.
11. J.J. Katz, J.R. Norris, L.L. Shipman, Brookhaven Symposia in Biology, 28 (1976) 17.
12. S.N. Vinogradov, R.H. Linnell, "Hydrogen Bonding" (Van Nostrand Reinhold Company, New York, 1971).
13. T.A. Evans, J.J. Katz, Biochim. Biophys. Acta, 396 (1975) 414.
14. T.M. Cotton, Thesis (1976), Evanston, Ill.
15. N.J. Turro, "Molecular Photochemistry" (Benjamin Inc. New York, 1967).
16. R.P.H. Kooyman, T.J. Schaafsma, J. Mol. Struct., in press (see also Chapter 7 of this thesis).
17. H.C. Chow, R. Serlin, C.E. Strouse, J. Am. Chem. Soc., 97 (1975) 7230.

6 NMR on chlorophyll monomer and dimers

6.1 INTRODUCTION

During the last decade, much work has been devoted to the elucidation of the identity of various chlorophyll species *in vivo* and *in vitro* (for some reviews, see ref. 1-5). Especially *in vitro* experiments provided valuable information concerning the occurrence of various forms of chlorophyll, as they depend on the nature of their environments. Moreover, these experiments gave important clues on the chlorophyll complexes which could be possibly present *in vivo*. In particular, two different chlorophyll a (Chl a) complexes have been proposed to be important in photosynthesis. These are the Chl a dimer (Chl a)₂ and the Chl a "special pair" (SP) (Chl a.L)₂. In (Chl a)₂ the two molecules are directly bonded to each other via a ring V keto-Mg interaction [2], whereas in (Chl a.L)₂ the two molecules are linked via two interstitial ligands L [2]. Katz [2,5] associates (Chl a)₂ with the plant "antenna chlorophyll" and (Chl a.L)₂ with the photosystem I "reaction center". For more details concerning the possible *in vivo* relevance of these complexes we refer to [2,5].

In assessing the validity of these complexes as model systems for the photosynthetic apparatus, it is important to have a knowledge of their geometries: the geometry will largely determine the specific properties, such as the absorption spectrum and the ionization potential, which make some chlorophyll complexes so well suited for their role in photosynthesis. The geometry of the SP was investigated using IR [6] and ESR [7] techniques. A structure was postulated in which two Chl a molecules are held in plane-parallel orientation via two ligands with both electron donor and electron acceptor properties [2,5]. A different structure has been proposed by Fong [8]. The geometry of the dimer (Chl a)₂ has been investigated using circular dichroism [9] and NMR [10]. From both studies it was concluded that the two macrocycles in (Chl a)₂ are $\sim 40^\circ$ tilted relative to each other. On the other hand, Shipman [11] has assumed that in (Chl a)₂ both macrocycle planes are perpendicular to each other.

In order to further investigate the geometrical structure of (Chl a)₂ and (Chl a.L)₂ we have carried out proton spin-lattice relaxation experiments on

these complexes. Furthermore, as an additional support for the conclusions drawn from the proton relaxation-experiments, we have also determined the deuterium spin-lattice relaxation times of perdeuterated Chl a. Finally, we have carried out ring current calculations on Chl a, (Chl a)₂ and (Chl a.L)₂.

A second goal of this investigation was to explore the possibility of investigating the overall structure of medium-sized molecules ($M \approx 2000$) with NMR techniques. It has been extensively demonstrated [12-15] that high-resolution NMR can provide detailed information about the molecular dynamics and structure of small molecules. NMR has also been widely used in the study of conformation and molecular motion of proteins [16], even up to a molecular weight of 10^7 . However, in the case of proteins the information provided by NMR is less detailed compared to small molecules; generally, only semi-quantitative results, which can nevertheless be very interesting, can be extracted from NMR studies on proteins.

6.2 NUCLEAR SPIN RELAXATION AND MOLECULAR STRUCTURE

Since techniques have become available for the selective determination of the spin-lattice relaxation times T_1 and spin-spin relaxation times T_2 of individual nuclei in a molecule, the usefulness of T_1 and T_2 data has been considerably enhanced in studying molecular structure and motion. In this Section, we will briefly discuss the relation between relaxation data and molecular structure and we will outline how this formalism is used to obtain information about Chl a and its dimers.

6.2.1 Theory

In the presence of a static magnetic field \vec{H}_0 , an ensemble of nuclear spin systems has a net longitudinal magnetization $\vec{M} = M_y$, parallel to \vec{H}_0 . If a perturbing resonant magnetic field $\vec{H}_1(t)$ is present (which can be either an externally applied rf field or a fluctuating magnetic field produced by random thermal motions), \vec{M} will shift from its equilibrium value M_y and will attain a transversal component M_x . By removing $\vec{H}_1(t)$, \vec{M} will relax to its equilibrium value. The time dependence of this relaxation process can be characterized by two parameters T_1 and T_2 . The spin-lattice relaxation (SLR) time T_1 is a characteristic time needed for \vec{M} to return to its equilibrium value M_y . This process is accomplished by energy exchange between the spin system and the lattice. The

spin-spin relaxation time T_2 measures the time needed for M_1 to return to its zero equilibrium value. This relaxation process is related to the loss of phase-coherence between the spin systems in the ensemble [17]. T_1 and T_2 depend in a complicated way on the random thermal motions of the molecule in a magnetic field H_0 , and on the particular relaxation mechanisms which are involved. In order to provide a relaxation mechanism for a nucleus with a resonance frequency ω_0 , the random thermal motions must have frequency components corresponding to ω_0 . For instance, it can be shown [18] that for dipolar relaxation of a proton pair, T_1 is given by a relation of the form

$$\frac{1}{T_1} = \frac{A}{r^6} \cdot [J(\omega_0) + 4 \cdot J(2\omega_0)] \quad (1)$$

where the function J is the spectral density distribution function describing the random motional behaviour of the molecule, r is the distance between the two protons and A is a constant. For T_2 a similar relation holds [18]. Depending on the model chosen for the molecular motion (rotational diffusion model, strong collision model, etc.), J is characterized by a set of correlation times τ_c [18], the physical meaning of which is also dependent on the model.

A widely used model is the rotational diffusion model [19]. Here, the motion of the molecule is described by a random walk over small angular orientations. It can be shown [20] that in this model the correlation times τ_c correspond to characteristic times during which the molecule "remembers" its orientational position relative to some fixed laboratory frame. By this definition, τ_c can be related to the shape of the molecule on the basis of a hydrodynamic approach, in which the molecular motion is described by an anisotropic rotational friction tensor. For molecules with ellipsoid shapes it has been shown [21] that a one-to-one correspondence exists between this friction tensor and the τ_c 's for rotational diffusion of the long and short axes of the molecule.

Thus, summarizing, determination of relaxation times of nuclei in a molecule can provide structural information in two ways:

- (1) assuming the rotational diffusion model to be valid, relaxation times can be theoretically calculated for a particular molecular structure and can be compared to the experimentally determined values.
- (2) assuming the rotational diffusion model *and* the hydrodynamic approach to be valid, experimentally determined rotational correlation times can be compared to the rotational friction coefficients which are to be expected for the molecule under study.

In the following we will only discuss the T_1 -relaxation process; further, the rotational diffusion model is assumed to be valid. For this model, Huntress [19,22] has treated the nuclear relaxation of nuclei in an anisotropically reorienting molecule. He has shown that, under certain conditions, all τ_c 's required for a complete description of the molecular reorientation, can be found by measuring the relaxation times of an appropriate set of nuclei in the molecule. It is found that for a nucleus i undergoing a T_1 process in the absence of internal mobility, the following relation holds:

$$\frac{1}{T_1} = F \cdot f(\vec{\Omega}_i, \vec{D}_R) \quad (2)$$

where F is a factor depending on the particular T_1 relaxation process which is operative, and f is a function of the diagonalized rotational diffusion tensor \vec{D}_R and a polar vector $\vec{\Omega}_i$. \vec{D}_R has a one-to-one correspondence to the above mentioned τ_c 's, and $\vec{\Omega}_i \equiv (\phi_i, \theta_i)$ are the polar angles of nucleus i relative to the molecular frame of reference which diagonalizes the rotational diffusion tensor.

We shall mainly be concerned with the (intramolecular) T_1 dipole-dipole relaxation process of $I = \frac{1}{2}$ nuclei (protons). Here, T_1 of a nucleus i being relaxed by $n-1$ other nuclei is given by the following form of eq. (2) [22]:

$$\frac{1}{T_1} = C \cdot \sum_{j \neq i} f(\vec{\Omega}_j, \vec{D}_R) \cdot \frac{1}{r_{ij}^6} \equiv \sum_j g(\vec{\Omega}_j, \vec{D}_R, r_{ij}) \quad (i, j = 1, \dots, n) \quad (3)$$

C is a constant depending on the type of nucleus studied, and r_{ij} is the distance between nucleus i and nucleus j . From the analytical form of f , given in ref. 22, it can be seen that f has the property:

$$f(\vec{\Omega}, \lambda \vec{D}_R) = \frac{1}{\lambda} f(\vec{\Omega}, \vec{D}_R) \quad (4)$$

where λ is some scalar.

We are primarily interested in relative values of the components of \vec{D}_R , since only these are relevant in studying structural features of the molecule. With the help of eq. (4) the problem of an *a priori* scaling of \vec{D}_R can be circumvented; simultaneously non-geometrical effects on \vec{D}_R , such as the influence of the temperature, are eliminated. If $\frac{1}{T_1}$ is scaled by $\langle T_1 \rangle$, which is the average of the T_1 -values, then

$$\frac{i T_1}{\langle T_1 \rangle} = \frac{\sum_j \sum_{i \neq j} g(\vec{\Omega}_j, \vec{D}_R, r_{ij})}{n \cdot \sum_{j \neq i} g(\vec{\Omega}_j, \vec{D}_R, r_{ij})} \equiv \frac{\sum_j \sum g(\vec{\Omega}_j, \lambda \vec{D}_R, r_{ij})}{\sum_j g(\vec{\Omega}_j, \lambda \vec{D}_R, r_{ij})} \quad (5)$$

$$(i, j = 1, \dots, n)$$

i.e. independent of λ . Given the functions g , which contain the structural information, and a set of n experimentally determined T_1 -values, eq. (5) can now be used to calculate relative T_1 -values; by considering the three diffusion constants D_{R_i} ($i = 1, 2, 3$) as adjustable parameters, one can try to fit the calculated T_1 -values to the experimental values. If a set of relative diffusion constants D_{R_i} has been found resulting in calculated relative T_1 -values corresponding to the experimental relative T_1 -values, then the absolute values of the components of \vec{D}_R are given by:

$$\vec{D}_R = \lambda \vec{D}_{R_i} \quad \text{with} \quad \lambda = \langle T_1 \rangle_{\text{exp}} / \langle T_1 \rangle_{\text{calc}} \quad (6)$$

For our purposes we wish to apply eq. (5) to a dimeric molecule, composed of two identical subunits. Then, in the limit of fast exchange between both monomer parts eq. (3) can be written as:

$$\frac{1}{i T_1} = \frac{1}{2} \cdot \left(\frac{1}{i T_1^{(1)}} + \frac{1}{i T_1^{(2)}} \right) \quad (3a)$$

where

$$\frac{1}{i T_1^{(u)}} = \sum_j g(\Omega_j, \vec{D}_R, r_{ij}) + \sum_j g(\Omega_j', \vec{D}_R, r_{ij}') \quad (u = 1, 2) \quad (3b)$$

In eq. (3b) the first term describes the relaxation caused by nuclei in the same subunit as the nucleus of which T_1 is observed, whereas the second term denotes the contribution from nuclei attached to the other subunit.

Of course, eqs. (3) are not very well suited to study a molecule, the structure of which is fully unknown; the number of unknown geometrical parameters r_{ij} , θ_i , ϕ_i would be much too large. However, if the monomeric structure is known, then the problem of studying dimer structures is tractable: one has then

6 geometrical parameters, 3 for rotation and 3 for translation.

6.2.2 Molecular structure of chlorophyll dimers from T_1 -measurements

The X-ray structure of ethylchlorophyllide a, which is Chl a without the phytol chain, has been determined [23] and we have used these data for the inter-atomic distances within one molecule. In order to be able to apply eq. (5), we must measure the T_1 -values of nuclei which have no internal mobility. For Chl a, there are only 4 protons which are rigidly attached to the macrocycle (in fig. 1 denoted by 1,2,3,4) and which have a reasonable intensity in the NMR spectrum. Of course, ^{13}C NMR measurements would be a better choice, but the availability of sizeable amounts of ^{13}C enriched Chl a is rather limited. Thus, we have determined the T_1 -values of these 4 nuclei. From the monomeric atomic coordinates, a dimer was generated by applying a translation \vec{V} and a rotation over the Euler angles $\vec{\Omega} = (\alpha, \beta, \gamma)$ on all atomic coordinates. The combination of the original and transformed coordinates thus forms the dimer. In determining the geometry of the Chl a dimers under study, we should seek for those \vec{V} and $\vec{\Omega}$ which give the "best" fit to the experimentally determined T_1 values with the help of eq. (5). The "best" fit is obtained by minimizing

$$\epsilon = \sum_i \left\{ \frac{(\langle T_1 \rangle)_{\text{calc}}}{\langle T_1 \rangle_{\text{calc}}} - \frac{(\langle T_1 \rangle)_{\text{exp}}}{\langle T_1 \rangle_{\text{exp}}} \right\}^2 \quad (7)$$

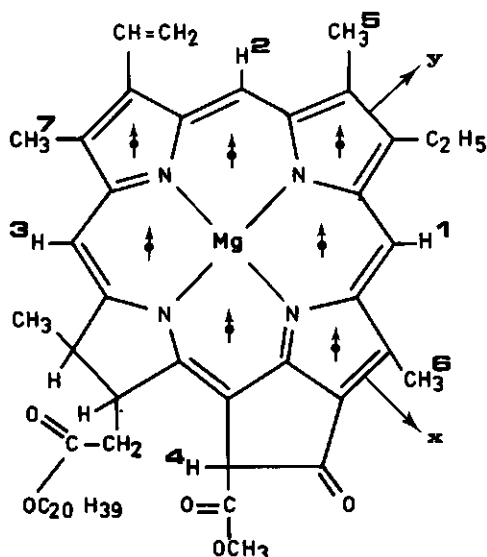


Fig. 1. Molecular structure of Chl a. The positions of the equivalent dipoles (Section 6.3) have been indicated by \uparrow . The relevant nuclei have been numbered by 1-7.

6.2.3 The choice of the molecular frame of reference

As already mentioned, eqs. (2)-(5) are only valid in a molecular axis system which diagonalizes the diffusion tensor. For molecules with sufficient symmetry, the diffusion tensor principal axis system is by symmetry coincident with the principal axis system of the moment-of-inertia tensor [22]. For a totally asymmetric molecule such as Chl a, the choice of the diffusion axis system is not *a priori* obvious, since it may be rotationally shifted from the principal inertial axes by intermolecular interactions. Nevertheless, since we do not know the orientation of the principal diffusion axis system in the chlorophylls, we have still used as a first approximation the easily determinable principal/inertial axis system of Chl a and of its dimers to coincide with the diffusion axis system. Some justification for this approximation lies in the fact that in Chl a the mass distribution is rather uniform; furthermore, it can be shown [24] that for a homogeneous mass distribution the diffusion axis system is coincident with the inertial axis system.

In order to obtain some experimental justification for this assumption, we have determined T_1 -values of deuterons in perdeuterated monomeric Chl a. Deuterons ($I = 1$) possess an electric quadrupole moment. Huntress has shown [19,22] that for a planar asymmetric molecule, the principal diffusion axis system can be unambiguously found if the relaxation times of four geometrically non-equivalent quadrupolar nuclei can be determined. An additional requirement is, that at least one nucleus has a non-zero asymmetry-parameter. Although not all these conditions are met in Chl a, we will see in Section 6.5.2 that the deuterium relaxation data of Chl a are consistent with the assumption of coinciding diffusion and inertial axis systems.

6.3 PROTON CHEMICAL SHIFTS AND MOLECULAR STRUCTURE

An alternate way to study molecular structure is the determination of the chemical shifts of individual nuclei in the molecule. The chemical shift of a nucleus in a static magnetic field H_0 is a measure of the magnetic shielding due to the H_0 -induced electronic currents, and is thus dependent on the local environment of that nucleus. By considering the chemical shifts of several magnetically inequivalent nuclei in a molecule, structural information on the molecule as a whole can in principle be obtained. Several mechanisms can contribute to the chemical shift of a particular nucleus in the molecule [25]. In aromatic mole-

cules, an important shift mechanism is caused by the presence of H_0 -induced ring currents, which arise from the circulation of the delocalized π -electrons. Several attempts have been undertaken to calculate the ring current-induced chemical shifts of the nuclei in such compounds [26-29]. In a widely used method, the π -electron current loop is replaced by an equivalent magnetic dipole [26,28]. To calculate the ring current induced chemical shifts in porphyrins, where several current loops are present, Abraham *et al.* [30] have refined this semi-empirical approach by dividing up the porphyrin ring into a number of current loops with equivalent dipoles placed at the center of each loop. In this way they were able to obtain fairly good agreement between the calculated and experimentally determined chemical shifts.

In view of the appreciable differences in the chemical shifts, which are experimentally found for Chl a monomer and dimers (see Section 6.5), these data should contain information about the geometry of the Chl a dimers which were investigated. To this end, we have adopted the approach of Abraham *et al.* [30] and we have extended this approach to describe the ring current induced chemical shifts of nuclei in Chl a dimers. This will now be discussed.

6.3.1 Ring current shifts in Chl dimers

To calculate the ring current shifts in chlorin (which is the basic skeleton of Chl), Abraham *et al.* [30] divided up the ring system into 7 closed rings (see fig. 1), 4 hexagons and 3 pyrrole rings, each of which contains two current loops. For each ring the two current loops were replaced by two equivalent dipoles, placed at the centre of the ring at a distance z_d above and below the chlorin plane. In a molecular coordinate system where the z -axis is perpendicular to the molecular plane, the ring current shift of a proton N is then given by [30]:

$$\Delta\delta(N) = \sum_{i=1}^8 \mu_H [1-3(z_{Ni}/r_{Ni})^2]/r_{Ni}^3 + \sum_{j=1}^6 \mu_P [1-3(z_{Nj}/r_{Nj})^2]/r_{Nj}^3 \quad (8)$$

where r_{Ni} and r_{Nj} are the distances from proton N to the equivalent dipoles i , placed in the hexagons and the dipoles j , placed in the pyrrole rings, respectively, and z_{Ni} , z_{Nj} are the z -coordinates of the vectors connecting proton N and the dipoles i and j , respectively. The constants μ_H and μ_P are the magnitudes of the dipoles placed in the hexagons and pyrrole rings, respectively.

If the distances are expressed in Å, and the dipole moments in Å³, then $\Delta\delta(N)$ is expressed in ppm.

To determine the ring current shifts in chlorin, Abraham *et al.* used as a reference pyrrole, and the experimental ring current shifts of chlorin relative to those of pyrrole were considered. By using μ_p , ν_H and z_d in eq. (8) as adjustable parameters, a fit was made between calculated and experimental ring current shifts.

We will now consider proton ring current shifts in a dimer. Suppose, the dimer consists of two identical molecules 1 and 2. Consequently, in a coordinate system fixed to molecule 1, the atomic coordinates and also the equivalent dipoles of molecule 2 can be generated from molecule 1 by applying a transformation \vec{R} (rotation and translation) on the atomic coordinates and equivalent dipoles of molecule 1. Thus, if we denote the set of dipoles, belonging to molecule 1 by $\{\vec{\mu}_1\}$, then the position of the set of dipoles, which are situated in molecule 2, will be given by $\{\vec{\mu}_2\} = \{\vec{R} \cdot \vec{\mu}_1\}$. Analogously, the atomic coordinates $\vec{r}_N = (N_x, N_y, N_z)$ of a nucleus N in molecules 1 and 2 are related by $\vec{r}_{N2} = \vec{R} \cdot \vec{r}_{N1}$.

Consider a proton N in molecule 1 with coordinates \vec{r}_{N1} . The ring current shift of this proton is composed of two parts: the shift due to the presence of dipoles in molecule 1 and the shift caused by the dipoles in molecule 2. This shift is given by:

$$\Delta\delta(N_1) = \Delta\delta(N_1)_{\{\vec{\mu}_1\}} + \Delta\delta(N_1)_{\{\vec{\mu}_2\}} \quad (9a)$$

where the braces denote to which set of dipoles is referred. For a proton N in molecule 2 with coordinates $\vec{r}_{N2} = \vec{R} \cdot \vec{r}_{N1}$ an analogous relation holds:

$$\Delta\delta(N_2) = \Delta\delta(N_2)_{\{\vec{\mu}_1\}} + \Delta\delta(N_2)_{\{\vec{\mu}_2\}} \quad (9b)$$

If the molecules 1 and 2 are indistinguishable on the NMR time scale, due to fast exchange of both monomer parts in the dimer, then the total ring current shift is the average of both contributions:

$$\Delta\delta(N)_{\text{dimer}} = \frac{1}{2} (\Delta\delta(N_1)_{\{\vec{\mu}_1\}} + \Delta\delta(N_2)_{\{\vec{\mu}_2\}} + \Delta\delta(N_1)_{\{\vec{\mu}_2\}} + \Delta\delta(N_2)_{\{\vec{\mu}_1\}}) \quad (10a)$$

Of course, the first and second term in eq. (10a) are equal, because these two terms reflect the monomeric ring current shift.

Thus:

$$\Delta\delta(N)_{\text{dimer}} = \frac{1}{2} \{ 2\Delta\delta(N_1)_{\{\vec{\mu}_1\}} + \Delta\delta(N_1)_{\{\vec{\mu}_2\}} + \Delta\delta(N_2)_{\{\vec{\mu}_1\}} \} \quad (10b)$$

The ring current shift of some particular proton can now be calculated by applying eq. (8) to each of the three terms in eq. (10b). Eq. (8) can directly be used to calculate the first and third term. The second term in eq. (10b) needs some closer examination, because the form of eq. (8) is only appropriate for dipoles which are placed parallel to the z-axis. The dipole set $\{\vec{R}, \vec{\mu}\}$ is not necessarily parallel to the z-axis, if in the transformation \vec{R} a rotation is included. Therefore, in order to be able to use eq. (8) in this case, we apply another transformation which places the dipoles in molecule 2 parallel to the z-axis. If the position vectors of a dipole μ_2 and a proton N are denoted by \vec{r}_μ and \vec{r}_N , respectively, and the rotational part of \vec{R} by \vec{R} , then it can be seen that the vectors:

$$(\vec{r}_N)' \equiv \vec{R}^{-1} \cdot (\vec{r}_N - \vec{r}_\mu)$$

and

$$(\vec{r}_\mu)' \equiv (0,0,0)$$

with μ_2 parallel to the z-axis, reflect the same relative positions of the

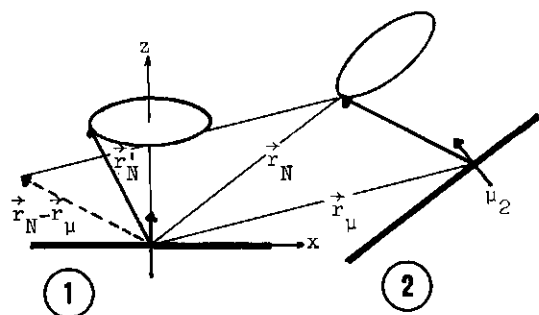


Fig. 2. Transformation of the position of nucleus N relative to μ_2 in molecule 2 to a position \vec{r}_N' relative to the origin in molecule 1. The heavy lines represent the molecules 1 and 2. The x and axes of the frame of reference have been indicated; the transformed μ is in the origin parallel to the z-axis (see text).

proton N and the dipole μ_2 as \vec{r}_N and \vec{r}_μ do (see fig. 2). Thus, the second term in eq. (10b) can now be evaluated with the help of eq. (8) for a proton N by applying this transformation to each dipole in the set $\{\vec{R}, \vec{\mu}\}$.

6.3.2 Calculations

Firstly, we have calibrated eq. (8) for Chl a using pyrrole as a reference compound. By considering the ring current shifts in the monomer, we have determined those μ_H and μ_P which result in an optimum fit between calculated and experimental ring current shifts. The positions of the 14 equivalent dipoles were kept constant; each loop contained two dipoles in its centre, which were situated at a distance 0.64Å above and below the chlorin plane, respectively.

Next, ring current shifts in Chl a dimers were considered, using the μ_H and μ_P as determined for the monomer. A dimer was generated in a manner, identical to that mentioned in Section 6.2.2. The ring current shifts of seven protons, in fig. 1 denoted by 1,...,7, were calculated: the positions of these protons in the molecule can be reasonably well determined, and, moreover, all these protons, including the methylgroups 5,6,7, exhibit a single resonance in the NMR spectrum, yielding well-defined chemical shifts. By varying the dimer geometry an optimum fit was sought between the calculated and experimental ring current shifts of these seven protons.

6.4 EXPERIMENTAL

6.4.1 Sample preparation

Three types of samples were prepared:

- (1a) Chl a dissolved in deuterated acetone, in which Chl a is monomeric [6].
- (1b) Fully deuterated Chl a in diethylether. This Chl was a gift from Dr. Norris.
- (2) Chl a in deuterated chloroform, in which Chl a mainly exists in the dimeric form (Chl a)₂ [6].
- (3) Chl a in deuterated toluene/ethanol, which at low temperature (T~260K) is partly in the "SP" form (Chl a.ethanol)₂ [6].

Chl a was extracted from spinach leaves and purified according to standard procedures [31]. Purity was checked by absorption spectrophotometry and thin-layer chromatography. No impurities were detected. The pure Chl a was extensively dried at low pressure (10^{-5} torr) at a temperature of ~60°C. Fully deuterated

solvents (Merck) were dried over 4A molecular sieves (Union Carbide) according to the procedure of Cotton [6], and thoroughly degassed. All sample preparations were done in a nitrogen-purged dry box. All samples were contained in sealed NMR tubes after preparation. In all experiments, the nominal concentration of Chl a varied between 0.01M and 0.05M. Sample 3 was prepared according to Cotton's procedure, with a molar Chl a/ethanol ratio of $\sim 1/4$. The effectiveness of this last sample preparation was checked by low temperature ($\sim 250\text{K}$) absorption spectra making use of a 25 μ pathlength microcell (Beckman Instruments). At low temperature, a 700 nm band occurred, such as described by Cotton, indicating the presence of (Chl a.ethanol)₂.

6.4.2 NMR experiments

All NMR experiments, except those on sample 3, were carried out at room temperature; sample 3 was studied at $T = 260\text{K}$. Proton experiments at 100 MHz were carried out with the samples 1a, 2, 3 on a Varian XL-100 NMR spectrometer. Additional experiments were done on a Bruker 360 MHz spectrometer. Deuterium NMR spectra with sample 1b were recorded at 61.4 MHz at the Bruker factory in Zürich. In the SLR measurements the inversion-recovery method was employed [32]. All proton NMR experiments were carried out in 5 mm NMR sample tubes, whereas for the deuterium experiments 10 mm sample tubes were used. Typically, an accumulation of 10 transients was needed for a good signal-to-noise ratio in the 100 MHz spectra. For the identification of the various resonance lines, the assignments of Katz *et al.* [33] were used. SLR times were determined for the three methine protons H1, H2, H3 and the single proton H4 (see fig. 1); these are the only protons with a rigid position with respect to the chlorin plane, and thus they reflect the dynamics of the macrocycle directly, contrary to, for instance, methylgroups which can have internal mobility. Moreover, the resonance lines associated with protons 1-4 are relatively isolated and their intensities can therefore be measured with satisfactory accuracy.

6.4.3 Data processing

SLR times for the various nuclei were determined with the help of a conventional semi-log plot. SLR times determinations making use of a non-linear least squares fit [34] yielded identical results. For the samples 2 and 3 the experimental SLR times could not be used directly, since in these samples an equilib-

brium exists between various forms of Chl a. For sample 2 an equilibrium constant was determined for the equilibrium



using a titration procedure with $L = \text{methanol}$, which has been previously described by Katz *et al.* [35]. Then, assuming fast exchange on the NMR time scale between the two species, the experimental SLR time of a nucleus can be written as a weighted average of two SLR times each associated with one species. In the same way, results of sample 3 were treated; here, an equilibrium of the form



was assumed [6].

Thus, if a fast equilibrium exists between two species A and B, then

$$\frac{1}{(T_1)_{\text{exp}}} = \frac{[A]}{[A] + [B]} \cdot \frac{1}{(T_1)_A} + \frac{[B]}{[A] + [B]} \cdot \frac{1}{(T_1)_B} \quad (13)$$

where $(T_1)_A$ and $(T_1)_B$ are the SLR times of a proton in species A and B respectively, and $[A]$ and $[B]$ are the concentrations of A and B in the sample.

The chemical shifts of various nuclei in the different samples were determined making use of the residual solvent proton resonances, which in turn can be related to the chemical shifts relative to TMS. The chemical shifts determined in this way were accurate to 0.2ppm, which is sufficient for our purpose. Analogously to what has been mentioned for the determination of the SLR times, the chemical shifts of the protons in the samples 2 and 3 are a weighted average of two chemical shifts each associated with one species.

6.5 RESULTS

The 360 MHz proton NMR spectrum of monomeric Chl a (sample 1a) is depicted in fig. 3. The chemical shifts of various protons agree with those earlier reported by Katz *et al.* [33].

In figs. 4 and 5 the 100 MHz spectra of sample 2 (Chl a dimer) and sample 3 (Chl a SP) are represented, respectively. Again, the chemical shifts in fig. 4 correspond to those published earlier [33], whereas the chemical shifts of pro-

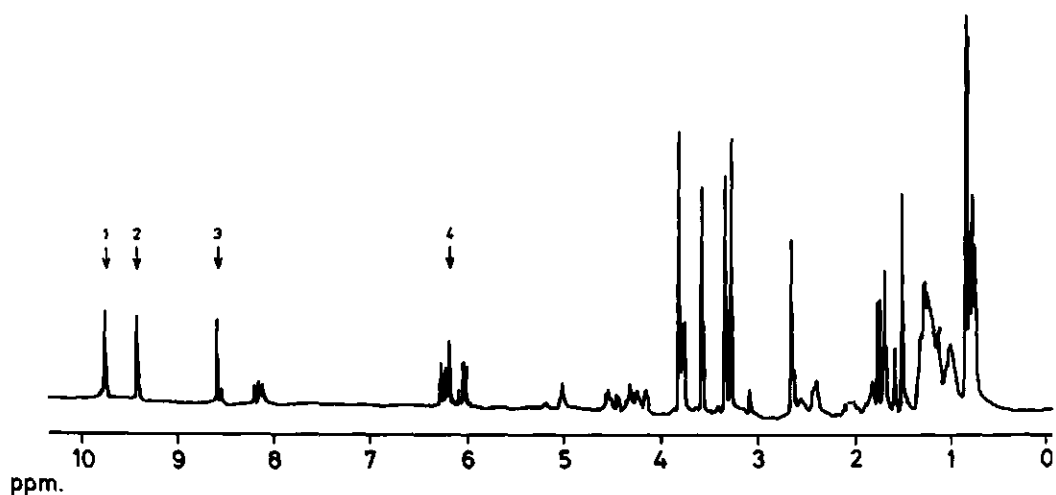


Fig. 3. 360 MHz proton NMR spectrum of sample 1a. 1 accumulation. Concentration: 0.04 M in deuterated acetone.

tons in Chl a SP have not been previously reported. However, as already mentioned in Section 6.4.3, these last two spectra do not represent the "pure" (Chl a)₂ and (Chl a.L)₂ SP, and are rather a weighted average of the mixture of species present in the samples 2 and 3, indicated by the equilibria (11) and (12), respectively. For equilibrium (11), it can be concluded from the value of the equilibrium constant which was determined at $k_1 \approx 40$ l/mol and the total Chl a concentration $C_0 \approx 5 \times 10^{-2}$ M that over 90% is in the dimeric form; in view of the experimental errors (see below), it is not appropriate to further correct the spectrum, depicted in fig. 4. For the spectrum of fig. 5 the situation is different: from the equilibrium constant $k_2 = 15$ (l/mol)² at 260 K [6] and the total Chl concentration $C_0 \approx 8 \times 10^{-2}$ M and [ethanol] ≈ 0.3 M, the ratio $\frac{[SP]}{C_0}$ is calculated to be ≈ 0.23 . As a consequence, the chemical shifts and SLR times determined for sample 3 do not reflect those of the "pure" Chl a SP, and they have to be corrected for the presence of (Chl a)₂. In order to obtain the chemical shifts and SLR times of the various protons in the "pure" Chl SP, these parameters were determined at $T = 260$ K for a sample consisting of Chl a in toluene without ethanol which is known to be in the dimeric form (Chl a)₂ [6]. Then, with the help of

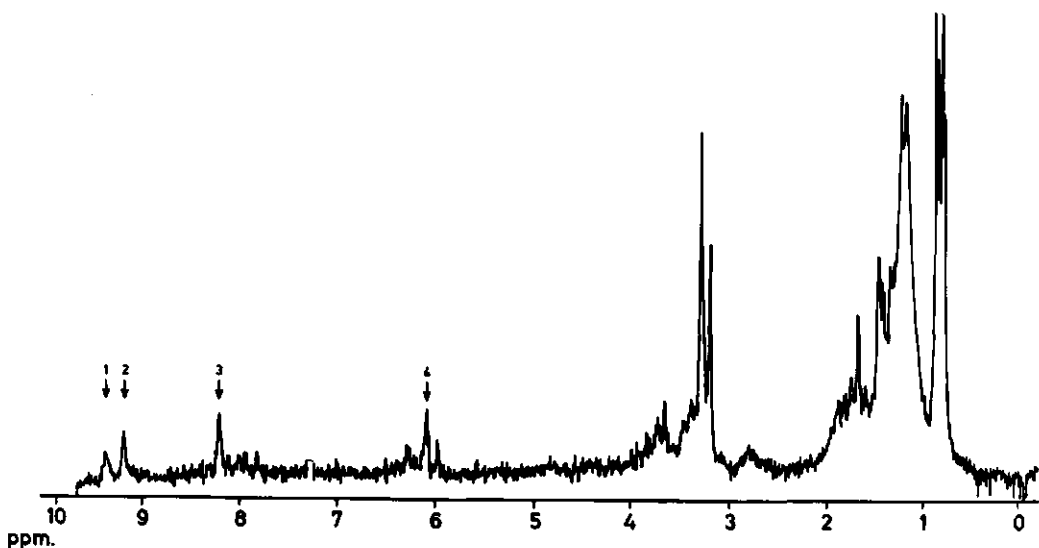


Fig. 4. 100 MHz proton NMR spectrum of sample 2. 200 accumulations. Concentration: 0.05 M in deuterated chloroform.

eq. (13) the SLR times and chemical shifts of the "pure" SP can be determined. All data (see below) concerning sample 3 have been corrected in this manner.

Finally, the ^2D 61.4 MHz NMR spectrum of sample 1b (monomeric Chl a) is shown in fig. 6. It is seen that this spectrum has a close resemblance to that of fig. 3, particularly in the low-field region, but with the difference that all lines are significantly broader, due to the inherently shorter spin-spin relaxation times of quadrupolar nuclei. In order to further compare figs. 3 and 6, a ppm scale in fig. 6 was constructed in such a way that the ppm-value of the strong line near 4 ppm in fig. 3 coincides with that of the corresponding line in fig. 6. It can then be seen that most corresponding resonances in figs. 3 and 6 have very similar chemical shifts. Further, it is nicely illustrated that in the deuterium spectrum the spin-spin splitting patterns which in the ^1H spectra are apparent for several protons, have collapsed into single lines (cf. the multiplets around 8 and 6 ppm in fig. 3 to the corresponding regions in fig. 6). As it is beyond the scope of this study, we will not further discuss the differences and similarities in figs. 3-6. Some comments on this subject may be found in ref. 33 for the Chl dimer and in ref. 36 for the deuterium spectrum. The numbering in the figs. 3-6 corresponds to that in fig. 1. For figs. 3 (monomer) and 4 (dimer), we followed the assignments of Katz *et al.* [33], which for Chl a monomer were later confirmed by Denniss *et al.* [37]. The assignment of the resonance lines

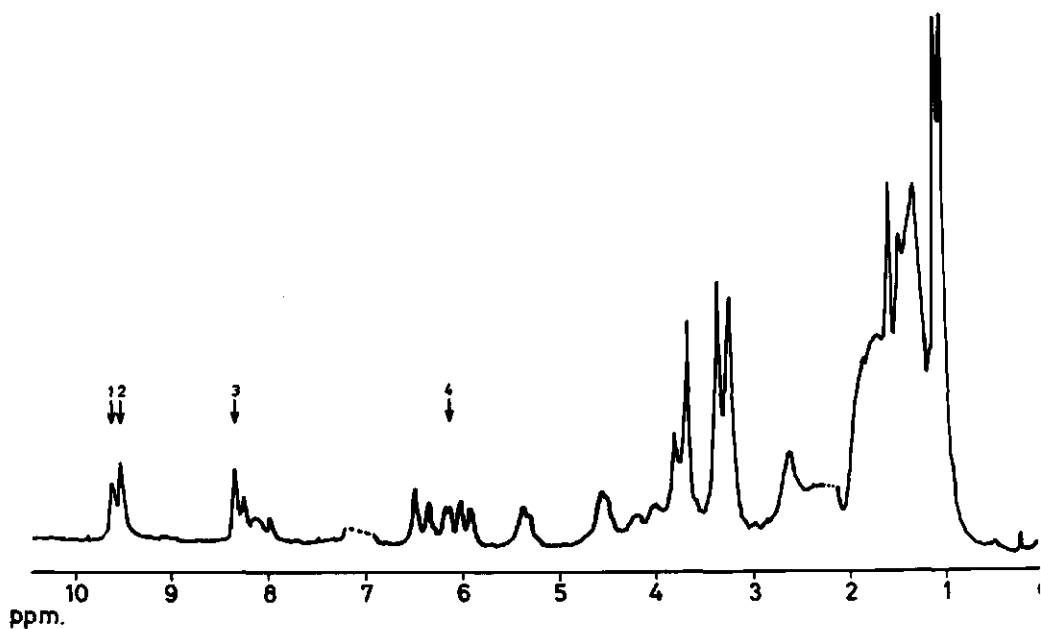


Fig. 5. 100 MHz proton NMR spectrum of sample 3. 200 accumulations. Concentration: 0.08 M in deuterated toluene + 0.3 M ethanol.

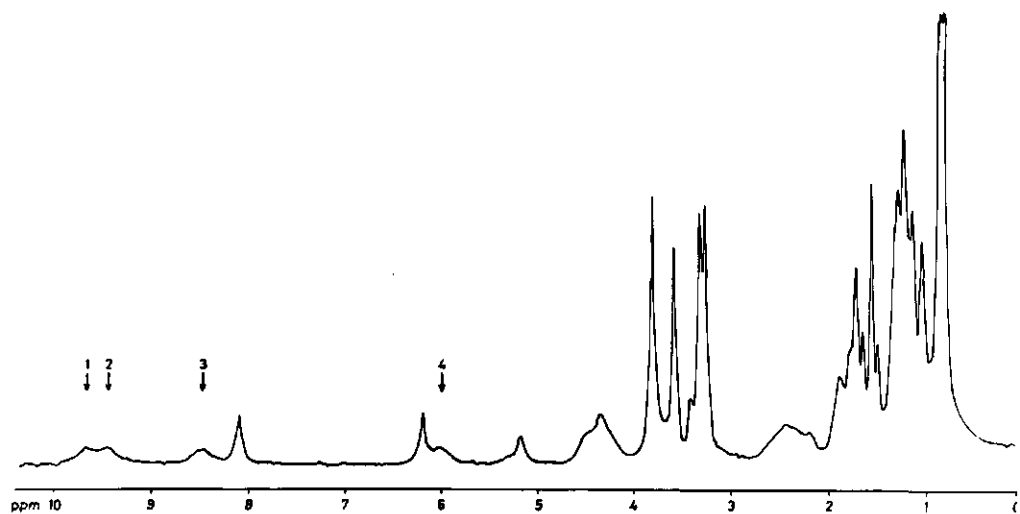


Fig. 6. 61.4 MHz deuterium NMR spectrum of sample 1b. 200 accumulations, line broadening 2 Hz. Concentration: 0.01 M in diethylether.

1...4 in fig. 5 (SP) is based on the following considerations: from previous NMR work on porphyrins [33,38] it is obvious that the lines 1,2,3 at the low-field side of the NMR spectrum correspond to the three methine protons. Furthermore, it is expected that the relative resonance positions of these protons, which are very close to the macrocycle plane, will not be seriously affected when one goes from monomer to dimer, because the ring current effects of the partner molecule which might shift the resonance positions of the methine protons are similar for these protons. Therefore we assume that the order of resonance positions of these protons is the same as that for the corresponding ones in the monomer. This assumption finds some support in the finding that also in the Chl a dimer (fig. 4) this order is the same as that in the monomer. In order to determine the resonance line in fig. 5 corresponding to proton 4, we have determined SLR-times for all resonance lines near 6 ppm. It was found that all SLR-times were about the same, except for one which was a factor 3 larger. In view of the relatively isolated position of proton 4, we assign the resonance line with the larger SLR time to this proton.

The assignments in the ^2D NMR spectrum of the Chl a monomer (fig. 6) can be straightforwardly made from a comparison with fig. 3: the deuterons in $^2\text{Chl a}$ have a local environment identical to the protons in $^1\text{Chl a}$, and thus the deuteron resonance positions should have the same ordering as those of the protons.

6.5.1 Dimer geometries from T_1 -data

In all samples, SLR times have been determined for the nuclei 1...4. We have also determined T_1 values for a more dilute monomeric ($\sim 10^{-3}\text{M}$) sample. SLR times determined for this sample were identical to those found for sample 1a. All experimental SLR times have been collected in Table I. Using these data, the calculations were carried out as indicated in Section 6.2.2.

In calculating the SLR time of some proton, the contributions of all other protons present in the molecule were included in the summation of eq. (5). Methyl groups with internal mobility, as judged from the non-exponential decay of the transverse magnetization [39], were treated by replacing such groups by 3 protons situated at their average positions.

To test the reliability of the fitting procedure, we have carried out calculations on the molecule pyrimidine, of which T_1 -data and rotational diffusion constants have been recently published [15]. Results of our calculations were identical to those published. Furthermore, only one set of rotational diffusion

Table I. SLR times of nuclei in various Chl a species³⁾

nr.nucleus	T_1 (sec) ¹⁾			
	monomer ^1H (sample 1a)	monomer ^2D (sample 1b)	dimer ^1H (sample 2)	dimer ^1H (sample 3) ²⁾
1	0.95 ± 0.06	0.03	0.40 ± 0.04	0.18 ± 0.03
2	1.07 ± 0.06	0.02	0.43 ± 0.04	0.31 ± 0.05
3	0.92 ± 0.06	0.03	0.32 ± 0.03	0.22 ± 0.04
4	1.45 ± 0.09	0.04	0.55 ± 0.05	0.41 ± 0.07

1) Errors are quoted as standard deviations and are the RMS sums of estimated instrument reproducibility and standard deviation of exponential fit. For sample 3 an additional error is introduced by the error in the equilibrium constant k_2 .

2) Corrected for the presence of $(\text{Chl } \underline{a})_2$ in the sample (cf. equil.(12) and eq. (13)).

3) For ^1H nuclei determined at 100 MHz.

coefficients corresponded with a good fit between experimental and calculated SLR times, indicating that no multiple minima were present. Then, having ascertained ourselves of the utility of the method, we turned to the Chl a SLR data. For the monomer and both dimers their respective principal axis systems of the moment of inertia tensor were used as molecular frames of reference (cf. Section 6.2.3). The inertia tensors were determined using the atomic coordinates of ethylchlorophyllide a published by Chow *et al.* [23]. To account for the effect of the presence of the phytol chain in Chl a on the inertia tensor, the phytol chain was simulated by a homogeneous rod of length 8.5Å (which corresponds to the gyration radius of the chain [40]); from a space-filling molecular model its average position relative to the macrocycle plane was estimated.

Firstly, the most simple case, Chl a monomer was examined, in which the geometry is fixed. As illustrated in fig. 7, where the fit results are presented, the agreement between experimental and calculated T_1 -values is fairly good. The corresponding diagonal elements of \vec{D}_R , and some other relevant quantities have been collected in Table II.

Next, "best" fits for various geometries of the $(\text{Chl } \underline{a})_2$ dimer were considered. For this type of dimer substantial evidence has been presented that it is linked by a Mg...ring V keto group coordination interaction [2,6] (see also Section 2.3.2) with a distance of closest approach of both molecules of $\sim 2\text{\AA}$ [6].

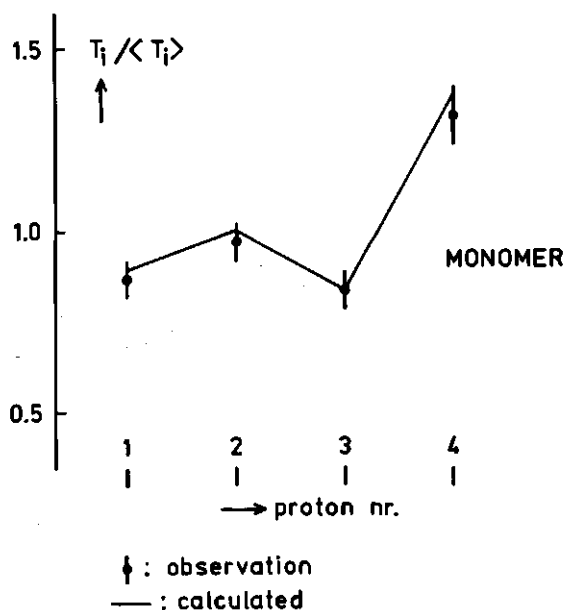


Fig. 7. Experimental and calculated T_1 values of the protons 1-4 in Chl a monomer.

These findings considerably restrict the range of possible geometries. Further, making the reasonable assumption that both molecules are roughly perpendicular to each other (cf. Section 2.3.2) and taking into account the local symmetry of the Mg orbitals and ring V keto lone pairs which are involved in bonding, this range can be further restricted. Some results of the fit procedure for (Chl a)₂ are given in fig. 8, assuming a perpendicular geometry with Eulerian angles (Goldstein convention [41]) $\vec{\Omega} = (90, 90, \phi)$. In this figure, also the results of the "best" fit for a non-perpendicular geometry, which has been earlier proposed [9,10] have been depicted. It is obvious that the results of this configuration are clearly outside the experimental error; therefore, this geometry does not seem very probable. Returning to the perpendicular configurations, and following the approach of accepting a geometry if and only if all calculated T_1 are within the experimental error, we conclude that the (Chl a)₂ dimer has a probable structure given by $\vec{\Omega} = (90, 90, 135 \pm 20)$. For the full geometrical description of the most probable geometry and the corresponding elements of \vec{D}_R , we refer to Table II. A pictorial view of this (Chl a)₂ dimer can be seen in fig. 6 of Chapter 7.

Finally, the geometry of Chl a SP was studied. For this type of dimer, two different geometries have been proposed by Fong [8] and by Shipman *et al.* [42], both of which have plane-parallel macrocycles (cf. Section 2.3.2). We have only calculated SLR times for these two configurations; the results are shown in

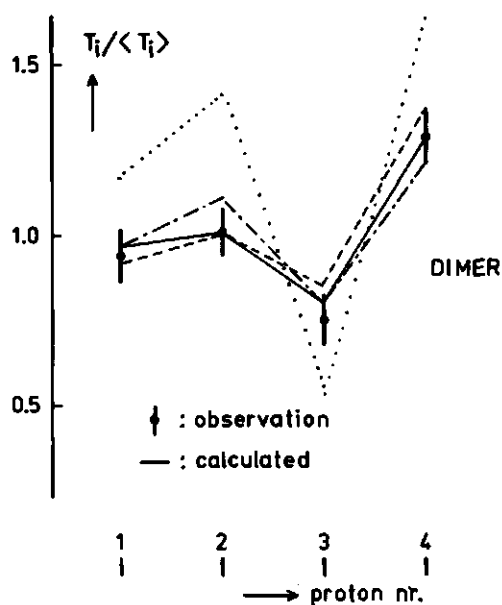


Fig. 8. Results of T_1 calculations for some geometries of Chl *a* dimer. ... geometry according to Katz *et al.* |10|.

--- $\vec{V} = (7.5, -0.65, 0)$, $\vec{\Omega} = (90, 90, 90)$

— $\vec{V} = (\" , \" , \")$, $\vec{\Omega} = (90, 90, 135)$

--- $\vec{V} = (\" , \" , \")$, $\vec{\Omega} = (90, 90, 120)$

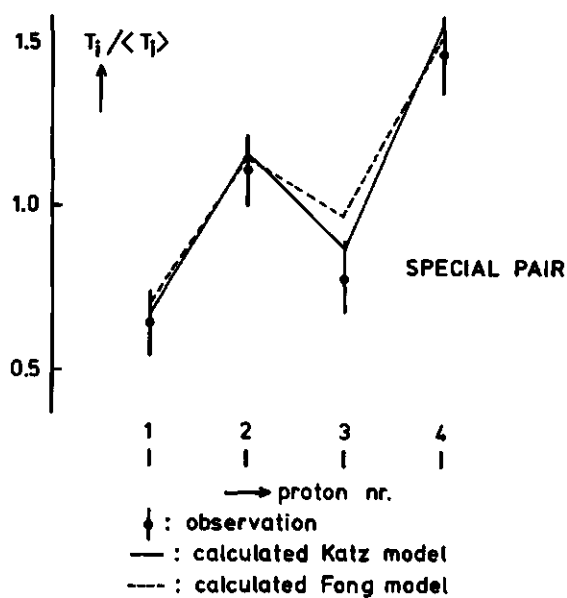


Fig. 9. Results of T_1 calculations for SP according to Fong and Shipman-Katz, respectively.

Table II. Results of proton SLR calculations on Chl a monomer, dimer, and special pair.

	Monomer	Dimer ³⁾	SP ³⁾
Geometry: ¹⁾			
\vec{r} (Å)	-	(7.5, -0.65, 0)	(7.7, -0.13, 3.6)
$\vec{\Omega}$ (degrees)	-	(90, 90, 135)	(0, 180, 180)
<hr/>			
I_{xx} (10^{-43} kg.m ²)	8	20	16
I_{yy} (10^{-43} kg.m ²)	1	20	7
I_{zz} (10^{-43} kg.m ²)	8	100	20
<hr/>			
D_{xx} (10^9 .sec ⁻¹)	5	0.6	0.5
D_{yy} (10^9 .sec ⁻¹)	2	3	0.5
D_{zz} (10^9 .sec ⁻¹)	5	2	3
$\langle D \rangle$ (10^9 .sec ⁻¹) ²⁾	4	1.9	1.3
<hr/>			
Principal axes: ¹⁾			
{x}	(1, 0.1, -0.1)	(0.25, -0.43, 0.87)	(0.91, 0, 0.42)
{y}	(-0.1, 1, 0.1)	(0.93, -0.15, -0.34)	(0, 1.00, 0)
{z}	(0.1, -0.1, 1)	(0.28, 0.89, 0.36)	(-0.42, 0, 0.91)

¹⁾ All vectors are expressed relative to a frame of reference as indicated in fig. 1.

²⁾ $\langle D \rangle \equiv (D_{xx} + D_{yy} + D_{zz})/3$

³⁾ These are the results corresponding to the optimum geometry.

fig. 9. From this figure, it can be inferred that our results are in favour of the Shipman-Katz SP model [42]. More numerical data on this model may be found in Table II. For a view of this Chl SP, we refer to fig. 4 in Chapter 2.

6.5.2 Deuterium T_1 -data and the diffusion axis system

As previously mentioned in Section 6.2.3, the choice of the inertial axis system as a frame of reference is for the chlorophylls not trivial and deuterium SLR data may be helpful in testing the validity of this assumption. Therefore, we have determined the deuteron SLR times of the nuclei 1...4 in Chl a monomer. These results are tabulated in Table I.

The asymmetry parameters η' of the nuclei 1,...,4 which are needed for a calculation of the quadrupolar SLR times of these nuclei are not known; however, for these singly bonded nuclei it is a good approximation to set all $\eta' = 0$. Following Huntress [19,22], this implies that the diffusion axis system can no longer be uniquely determined. With the available data we still can check whether the deuterium SLR times are consistent with the assumed axis system. As it turns out, however, the results of these calculations are not very conclusive, since, unfortunately, the nuclei 1,3 and 2,4 are equivalent by a $\sim 180^\circ$ in-plane rotation, implying that in Huntress' formalism only 2 non-equivalent nuclei are relevant. Using the rotational diffusion constants of the monomer (see Table II) and assuming that Chl a monomer is planar (implying that one diffusion axis is perpendicular to the plane), we have calculated relative quadrupolar SLR times as a function of the in-plane orientation of the diffusion axes. It is found that the experimental relative quadrupole SLR times are consistent with the calculated ones if the D_{xx} -axis has an angle ϕ with the x-axis in fig. 1 such that $-15^\circ < \phi < 110^\circ$. The inertial x-axis is also in this range and thus the quadrupole relaxation data do not contradict the assumption of coinciding inertial and diffusion axis systems.

6.5.3 Dimer geometries from ring current shifts

Table III contains the experimental chemical shifts of various protons in the monomer and both dimers; furthermore, the ring current shifts relative to those of the corresponding nuclei in pyrrole, have been indicated. For pyrrole, we have used the chemical shifts and ring current shifts as indicated by Abraham *et al.* [30]. Firstly, we have calibrated eq. (8) in Section 6.3.1 for Chl a by

Table III. Chemical shifts (δ) and ring current shifts ($\Delta\delta$) in chlorophyll¹⁾.

proton nr.	Monomer			Dimer			SP ³⁾		
	δ	$\Delta\delta_{\text{mono}}$ exp calc ²⁾		δ	$\Delta\delta_{\text{dimer}} - \Delta\delta_{\text{mono}}$ exp calc		δ	$\Delta\delta_{\text{SP}} - \Delta\delta_{\text{mono}}$ exp calc	
1	9.70	4.58	4.42	9.40	-0.30	-0.23	9.90	0.20	-0.30
2	9.36	4.24	4.42	9.20	-0.16	-0.03	9.87	0.51	0.20
3	8.54	3.42	3.57	8.22	-0.32	-0.06	8.87	0.33	0.19
4	6.17		1.84	~4.70	-1.47	-0.91	~8	1.83	0.70
5	3.27	1.77	2.01	3.22	-0.05	0.04			
6	3.58	2.08	1.97	2.80	-0.78	-0.55			
7	3.33	1.83	1.90	3.31	-0.02	-0.16			

¹⁾ δ (ppm) relative to TMS; $\Delta\delta$ (ppm) relative to pyrrole, calculated according to $(\Delta\delta)_{\text{Chl}} = \delta_{\text{Chl}} - \delta_{\text{pyrrole}} + (\Delta\delta)_{\text{pyrrole}}$.

²⁾ Results for $\mu_{\text{H}} = 21\text{\AA}^3$, $\mu_{\text{P}} = 18\text{\AA}^3$ (see eq. (8)).

³⁾ Corrected for the presence of $(\text{Chl } a)_2$ dimer (cf. equil. 12); the calculated results for the Shipman-Katz structure have been indicated.

using the experimental monomer ring current shifts to determine the optimum μ_{H} and μ_{P} . In these calculations we have used the shifts of the nuclei 1,2,3 and 5,6,7; proton 4 cannot be used since no corresponding proton is present in pyrrole. The results of this calculation with $\mu_{\text{H}} = 21\text{\AA}^3$, $\mu_{\text{P}} = 18\text{\AA}^3$ may be seen in Table III. Having determined μ_{H} and μ_{P} , we subsequently calculated the dimer and SP ring current shifts with the help of eq. (10b) as a function of the dimer geometry. We were not able to obtain full quantitative agreement between calculated and experimental ring current shifts for any dimer geometry. However, from a more qualitative viewpoint, by considering the signs and relative magnitudes of the dimer ring current shifts relative to the monomer shifts, some conclusions can be drawn about the dimer geometries.

Consider first the $(\text{Chl } a)_2$ dimer. It is seen from Table III that all experimental dimer ring current shifts are smaller than those of the corresponding protons in the monomer, with the protons 4 and 6 having the largest shifts. If we try to reproduce these experimental findings in the calculations, then we find that the geometries:

$$\vec{V} = (7.5 \pm 0.3, -0.3 \pm 0.7, -0.4 \pm 0.4)$$

and

$$\vec{Q} = (90 \pm 10, 90 \pm 10, 100 \pm 10)$$

yield calculated ring current shifts in qualitative agreement with the experimentally determined ones (see Table III).

Turning to Chl a SP, we note that now all experimental dimer ring current shifts are positive relative to those of the monomer, with the shift of proton 4 being the larger one. (For Chl a SP the number of monitor protons is restricted to 4, because we do not know to which resonance lines the protons 5,6,7 correspond in fig. 5.) As in the proton SLR calculations on the SP, we have only investigated the Fong [8] and the Shipman-Katz [42] SP geometry. From our calculations, all ring current shifts in the Fong configuration prove to be negative relative to those of the monomer, whereas in the Shipman-Katz configuration most shifts are positive (see Table III), with proton 4 having the largest shift. Thus, also from ring current calculations, the Shipman-Katz structure seems to be the most probable SP geometry.

6.6 DISCUSSION

6.6.1 *Validity of calculation procedures*

In this Section we will discuss whether the various assumptions underlying the calculations can be considered to be valid.

The main assumptions for the proton SLR calculations are:

- (1) the rotational diffusion model is valid;
- (2) only the intramolecular dipole-dipole relaxation mechanism is operative;
- (3) the condition $\omega\tau_c \ll 1$ applies;
- (4) the diffusion axis system of the molecule is coincident with the inertial axis system.

Ad (1). As a rule-of-a-thumb, this condition can be checked by considering the ratio between the rotational correlation time $\tau_c \equiv 1/6D_R$ and the free rotor time $\tau_f \equiv (2\pi/9) \cdot I/kT$. If $\tau_c/\tau_f \gtrsim 5$, then the rotational diffusion model is considered to be valid [43]. From the data in Table II it can be concluded that for the Chl dimers this condition is met, whereas for Chl a monomer other reorientational mechanisms besides rotational diffusion might contribute.

Ad (2). Additional relaxation mechanisms, which might be operative are [32]: intermolecular dipole-dipole relaxation, spin rotation relaxation and scalar (spin-spin) relaxation.

As already noted (Section 6.5.1), SLR times of a dilute sample were within the

margin of error identical to those quoted in Table I, indicating that an intermolecular SLR mechanism could not be detected. In addition, all proton SLR measurements were done using fully deuterated solvents, thus further avoiding intermolecular relaxation processes.

Most probably, the contribution of spin rotation relaxation can be considered to be negligible: this mechanism is only important for molecules of which the motional behaviour is inertial [32]. Moreover, this relaxation mechanism is less important for protons [32].

Scalar relaxation is only important for nuclei which exhibit spin-spin coupling [32]. In our SLR calculations, we have only considered protons which in the NMR spectra correspond to single resonances; we may thus rule out this relaxation mechanism.

Ad (3). A way to check this assumption is determination of SLR times at another rf frequency. We have determined SLR times of $(\text{Chl } a)_2$ dimer at an NMR frequency of 360 MHz. It is found that the SLR times at 360 MHz are a factor ~ 2 larger than those measured at 100 MHz, implying that at 360 MHz the condition $\omega\tau_c \ll 1$ is not fulfilled. By plotting the well-known relation $1/T_1 = \tau_c / (1 + \omega^2 \tau_c^2) + 4\tau_c / (1 + 4\omega^2 \tau_c^2)$ [18] as a function of ω it can be readily seen that, given the experimental ratio $(T_1)_{360\text{MHz}} / (T_1)_{100\text{MHz}} \approx 2$, for 100 MHz, the condition $\omega\tau_c \ll 1$ is fulfilled. Thus, for the chlorophyll dimers only T_1 data determined at 100 MHz can be used in our calculations.

Ad (4). This assumption seems to be the most difficult one to justify. As can be judged from the results in Section 6.5.2, the deuterium data are not very conclusive; it can only be said that these data do not contradict the assumption of coinciding diffusion and inertial axis systems. However, some additional comments can be made. On one hand, as already mentioned in Section 6.2.3, for a homogeneous mass distribution the principal axis system of the rotational friction tensor is coincident with that of the inertia tensor [24]. Although this statement only holds rigorously for macroscopic bodies in a viscous fluid, this can be taken as a first approximation for the fairly large chlorophylls having rather homogeneous mass distribution. Moreover, the relative values of the SLR times, calculated from eq. (5), turn out to be not very sensitive to moderate variations in the orientation of the frame of reference. On the other hand, solvent-solute interactions, such as electric dipole and steric interactions, may shift the rotational diffusion axis system away from the moment of inertia system [19,22]. For a limited number of asymmetric molecules the orientation of the diffusion axis system relative to that of the moment of inertia has been studied [19,44]. In these in-

vestigations it was found that the two axis systems are at most 20° rotated relative to each other, even for molecules with a relatively high dipole moment. Extrapolating these findings to the chlorophylls, of which the dipole moment is not very high [45], and in view of the aforementioned insensitivity of eq. (5) to small variations in the orientation of the axis system, we may also from this viewpoint expect that our choice of axis system does not lead to erroneous results.

For the monomer, we note the following: Chl a monomer is planar, and thus we expect that one diffusion axis is perpendicular to the molecular plane. Furthermore, it is expected that the presence of the phytol chain introduces some axial symmetry about this chain. The axis system, dictated by these symmetry arguments is in line with the axis system indicated in Table II. This adds some further justification for our choice of the frame of reference. For Chl a SP, we may *a posteriori* rationalize the choice of one principal axis: here, the phytol chains of both monomeric units are roughly parallel and we therefore assume, analogously to the Chl a monomer, that the phytol chains may be considered to form a symmetry-axis. This is in agreement with the orientation of the y-axis in Chl a SP (see Table II).

For the Chl a dimer, no symmetry arguments can be used to rationalize one or another principal axis, because of the absence of any symmetry in this type of dimer, and we must rely on the more general considerations, mentioned earlier.

We will now consider the ring current calculations. For a discussion on the validity of the "double dipole" model (eq. (8)) in the monomer, we refer to Abraham *et al.* [30]. For Chl a monomer the agreement between calculated and experimental ring current shifts is comparable to that found by Abraham *et al.* [30] for chlorophyll e_6 trimethylester.

One may wonder why for the monomer a quantitative fit is possible, whereas for the dimers only general trends in the ring current shifts can be made in agreement with experiment (cf. Table III). Of course, it is expected, in view of the results for the monomer (see Table III), that for the dimers the agreement between experiment and calculation will be worse than that for the monomer. But, there may be some other reasons, originating from limitations in the model, why we are not able to obtain quantitative agreement between calculation and experiment for the dimers. The most important one is thought to be that in the dimers the various current loops, represented by equivalent dipoles, may be perturbed relative to those of the monomer. A current loop finds its origin in the presence

of circulating π -electrons. If two π -systems are brought together, such as is the case for a dimer, then both systems will be perturbed, for instance by polarization or charge transfer effects. This implies that the positions and magnitudes of the equivalent dipoles, associated with the local π -electron densities will be different from those in the monomer. We have optimized the μ_H and μ_P for the monomer, and thus it is not very surprising that we were not able to calculate the dimer ring current shifts quantitatively.

Furthermore, two other effects might be of importance.

(1) Abraham *et al.* [30] have noted that the calculated ring current shifts for nuclei situated at positions near to and immediately above or below the macrocycle exhibit larger deviations from the experimental values than other nuclei. In the monomer we have only considered nuclei which are at the periphery of the macrocycle, and their calculated ring current shifts should thus not suffer too much from this shortcoming of the double dipole model. On the other hand, in the dimers some nuclei of one molecule are situated above or below the macrocycle plane of the other molecule at relatively small distances, implying that this effect may be noticeable.

(2) An additional reason for the lack of quantitative agreement may be that we have only considered ring current shifts in the dimers, and not the additional chemical shifts which may arise if two chemical groups approach each other, distorting the electron distribution in the monomer parts of the dimer.

All these effects are very difficult to quantify, and more refined methods are required to adequately account for these chemical shift mechanisms. Therefore, and in view of the simplicity of the double dipole model, the obtained qualitative agreement seems quite satisfactory.

6.6.2 Dimer geometries

It is gratifying that data from such completely different methods as proton SLR and ring current measurements yield very similar geometries for the Chl a dimer as well as for the Chl a SP. Also, calculations on the excited state properties of these dimers [46] are in agreement with the geometries mentioned in Section 6.5.

Although in searching dimer geometries using proton SLR calculations no evidence was found for the presence of multiple minima, we want to emphasize that, given the obtained experimental accuracy, the method does not allow an unambiguous determination of the geometry of the Chl a dimer or SP from the experimental

data. This especially holds for Chl a SP, where the experimental error in the proton SLR data is fairly large. Additional and independent evidence will then be required to make a reasonably firm statement about the dimer geometry. In principle, this evidence can be presented by the results of the proton SLR calculations themselves. We recall that in the SLR calculations a set of rotational diffusion constants is found. If the values of these diffusion constants can be related to the dimer geometry, then further confidence in the results of the calculations is obtained. However, rotational diffusion constants are in general rather difficult to interpret in terms of molecular geometry and also for the chlorophylls we failed to give a satisfactory interpretation (see Section 6.6.3). This is one of the reasons why we have carried out ring current calculations. These provide, as has been demonstrated, the necessary additional evidence.

6.6.3 Rotational diffusion constants

From Table II it can be seen that the average diffusion constants $\langle D_R \rangle$ of the monomer is approximately twice that of the dimers. From a simple hydrodynamic Stokes-Einstein model where the molecule is assumed to be spherical, it follows that $\langle D_R \rangle \propto \eta T / M$ [47], where M is the molecular weight of the molecule under study, η is the solvent viscosity, and T is the absolute temperature. Thus, in this respect the $\langle D_R \rangle$ of the monomer and dimers agree with the predictions from the Stokes-Einstein model. $\langle D_R \rangle$ of Chl a SP is somewhat smaller than that of Chl a dimer since SP measurements were carried out at lower temperature and higher solvent viscosity.

Beyond this point the agreement between hydrodynamic theory and experimental diffusion constants ends: when one tries to apply a more refined hydrodynamic model, where the anisotropy of the molecule is included by approximating it by an ellipsoid [21], then it turns out that neither for the monomer, nor for the dimer the experimental relative values of \bar{D}_R agree with the theory. However, we should be aware of some presumptions of the hydrodynamic model. Firstly, the hydrodynamic model is essentially macroscopic, where the body (molecule) is assumed to move in a homogeneous, continuous medium (solvent). It is to be expected that for large molecules, such as proteins ($M \approx 10^5$) this is a better approximation than for Chl a ($M \approx 1000$), and, consequently, for proteins hydrodynamic theory is fairly successful [48]. Another consequence of the macroscopic nature of hydrodynamic theory is that more specific microscopic solvent-solute interactions, such as reorienting electric dipoles or hydrogen bonding at specific sites of the solute

are ignored. It has been demonstrated that these effects can largely determine the rotational behaviour of the molecule under study [15,43]. Secondly, if still the hydrodynamic model is assumed to be valid for the chlorophylls, then the shape of the molecules cannot simply be represented by ellipsoids as can be concluded from the molecular geometries of Chl a monomer and its dimers.

Other models on molecular reorientation are extremely complex, and up to now only very simple model systems such as linear or spherical top molecules have been treated mathematically [49]. It seems therefore that a physical interpretation of the rotational diffusion constants of Chl a monomer and dimers is not yet possible.

6.7 CONCLUSIONS

1. Proton SLR data can be fruitfully used to check geometries of dimers with molecular weight $M \lesssim 2000$, provided that the monomeric geometry is known. If it is required to determine molecular geometries unambiguously, then additional data are needed, which in our case is provided by ring current calculations.

2. Ring current calculations can also be applied to molecular dimers. Only qualitative agreement with the experimental results can be expected.

3. Although quantitative agreement cannot yet be obtained, ring current calculations seem to be a more direct way to study dimer geometries in view of the higher sensitivity to geometrical parameters and the less severe assumptions associated with these calculations as compared to the proton SLR method.

4. For the chlorophylls, the hydrodynamic model is unable to interpret measured rotational diffusion constants in terms of molecular geometry.

5. Both proton SLR calculations and ring current calculations yield geometries for the Chl a dimer and the SP, which are very similar to those reported previously: the Chl a dimer consists of two molecules which are approximately perpendicular to each other, whereas the Chl a SP has the Shipman-Katz geometry.

6.8 REFERENCES

1. G.R. Seely, in "Primary Processes of Photosynthesis" (Ed. J. Barber), Ch.1, Elsevier Publ. Comp., Amsterdam (1977).
2. J.J. Katz, J.R. Norris, L.L. Shipman, Brookhaven Symposia in Biology, 28 (1976) 17.
3. K. Sauer in "Bioenergetics of Photosynthesis", Ch. 3 and references therein (Ed. Govindjee) Acad. Press, New York (1975).
4. R.E. Fenna, B.W. Matthews in ref. 2, pp. 170-182.

5. J.J. Katz, L.L. Shipman, J.R. Norris, in "Chlorophyll Organization and Energy Transfer in Photosynthesis", Ciba Foundation 61 (new series) Excerpta Medica, Amsterdam (1979).
6. T.M. Cotton, Thesis, Northwestern Univ., Evanston, Ill. (1977).
7. R.P.H. Kooyman, T.J. Schaafsma, J.F. Kleibeuker, Photochem. Photobiol. 26 (1977) 235.
8. (a) F.K. Fong, Appl. Phys. 6 (1975) 151;
(b) F.K. Fong, "Theory of Molecular Relaxation: Applications in Chemistry and Biology", Ch. 9, Wiley-Interscience, New York (1975).
9. C. Houssier, K. Sauer, J. Am. Chem. Soc. 92 (1970) 779.
10. J.J. Katz, J.R. Norris, Curr. Top. Bioen. 5 (1973) 41.
11. L.L. Shipman, J. Phys. Chem. 81 (1977) 2180.
12. D. Wallach, W.T. Huntress, J. Chem. Phys. 50 (1969) 1219.
13. R.L. Vold, R.R. Vold, J. Chem. Phys. 68 (1977) 1202.
14. W.M.M.J. Bovée, Thesis, University of Delft (1975).
15. E.J. Pedersen, R.R. Vold, R.L. Vold, Mol. Phys. 35 (1978) 997.
16. K. Wüthrich, "NMR in Biological Research: Peptides and Proteins", North-Holland Publ. Comp., Amsterdam (1976).
17. C.P. Slichter, "Principles of Magnetic Resonance", Springer, Berlin (1978).
18. A. Abragam, "The Principles of Nuclear Magnetism", Clarendon Press, Oxford (1961).
19. W.T. Huntress, Advan. Magn. Res. 4 (1970) 1.
20. N. Bloembergen, E.M. Purcell, R.V. Pound, Phys. Rev. 73 (1948) 679.
21. H. Shimizu, J. Chem. Phys. 40 (1964) 754.
22. W.T. Huntress, J. Chem. Phys. 48 (1968) 3524.
23. H.C. Chow, R. Serlin, C.E. Strouse, J. Am. Chem. Soc. 97 (1975) 7230.
24. H. Brenner, Chem. Eng. Sci. 19 (1964) 519.
25. J.W. Emsley, J. Feeney, L.H. Sutcliffe, "High Resolution Nuclear Magnetic Resonance Spectroscopy", Vol. 2, Pergamon Press, Oxford (1968).
26. J.A. Pople, J. Chem. Phys. 24 (1956) 1111.
27. C.E. Johnson, F.A. Bovey, J. Chem. Phys. 29 (1958) 1012.
28. R.J. Abraham, Mol. Phys. 4 (1961) 145.
29. R. Ditchfield, in "Specialist Periodical Report on NMR Spectroscopy", Vol. Ch. 1, Chemical Society, London (1976).
30. R.J. Abraham, S.C.M. Fell, K.M. Smith, Org. Mag. Res. 9 (1977) 367.
31. H.H. Strain, W.A. Svec, in "the Chlorophylls", Ch. 2 (Eds. L.P. Vernon and G.R. Seely), Acad. Press, New York (1966).
32. T.C. Farrar, E.D. Becker, "Pulse and Fourier Transform NMR", Acad. Press, New York (1971).
33. J.J. Katz, R.C. Dougherty, L.J. Boucher, in ref. 31, Ch. 7.
34. S.W. Provencher, J. Chem. Phys. 64 (1976) 2772.
35. J.J. Katz, H.H. Strain, D.L. Leussing, R.C. Dougherty, J. Am. Chem. Soc. 90 (1968) 784.
36. R.C. Dougherty, G.D. Norman, J.J. Katz, J. Am. Chem. Soc. 87 (1965) 5801.
37. I.S. Dennis, J.K.M. Sanders, J.C. Waterton, J. Chem. Soc., Chem. Comm. (1976) 1049.
38. R.J. Abraham, P.A. Burbidge, A.H. Jackson, G.W. Kenner, Proc. Chem. Soc. (1963) 134.
39. P.S. Hubbard, J. Chem. Phys. 52 (1970) 563.
40. C. Tanford, "Physical Chemistry of Macromolecules", Wiley, New York (1961).
41. H. Goldstein, "Classical Mechanics", pp. 107-109, Addison-Wesley, London (1964).
42. L.L. Shipman, T.M. Cotton, J.R. Norris, J.J. Katz, Proc. Natl. Acad. Sci. U.S.A., 73 (1976) 1791.
43. K.T. Gillen, J.H. Noggle, J. Chem. Phys. 53 (1970) 801.

- 44. R.L. Somorjai, R. Deslauriers, J. Am. Chem. Soc. 98 (1976) 6460.
- 45. J.D. Petke, G.M. Maggiora, L.L. Shipman, R.E. Christoffersen, J. Mol. Spectr. in press.
- 46. R.P.H. Kooyman, T.J. Schaafsma, J. Mol. Struct., in press (see also Chapter 7 of this thesis).
- 47. See, for example, R.A. Dwek, "NMR in Biochemistry", Clarendon Press, Oxford (1973).
- 48. T. Tao, Biopolymers, 8 (1969) 609.
- 49. J.G. Powles, G. Rickayzen, Mol. Phys. 33 (1977) 1207.

7 A charge resonance-exciton description of chlorophyll and pheophytin dimers

7.1 INTRODUCTION

In order to obtain structural information about complexes of photosynthetic pigments *in vivo* and *in vitro*, several methods have been employed:

- Infrared and high-resolution NMR of *in vitro* chlorophyll complexes in solution [1-3].
- X-ray diffraction of *in vitro* [4-6] and *in vivo* complexes [7], resulting in the solid state geometry of these complexes.
- Resonant Raman-scattering of *in vivo* complexes [8].
- Measurement of nuclear spin-lattice relaxation times of *in vitro* complexes [9], yielding the complex geometry in solution.
- Low-temperature electron spin resonance of the lowest excited triplet state relating triplet-state parameters to the structure of the complex [10-12].

In the last method, zero-field-splitting (ZFS) and kinetic parameters of the lowest excited triplet state of the complex are determined. A simple triplet exciton model has been developed correlating these parameters to the geometry of a dimeric complex [10-12]. Because these parameters can be obtained from experiment rather easily and their interpretation is relatively straightforward in terms of this "pure" exciton model, this method seems to be an attractive means to study structural features of chlorophyll-like dimers. Using the triplet exciton model, Clarke et al. have derived geometries for the bacterial reaction center [11], and for chlorophyll dimers in solution [13]. However, some findings indicate that this model may be too simple:

(1) ZFS-values are known to be dependent on the environment of the molecule under study [14]; especially the E-value (for a definition see chapter 1), which is a measure of the in-plane symmetry of the molecule, can exhibit large variations if the molecule is studied in different environments. This is nicely illustrated by molecules in Shpol'skii-matrices [15] where different sites can be present each with their own local environment and their own ZFS-values. In the pure exciton model, where environmental effects are not

included, results lean heavily on the E-value; without having a precise knowledge of the environmental effects on the E-value, it seems inappropriate to use this parameter in studying dimer geometries.

(2) It is not a priori obvious whether to choose a coherent or an incoherent exciton model. In the coherent case the dimer eigenfunctions which should be used in calculating dimer triplet parameters are the symmetric and antisymmetric linear combinations of the monomer excited states, whereas in the incoherent model the excitation hops stochastically between the two molecules; in this case the dimer triplet parameters are given by a weighted average of the corresponding monomer quantities. In contrast with the expressions for the dimer ZFS-values, the formulae for the dimeric kinetic constants are generally dependent on this particular choice [16]. Only if the dimer has C_2 symmetry, both descriptions yield identical results [17]. Thus, the question of coherent versus incoherent exciton model not yet being answered, the usefulness of kinetic constants in determining a dimer geometry is rather limited. This might be one of the reasons why Hoff [18] found that the combined use of ZFS-values and kinetic constants in determining a geometry for the bacterial reaction center leads to contradictory results.

(3) Another reason for incompatible ZFS and kinetic values may be sought in the neglect of ionic (charge resonance) contributions to the triplet state. An example of the importance of including such states is the finding [19-21] that for plane-parallel cyclophanes the ZFS-values are appreciably lower than those for the corresponding monomers, whereas the pure exciton model predicts no change. There is no a priori reason why charge resonance (CR) should not be included in the wavefunctions for dimers of chlorophyll and related compounds: there is substantial evidence [22-25] that both the ion-radicals of the plant reaction center ($P700^+$) and of the bacterial reaction center ($P870^+$) are composed of an aggregate, the unpaired electron of which is completely delocalized over at least two molecules. This makes it very probable that the monomer wavefunctions of a pair of molecules have appreciable overlap, implying that the excited state of a dimer is not only composed of localized (exciton) states, but, as will be outlined in Section 7.2, also of CR states.

Refinements with respect to (1) and (2) mentioned above are difficult to make with the present knowledge about the chlorophylls, and more experimental and theoretical work is needed to clarify them; especially high-resolution optical and magnetic resonance work should be able to solve the abovementioned problems. The third problem is relatively simple and in the following we shall try to refine the pure exciton model by including CR states; it will be indicated how geometries of dimers can be determined without leaning on the triplet

E-value and the triplet kinetic constants. A short account of this attempt has been given elsewhere [26].

7.2 THEORY

The relatively large number of unknown dimer parameters (the CR-percentage and the six coordinates - 3 for rotation and 3 for translation - defining its geometry) requires both singlet and triplet data of the dimer for the assignment of its geometry. Combining these two sets of data yields an internally consistent description of the dimer.

The approach is based upon a consideration of the configuration interaction between the relevant states involved in a description of the dimer. Considering two molecules A and B with mutual interaction, the dimer singlet wavefunction with energy E_k can be written as a sum of zeroth-order basisfunctions (see fig. 1):

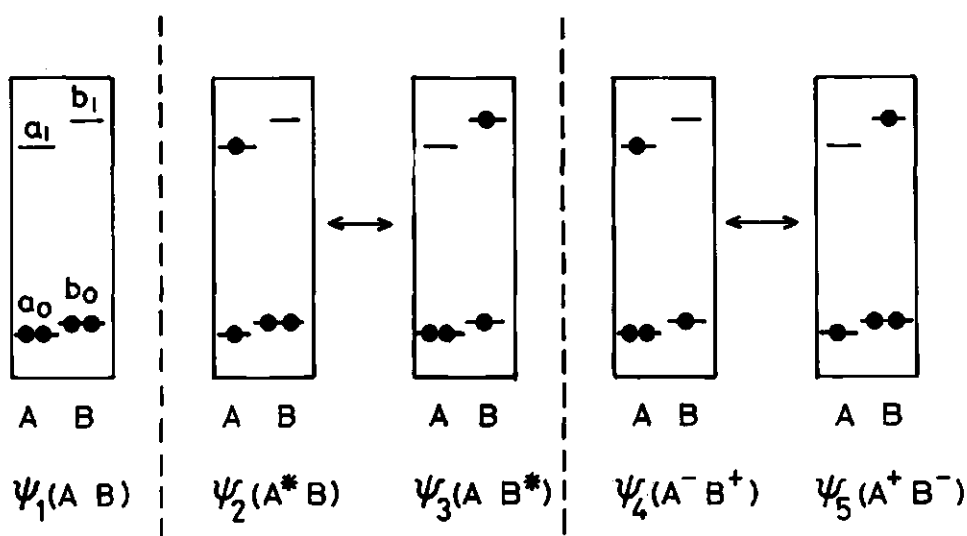


Fig. 1. MO scheme of the singlet excited state of a dimer composed of two molecules A and B. Only the HOMO's and LUMO's are indicated.

a_0, a_1 MO's of molecule A
 b_0, b_1 MO's of molecule B

$$\psi_k = c_{k1}\psi_1(AB) + c_{k2}\psi_2(A^*B) + c_{k3}\psi_3(AB^*) + c_{k4}\psi_4(A^-B^+) + c_{k5}\psi_5(A^+B^-)$$

$$\equiv \sum_i c_{ki}\psi_i \quad (i, k = 1, \dots, 5) \quad (1)$$

where ψ_1 represents the no-bond groundstate of the dimer, ψ_2 and ψ_3 are the wavefunctions of the locally excited states A^*B and AB^* , and ψ_4 and ψ_5 are the CR wavefunctions.

Of course, this basis-set is rather restricted, but, in order to keep things simple and tractable, it seems wise not to expand this set by including other excited states; besides, extensive MO calculations [27-29] have indicated that the highest occupied MO's (HOMO's) and lowest unoccupied MO's (LUMO's) of chlorophyll-like molecules are relatively isolated from the other MO's, implying that only a limited configuration interaction is sufficient for a satisfactory description of excited states.

In the dimer, stabilization is the result of the Coulomb attraction energy C between A^- and B^+ or A^+ and B^- , the exchange energy J between A^*B and AB^* , and by the intermolecular overlap S between the various MO's of A and B involved in bonding. Furthermore, the van der Waals attraction energy between A and B will contribute to the stabilization of the dimer. In our calculations, this contribution has been neglected. We wish to determine the geometry of the dimer using the coefficients c_{k1}, \dots, c_{k5} as variables, whereas monomeric properties (ionization potential IP, electron affinity EA, MO coefficients of A^\pm and B^\pm , transition energies of the lowest excited singlet and triplet state, ZFS parameters) and some experimental dimeric properties (ZFS parameters, transition energy of the lowest excited singlet state) are known.

7.2.1 Singlet state properties

For the excited singlet state of the dimer we want to fit the calculated transition energy to the experimental value by solving the secular determinant in the basis ψ_k ($k = 1, \dots, 5$):

$$|\mathcal{H} - E.S| = 0 \quad (2)$$

The non-diagonal matrix elements $\langle \psi_i | \mathcal{H} | \psi_j \rangle$ have been shown to be proportional to the overlap elements between the various MO's [30], whereas for the diagonal

elements $\langle \psi_i | \mathcal{H} | \psi_i \rangle$ the usual expressions hold [31]. The full Hamiltonian matrix is given in Table I.

The geometry of the dimer enters via the Coulomb energy, the exchange energy and via the intermolecular overlap integrals. Thus, for a particular geometry eq. (2) can be solved yielding the coefficients c_{ki} and the corresponding dimeric energies E_k , from which the transition energies $E_{kk'} \equiv E_{k'} - E_k$ can be determined and compared to the experimental transition energy. In order to determine which $E_{kk'}$ correspond to allowed transitions, the dimeric transition moments $\vec{M}_{kk'}$ have been calculated according to

$$\vec{M}_{kk'} = \sum_{ij} c_{ki} c_{k'j} \langle \psi_i | e\vec{r} | \psi_j \rangle \quad (3)$$

where the ψ_i can be written as Slater determinants which can be evaluated in the usual way [32].

7.2.2 Triplet state properties

In principle, the same formalism can be used in calculating the transition energy in the triplet state, except that in eq. (1) $c_{k1} \equiv 0$ due to the fact that ψ_1 cannot be written as a triplet wavefunction. In fact, consideration of the triplet state dimer energies directly reflect possible CR contributions because the optical triplet energies are hardly affected by exciton interactions, which are very small for the triplet as compared to the singlet [33]. Unfortunately, the experimental dimer triplet transition energy is unknown in most cases, so we will not consider the triplet optical transitions here.

For the ZFS parameters of the dimer the following expression can be derived

$$\langle \vec{D} \rangle = \sum_i c_i'^2 \langle \psi_i | \vec{D} | \psi_i \rangle + \sum_{i \neq j} c_i' c_j' \langle \psi_i | \vec{D} | \psi_j \rangle \quad (4)$$

where \vec{D} is the ZFS tensor [34], and c_i' are the CI coefficients in the triplet state.

The first summation on the right hand side of eq. (4) is composed of locally excited (exciton) and CR terms. Again, the matrix elements $\langle \psi_i | \vec{D} | \psi_j \rangle$ can be calculated for a particular dimer geometry and a fit can be made to the experimental values.

$\psi_1(AB)$	0	$\psi_2(A^*B)$	$\psi_3(AB^*)$	$\psi_4(A^+B^+)$	$\psi_5(A^+B^-)$
$\psi_2(A^*B)$	0	$1E(A^*B)$			
$\psi_3(AB^*)$	0	J	$1E(AB^*)$		
$\psi_4(A^+B^+)$	$\sqrt{2} \cdot S(b_0, a_1) \cdot \Gamma$	$-S(b_0, a_0) [\Gamma + 1E(A^*B)]$	$S(b_1, a_1) \cdot \Gamma$	IP-EA-C	
$\psi_5(A^+B^-)$	$\sqrt{2} \cdot S(b_1, a_0) \cdot \Gamma$	$S(b_1, a_1) \Gamma$	$-S(b_0, a_0) [\Gamma + 1E(AB^*)]$	0	IP-EA-C

Table I. Matrixelements $\langle \psi_i | \mathcal{H} | \psi_j \rangle$ describing the excited singlet state of the dimer [30].

Abbreviations: J: exchange energy (see eq. (6))

$$\Gamma = -16 \rightarrow IP - \frac{1}{2}C - [E(A^*B) - \frac{1}{2}E(A^*B)]$$

$$S(b_n, a_n) = \langle b_n | a_n \rangle, n = (0, 1) \quad (\text{see eq. (7)})$$

C: Coulomb energy (see eq. (5))

IP: ionization potential

EA: electron affinity

7.2.3 Calculation procedure

In the following we shall consider the case $A = B$, i.e. two identical molecules.

In the singlet calculations the geometry-dependent parameters are the Coulomb energy C , the exchange energy J , and the intermolecular overlap integrals S . For C a point-charge approximation was applied, assuming zero differential overlap (ZDO):

$$C \approx \sum_{pq} \sum \gamma_{0p}^2 \delta_{1q}^2 \frac{1}{R_{pq}} \quad (5)$$

where γ_{0p} is the coefficient of the p th atomic orbital (AO) in MO a_0 of molecule A^+ , δ_{1q} is the coefficient of the q th AO in MO b_1 of molecule B^- , and R_{pq} is the distance between center p on A^+ and center q on B^- .

For our purpose, the point-charge approximation seems justified because of the exclusively intermolecular character of this interaction.

The intermolecular exchange energy J was calculated in a dipole-dipole approximation [35]:

$$J = \frac{\vec{M}_A \cdot \vec{M}_B}{|r|^3} - \frac{3(\vec{M}_A \cdot \vec{r})(\vec{M}_B \cdot \vec{r})}{|r|^5} \quad (6)$$

where \vec{M}_A and \vec{M}_B are the transition dipole moments of A and B , respectively, and $\vec{r} = \vec{r}_A - \vec{r}_B$ is the vector joining both transition moments.

The intermolecular overlap integrals were calculated according to (see fig. 1)

$$S(a_n, b_m) = \sum_{pq} \gamma_{np} \delta_{mq} \langle \phi_p^A | \phi_q^B \rangle \quad (n, m = 0, 1) \quad (7)$$

where ϕ_p^A and ϕ_q^B are the $2p_z$ AO's of the two components; assuming Slater-type AO's with exponent 1.625, the AO overlap integrals were calculated by interpolating from the Table given in ref. 36.

The monomer MO coefficients γ_{np} and δ_{np} ($n = 0, 1$) were calculated using a SCF-Pariser-Parr-Pople scheme.

In the triplet calculations we used for the excitonic part of the ZFS tensor, denoted by \vec{D}_{exc} , the phenomenological formulae, originally derived by Sternlicht

and McConnell [37], thereby avoiding the complicated and tedious procedures involved in calculating intramolecular multi-center integrals. \vec{D}_{exc} can be written in the form:

$$\vec{D}_{exc} = \frac{1}{2}(\vec{D}_m + \vec{R}^{-1} \cdot \vec{D}_m \cdot \vec{R}) \quad (8)$$

where \vec{R} is a matrix specifying the orientation of one monomer relative to the other, and \vec{D}_m is the ZFS-tensor for the monomers. This approximation is appropriate, provided the ZFS parameters are much smaller than the exciton splitting in the triplet state, which is certainly the case for large molecules, such as chlorophyll.

For the CR part in eq. (4) a point-dipole approximation was used, which is justified because of the intermolecular character of these contributions.

Making use of the ZDO approximation it is found that

$$\langle \psi_i | \vec{D} | \psi_i \rangle = \frac{1}{2} (gS)^2 \sum_{pq} \gamma_{0p}^2 \delta_{1q}^2 \frac{3\vec{R}_{pq} \cdot \vec{R}_{pq} - R_{pq}^2}{R_{pq}^5} \cdot \vec{1} \equiv \langle \vec{D} \rangle_{CR} \quad (9)$$

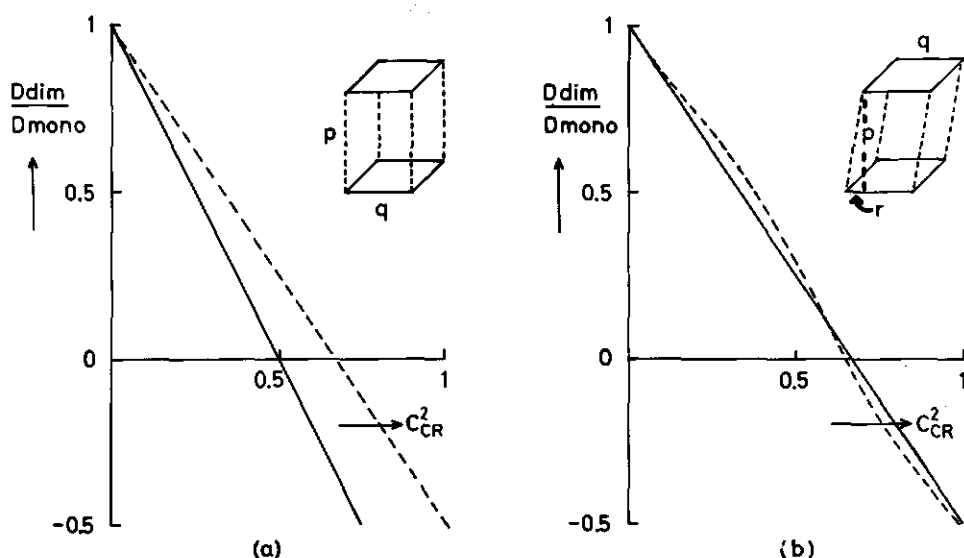


Fig. 2. Primitive calculation of ZFS-parameter D for a plane-parallel two-squares dimer as a function of the CR-percentage.

Both the excitonic and CR part of the ZFS-tensor have been calculated using the point-dipole approximation.

(a) $p/q = 1.5$ (—); $p/q = 2$ (---)

(b) $p/q = 2$, $q/r = 2$ (—); $p/q = 2$, $q/r = 4$ (---)

\vec{R}_{pq} , γ_{0p} and δ_{1q} have been defined before; $\vec{1}$ is the unit tensor; $g = 2$ and β is the Bohr magneton. (Note that in eq. (9) the product $\vec{R}_{pq} \vec{R}_{pq}$ is a tensor of rank two).

A similar expression was used by Keijzers et al. [38] in a study of PMDA-phenanthrene complexes.

Finally, the crossterms in eq. (4) vanish by virtue of the ZDO approximation. Since we choose $A = B$, $c_2' = |c_3'|$ and $c_4' = |c_5'|$, and only one adjustable parameter $c_{CR}^2 \equiv \frac{1}{2}(1 - 2c_4'^2)$ appears in eq. (4). Then, for a particular geometry, c_{CR} can be adjusted to fit the calculated ZFS parameters to the experimental values.

As a simple illustration of the qualitative effects resulting from including CR contributions to the dimer ZFS tensor, consider a dimer consisting of two squares. From fig. 2a it is seen that for a plane-parallel dimer the D-value decreases with increasing CR percentage; for large CR contributions D is negative, which is a consequence of the fact that in this case both electronspins are mainly localized on different molecules. Secondly, as is shown in fig. 2b, the D-value depends also on the relative displacement of one molecule relative to the other. This dependence is not found in the pure exciton model; here, only relative rotations affect the D-value (see eq. (8)). This difference is a consequence of the fact that in the pure exciton model the triplet excitation as a whole jumps between the two monomerparts, each of which has its own ZFS-axes system relative to some fixed reference frame. For a plane-parallel dimer, the Z-axis, averaged over both monomerparts, is the same as that for the single molecule; consequently the D-value does not change with respect to that of the single molecule. This same circumstance is the origin of the fact that for translationally displaced plane-parallel dimers inclusion of CR generally results in a shift of the dimer ZFS principal axes: they tend to align with the symmetry axes of the dimer as a whole.

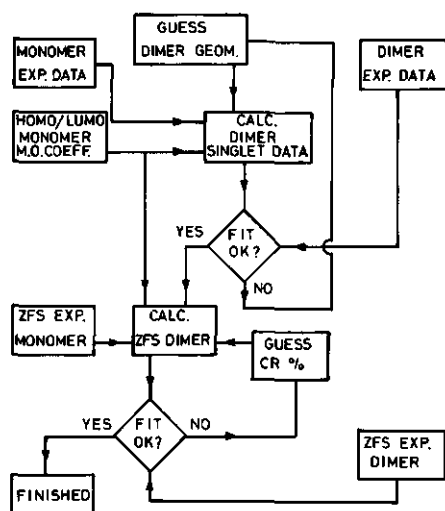


Fig. 3. Outline of calculation procedure.

Before turning to more realistic molecules, it is appropriate to outline the algorithm thus used in determining a dimer geometry. We used the scheme as indicated in fig. 3. As can be seen from this figure, the singlet calculations are used in determining the geometry, yielding a restricted set of possible geometries. Because of the presence of two independent ZFS parameters, the triplet calculations can in principle be used to further reduce this range of possible geometries. However, as already noted in Section 7.1, the E-value can be strongly dependent on other factors; thus, in our examples we have only used the D-value to calculate the CR percentage in the triplet state.

7.3 APPLICATIONS

We have studied three types of dimers: the pheophytin a dimer (Ph a)₂ [39], the chlorophyll a "special pair" dimer (Chl a.L)₂ [2,40,41], and the chlorophyll a "pure" dimer (Chl a)₂ [2,42]. For the Ph a monomer, MO coefficients were obtained from a ground state SCF-PPP calculation; for Chl a these coefficients were taken from open-shell SCF-PPP calculations on the cation and anion.[†]

The monomer molecular geometry was slightly idealized compared to that published by Strouse [5]. A righthanded Cartesian frame of reference was chosen such that the Mg-atom lies in the origin, the positive X-axis passes through the nitrogen-atom of ring III (see fig. 1 of chapter 2), and the Z-axis is perpendicular to the molecular plane. The electron affinity and ionization potential were estimated from experiment [43,44] and ab-initio calculations [29] (see Table II); further input data were obtained from experiment [2,39,42].

[†] The calculations were performed by H. van Osnabrugge at Leiden University.

Table II. Monomeric inputdata for Ph a and Chl a

		Ph <u>a</u>	Chl <u>a</u>
IP	(eV)	6.4 ^e	6.1 ^a
EA	(eV)	0.7 ^b	0.9 ^b
¹ E(A [*] B)	(eV)	1.85 ^c	1.88 ^c
³ E(A [*] B)	(eV)	1.32 ^d	1.26 ^d

- a. ref. 29a, 43a
- b. ref. 43b
- c. ref. 43c
- d. ref. 43d
- e. ref. 29b

In determining geometries, which fit to the experimental results, three criteria were used:

- (1) the calculated dimer singlet transition energy E should agree with the experimental value.
- (2) the stabilization-energy of the dimer in the ground state should be a maximum: experimentally, dimers are prepared in the groundstate by freezing a solution in the absence of light. Thus, the dimer-geometry is determined by ground state interactions.
- (3) the singlet transition of the correct energy should be strongly allowed with respect to that of the other calculated dimer singlet transitions; experimentally the dimer transition is rather strong.

By employing these criteria simultaneously, it turns out that only a rather narrow range of geometries is possible. In specifying a dimer geometry, use is made of a Cartesian translation vector $\vec{V} = (x, y, z)$ in Ångstrom units, denoting the displacement of the center of one molecule relative to that of the other one (Note that the notation is different in ref. 26). Further, a set of Eulerian angles $\vec{\Omega} = (\alpha, \beta, \gamma)$ [45] specifies the rotation of the coordinate system of one molecule with respect to that of the other one.

7.3.1. The pheophytin dimer

Experimental results on $(\text{Ph } \underline{a})_2$ have been published elsewhere; it is assumed that $(\text{Ph } \underline{a})_2$ is a plane-parallel π - π complex [39]. By determining the geometry a

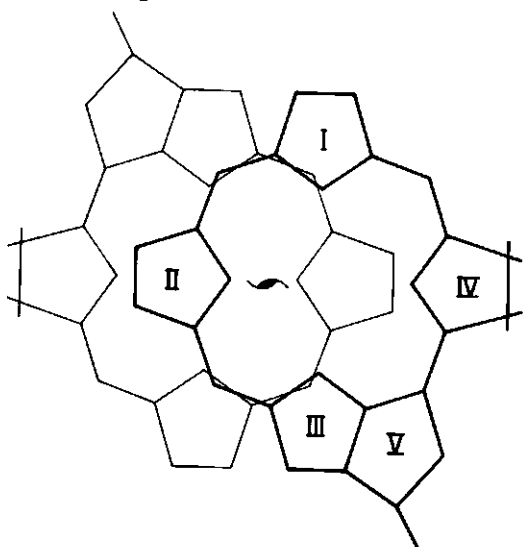


Fig. 4. In-plane projection of $(\text{Ph } \underline{a})_2$ dimer.

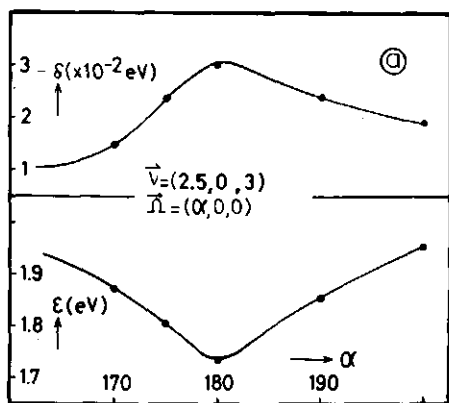


Fig. 5. Stabilization energy δ and allowed singlet transition energy ϵ of $(\text{Ph } \frac{a}{2})_2$ as a function of
 (a) α
 (b) y
 (c) x

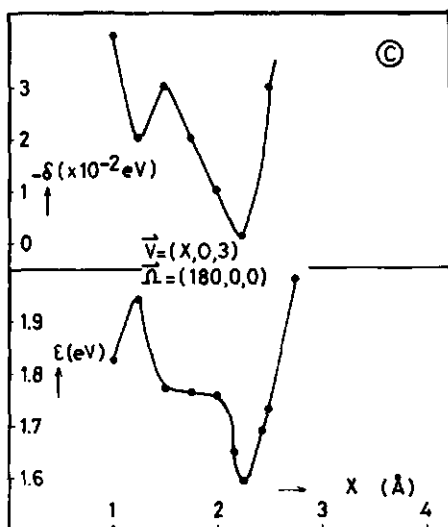
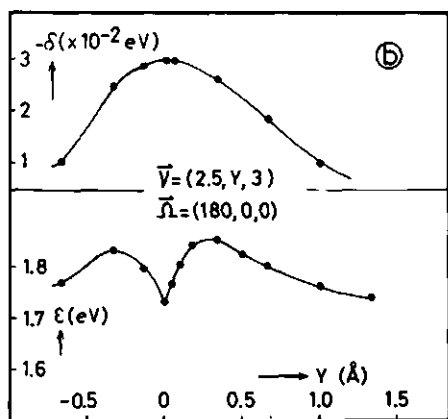


Table III. Calculated results for Ph a

input data ^a		calculated dimer data						
	D(10 ⁻⁴ cm ⁻¹)	ε [†] (eV)	\vec{V} (Å)	$\hat{\Omega}$ (degrees)	J (eV)	C (eV)	δ (eV)	% CR singlet triplet
Monomer	350	1.85	(2.5,0,3)	(180,0,0)	0.1	2.64	-0.03	10 5
Dimer	324	1.73						

a. ref. 39

+ $\epsilon \equiv {}^1E(S_1) - {}^1E(S_0)$

Table IV. Calculated results for Chl a "special pair" dimer

input data				calculated dimer data					
	D (10^{-4} cm^{-1})	ϵ (eV)	\vec{V}^c (Å)	$\vec{\Omega}^c$ (degrees)	J (eV)	C (eV)	δ (eV)	ϵ (eV)	% CR singlet triplet
Monomer	309 ^a	1.88							
Dimer	286 ^a	1.77 ^b	(6.4, 0, 3)	(0, 180, 180)	-0.1	1.57	~0	1.78	~3 ~7

a. ref. 47 b. ref. 2 c. from ref. 40

Table V. Calculated results for Chl a "pure" dimer

input data		calculated dimer data						
	D (10^{-4} cm^{-1})	E (eV)	\vec{V} (Å)	$\vec{\Omega}$ (degrees)	J (eV)	C (eV)	δ (eV)	% CR singlet triplet
Acceptor	309 ^b	1.818 ^a						
	309 ^b	1.87 ^a						
	270 ^c	1.83 ^d						
Donor			I (7.5, -0.65, 0)	(90, 90, 50)	0.08	1.95	~0	~5
Dimer			II (7.5, -0.65, 0)	(90, 90, 135)	-0.01	1.64	~0	~7

a. ref. 42 b. ref. 47 c. ref. 48 d. ref. 2

described above, assuming 3 Å interplanar distance [46], we find as an optimum (see table III and fig. 4):

$$\vec{V} = (2.5, 0, 3) \quad \text{and} \quad \vec{\Omega} = (180, 0, 0)$$

In fig. 5 the calculated energy E of the allowed singlet transition and the ground state stabilization energy δ are shown as functions of \vec{V} and $\vec{\Omega}$ for small deviation from the optimum geometry. From these figures it is seen that for small deviations from the optimum α and γ , δ is indeed a maximum for $\gamma = 0$ and $\alpha = 180^\circ$. δ as a function of x does not exhibit a maximum: however, using the first criterion, fig. 5c determines the geometry: δ is relatively high for the corresponding value of x . The dependence of δ and ϵ on the geometry is mainly due to variations in the intermolecular overlap integrals, whereas C and J vary much less.

Turning to the triplet state, we note that from a comparison of ZFS values for the monomer and dimer it follows from the application of the pure triplet exciton model that the $(\text{Ph a})_2$ dimer is composed of two molecules which are $\sim 30^\circ$ tilted with respect to each other. Furthermore, as already explained in section 7.2.3, this model is unable to predict a translation vector. Applying the CR-exciton model the lowering of the experimental D-value with respect to that of the monomer, assuming the abovementioned plane-parallel geometry (which in fact is justified by the results of the singlet calculations), can be accounted for with a CR percentage as low as $\sim 5\%$. We conclude therefore, that even for low CR percentages the pure triplet exciton model is inadequate to correctly predict dimer geometries from ZFS-values.

7.3.2 The chlorophyll "special pair" dimer

A model of the photosystem I (P700) reaction center in the plant has been proposed [40], consisting of a "special pair" (SP) of plane-parallel Chl molecules (see chapter 2). This dimer can be prepared *in vitro* [2]. Its singlet [2] and triplet (ZFS) [13,47] properties have been measured (see Table IV). Here, also, it is found that the dimer D-value is reduced with respect to that of the monomer, indicating some CR character of the dimer triplet state, provided it is plane-parallel. By applying the CR-exciton model on the proposed SP geometry, we calculate a transition at 700 nm with a transition moment comparable to that of the allowed monomer transition in the visible region, in agreement with the experimental results (see Table IV). Thus, in the CR-exciton model the proposed SP geometry [40] is compatible with the experimental results. For the triplet state a CR percentage of $\sim 7\%$ is calculated for this geometry.

7.3.3 The chlorophyll "pure" dimer [2,42]

In non-electrondonating solvents, such as toluene, carbon tetrachloride, and *n*-octane, Chl a readily forms dimers and higher aggregates; the "pure" dimer (Chl a)₂ consists of a pair of Chl a molecules where one molecule - by the presence of its ring V keto group - donates an electron to the electron-deficient Mg-atom of the other molecule (see chapter 2). In contrast to the dimers discussed in Sections 7.3.1 and 7.3.2, the (Chl a)₂ dimer can be considered as composed of two different molecules: the donor (B) and acceptor (A) molecule. From a deconvolution of the visible absorption spectrum of (Chl a)₂ Shipman et al. [42] determined the absorption spectrum of donor and acceptor Chl. They found for B and A transitions at 1.87 eV and 1.818 eV, respectively. Experimentally, the dimer transition energy is found at 1.83 eV [2]. It is easily shown that exciton interaction alone (eq. 6) cannot account for a dimer transition in between the pure A and B transition energies. We conclude therefore that a certain amount of CR must be present in the description of the excited state, which is indeed to be expected in view of the inequivalent roles of both monomers constituting the dimer.

To determine the geometry of (Chl. a)₂, we applied the CR-exciton model, using as input data IP, EA and MO coefficients as those in Section 7.3.2, and $E(A^*B) = 1.818$ eV, $E(AB^*) = 1.87$ eV. As possible geometries we find

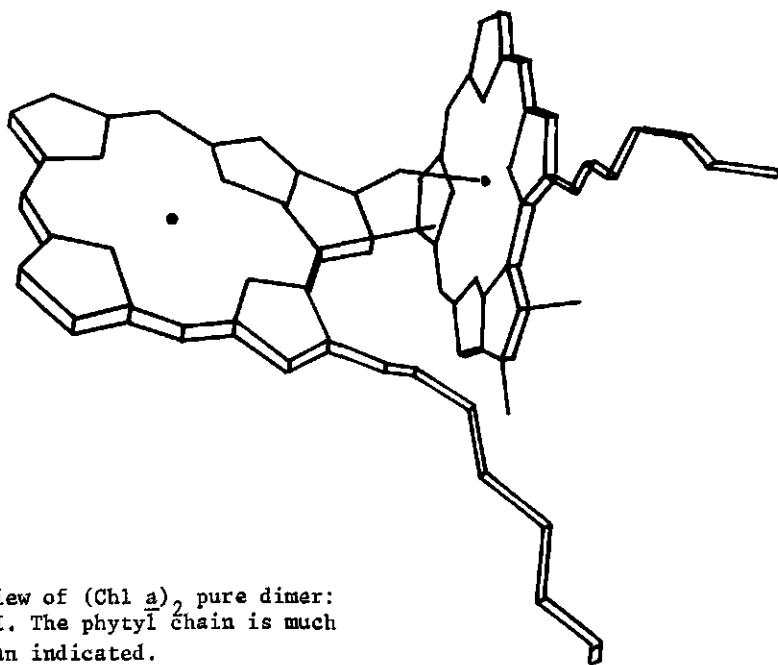


Fig. 6. View of (Chl a)₂ pure dimer: geometry I. The phytyl chain is much longer than indicated.

$$\vec{V} = (7.5, -0.65, 0), \vec{\Omega} = (90, 90, 135) \quad (I)$$

or

$$\vec{V} = (7.5, -0.65, 0), \vec{\Omega} = (90, 90, 50) \quad (II)$$

In fig. 6 a visual impression of geometry I is given.

For the excited singlet state the following wavefunctions are found:

$$I : \quad {}^1\psi_I^* = 0.92 \psi_3(AB^*) - 0.27 \psi_2(A^*B) + 0.27 \psi_4(A^-B^+)$$

$$II : \quad {}^1\psi_{II}^* = 0.85 \psi_3(AB^*) - 0.47 \psi_2(A^*B) + 0.23 \psi_4(A^-B^+)$$

In considering the triplet state we note that for $A \neq B$, generally, in eq. (4) $c_2' \neq |c_3'|$ and $c_4' \neq |c_5'|$. However, due to the very small exciton interaction in the triplet state, because of the spin-forbidden character of the singlet \rightarrow triplet transition, the excitation in this state will be mainly localized at one molecule, i.e. $c_2' \approx 0$ or $c_3' \approx 0$.

Thus, in considering the ZFS parameters due to localized excitations, we only need to know the ZFS of the monomer. The D-values of B and A are about the same [47], so for the calculations it is irrelevant to make an a priori choice where to locate the excitation.

For the ionic contributions in eq. (4) we made the assumptions that the spindensities in A^- and B^- are equal, and analogously for A^+ and B^+ , implying that $\langle \psi_4 | \vec{D} | \psi_4 \rangle = \langle \psi_5 | \vec{D} | \psi_5 \rangle$. A justification of this assumption is found in the fact that for such large molecules as Chl spindensities on different centers are rather low (typically 0.03); relatively large variations in the spindensities will have only a moderate effect in the summation of eq. (9). Furthermore, it was demonstrated by Keijzers et al [38] that even for small molecules this argument holds.

Thus, for $(Chl\ a)_2$ the following expression is found:

$$\langle \vec{D} \rangle_{\text{dimer}} = c_{\text{loc}}^2 \langle \vec{D}_m \rangle + c_{\text{CR}}^2 \langle \psi_4 | \vec{D} | \psi_4 \rangle \quad (4a)$$

$$\text{with } c_{\text{CR}}^2 \equiv c_4'^2 + c_5'^2 \quad \text{and } c_{\text{loc}} \equiv c_2' \text{ or } c_3'.$$

Fitting to the experimentally determined value $D = 270 \times 10^{-4} \text{ cm}^{-1}$ [48], a CR percentage of $\sim 5\%$ is found, irrespective whether geometry I or II is assumed.

7.4 DISCUSSION

7.4.1 *The model*

Notwithstanding the satisfying agreement between experimental and calculated results, a number of objections may be raised against the CR-exciton model. Some of them will be listed below, together with arguments justifying the use of the CR-exciton model, as outlined in Section 7.2.

- Theorists might argue that the CR-exciton model does not seem very satisfying: a supermolecule description, such as has been published by Chandra & Lim [49], in which the dimer is treated as one single molecule, would be preferable. However, from a practical point of view, the CR-exciton model has the definite advantage that the point of departure is the accurately known transition energy of the excited singlet state of the monomer, and not the energy levels of the monomer MO's. The dimers, such as described in Section 7.3 are composed of large monomers (~ 35 relevant atomic centers) and only in rather sophisticated MO calculations, such as CNDO, INDO and ab-initio procedures, a reasonably accurate description of the monomer ground and excited states can be obtained. For a dimer one has then the choice between performing these calculations, which are nearly intractable, and a simple π -electron calculation, which for this class of molecules has a low-grade reliability on a quantitative level. In the CR-exciton model, contrarily, errors due to miscalculations on the monomer which propagate in the supermolecule calculations are avoided and one can focus on the small interactions which are important in forming the dimer. The number of required experimental parameters (IP, EA, energy of the monomeric excited states) is increased with the aim of obtaining a more reliable result. Moreover, for our purposes the final results of a CR-exciton calculation lead to a more clear description of the electronic structure of the dimer, which is directly expressed in terms of monomolecular states.

- The use of zeroth-order basisfunctions in eq. (1) without including intermolecular overlap is justified, since it can be shown [30] that corrections are of second order in S , while in our examples $S \ll 1$.

- For pheophytins and chlorophylls, there are two relatively close-lying transitions, denoted by Q_y and Q_x (see Chapter 2) with approximately perpendicular transition moments. The Q_y transition moment is about 5 times as large as the Q_x moment. [29c]. In a dimer, these moments may interact, depending on the geometry of the dimer. We have estimated the maximum interaction between Q_y and Q_x to

shift the allowed dimer transition with at most 0.01 eV.

- The sensitivity of the final results to variations in the input parameters determines the accuracy of the specified optimum geometry. IP and, in particular, EA deserve attention because these parameters are not accurately known, and are treated as empirical input parameters in contrast to C and J.

Fitting the experimental dimer transition at geometries in the vicinity of the optimum one by using EA and IP as adjustable parameters provides an indication about the accuracy of the specified optimum geometry. For the $(\text{Ph } \underline{a})_2$ dimer it is found that if the optimum geometry is specified as

$$\vec{V} = (2.3 \pm 0.2, 0 \pm 0.5, 3), \vec{\Omega} = (185 \pm 10, 0, 0)$$

then IP may vary by 10% and EA by 60%. Thus, sizeable variations in EA and IP can be tolerated within a reasonable range of geometries. Roughly the same applies for the case where C and J are treated as adjustable parameters. Here, a variation of C by 10% and of J by 70% leaves the specified geometry within its error limits indicated above. We feel that in our examples the point charge approximations for C and J are accurate enough to cause errors in the calculated geometry within the limits quoted above.

- In Section 7.1 the influence of the solvent on the positions of the singlet transitions has been completely ignored. It is not a priori clear whether such approximation is justified. However, the Q_y transition dipole moment of Chl is not very sensitive to the polarity of the solvent: variations are at most $\sim 10\%$ [50], indicating a relatively weak solvent-solute interaction. Furthermore, the shift in transition energy due to solvent-solute interactions can be shown to be proportional to the difference in solvent polarization energy ΔE_{pol} between ground and excited state of the solute [51]. For nonpolar solvents, ΔE_{pol} is rather low consequently only a minor shift of the solute transition energy is expected. The experimental transition energies that we used in the calculations were all obtained from experiments carried out in nonpolar solvents. This circumstance justifies the neglect of solvent effects in our calculations.

7.4.2 *The dimers*

For a discussion of the geometries of $(\text{Ph } \underline{a})_2$ and the Chl \underline{a} SP we refer to previous work [39,40]. The geometry of $(\text{Ph } \underline{a})_2$, indicated in the early NMR work of Katz' group [1] is confirmed by our calculations.

It may be somewhat surprising that in the CR-exciton model the ground state stabilization energy of the Chl a SP dimer is found to be vanishingly small. It has been previously pointed out [39] that binding mechanisms in $(\text{Ph } \underline{a})_2$ and Chl a SP are essentially different. The finding that for Chl a SP $\delta \approx 0$ is another indication of this difference: other binding mechanisms which are not included in the CR-exciton model are required to stabilize this dimer. Here, bifunctional ligands, such as water or ethanol, provide the binding between both monomerparts. In contrast to $(\text{Ph } \underline{a})_2$, where both monomers, due to the presence of appreciable intermolecular overlap, as a whole are involved in forming the dimer, the Chl a SP dimer is stabilized by local interactions, such as hydrogen bonding to some specific center, i.e. Mg and the ring V keto group. In the case of Chl a SP, these local interactions do not severely perturb the monomer π -system. Therefore, although the CR-exciton model is unable to correctly calculate the ground state stabilization energy of Chl a SP, this model is expected to correctly predict π -properties such as the transition energy and the CR percentage. The same reasoning holds for the $(\text{Chl } \underline{a})_2$ "pure" dimer, where no ground state stabilization energy is found either.

In section 7.3.3 two possible geometries were mentioned for $(\text{Chl } \underline{a})_2$. It is remarkable that geometry I was also obtained in a completely independent way by measuring the proton spin-lattice relaxation times [9]. The fact that with the CR-exciton model two geometries are found is conceivable in view of the fact that both geometry I and II correspond to a situation where a line in the acceptor molecule joining the Mg-atom and the center of ring III makes an angle of $\sim 45^\circ$ with the plane of the donor molecule (see fig. 7). Since the relative orientations of the π -systems of both monomers in I and II are nearly equivalent, the CR-exciton model cannot discriminate between these two geometries.

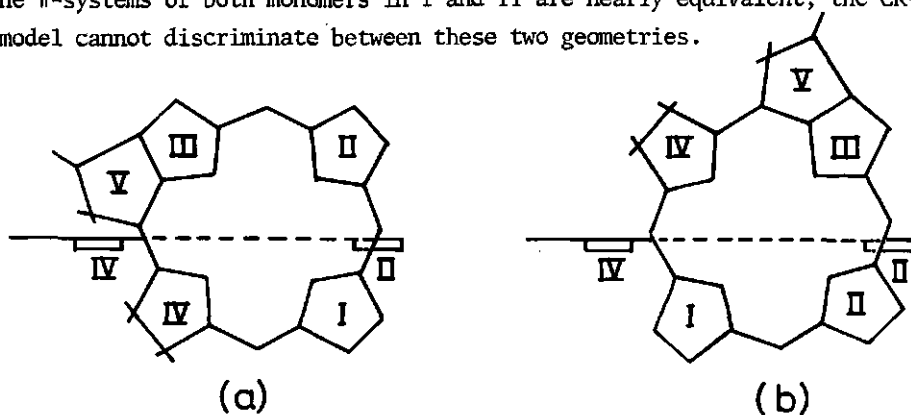


Fig. 7. $(\text{Chl } \underline{a})_2$ pure dimer schematically viewed in the plane of the donor molecule. Rings II and IV of the donor molecule are indicated.

(a) geometry I (b) geometry II.

Turning to the singlet excited state wavefunction of $(\text{Chl } a)_2$ we note that the excitation is mainly located on one molecule, in agreement with previous calculations by Shipman et al. [42]. There is also a small but significant CR contribution, indicating that indeed molecule A serves as an acceptor for molecule B.

7.5 CONCLUSIONS

The CR-exciton model provides a reasonably satisfying means to describe chlorophyll-like dimers. Even for low CR percentages the pure triplet exciton model applied to ZFS-parameters is generally inadequate to correctly predict dimer geometries: for $(\text{Ph } a)_2$ a 5% CR percentage in the CR-exciton model is equivalent to a tilting angle of $\sim 30^\circ$ in the pure exciton model. In contrast to the pure exciton model, the CR-exciton model can also be applied to hetero-dimers.

7.6 REFERENCES

1. J.J. Katz, R.C. Dougherty, L.J. Boucher in "the Chlorophylls", Eds. L.P. Vernon and G.R. Seely (Acad. Press, New York, 1966) Chapter 7.
2. T.M. Cotton, Thesis (1976), Northwestern Univ. Evanston, Ill.
3. T.M. Cotton, P.A. Loach, J.J. Latz, K. Ballschmiter, Photochem. Photobiol. 27 (1978) 735.
4. C. Krathy, Thesis (1976), Technische Hochschule, Zürich.
5. H.C. Chow, R. Serlin, C.E. Strouse, J. Am. Chem. Soc. 97 (1975) 7230.
6. R. Serlin, H.C. Chow, C.E. Strouse, J. Am. Chem. Soc. 97 (1975) 7237.
7. R.E. Fenna, B.W. Matthews, Nature 258 (1975) 573.
8. M. Lutz, Biochim. Biophys. Acta 460 (1977) 408.
9. R.P.H. Kooyman, T.J. Schaafsma, Chapter 6 of this thesis.
10. W. Hägele, D. Schmid, H.C. Wolf, Z. Naturforsch. A, 33 (1978) 94.
11. R.H. Clarke, R.E. Connors, H.A. Frank, Biochem. Biophys. Res. Commun., 71 (1976) 671.
12. R.H. Clarke, R.E. Connors, H.A. Frank, J.C. Hoch, Chem. Phys. Lett., 45 (1977) 523.
13. R.H. Clarke, D.R. Hobart, W.R. Leenstra, J. Am. Chem. Soc., 101 (1979) 2416.
14. J.F. Kleibeuker, Thesis (1977), Agricultural University, Wageningen
15. (a) G. Jansen, Thesis (1977), University of Leiden
(b) R.J. Platenkamp, personal communication.
(c) Chr. Bräuchle, H. Kabza, J. Voigtländer, Z. Naturforsch. 34a, (1979) 6.
16. W. Hägele, Thesis (1977), University of Stuttgart.
17. M.K. Bowman, J.R. Norris, Chem. Phys. Lett., 54 (1978) 45.
18. A.J. Hoff, H. Gorter de Vries, Biochim. Biophys. Acta 503 (1978) 94.
19. D. Schweitzer, K.H. Hausser, Chem. Phys. 29 (1978) 181.
20. J.P. Colpa, K.H. Hausser, D. Schweitzer, Chem. Phys. 29 (1978) 187.
21. H. Vogler, G. Ege, H.A. Staab, Mol. Phys. 33 (1977) 923.
22. D.L. Williams-Smith, P. Heathcote, C.K. Sihra, M.C.W. Evans, Biochem. J. 170 (1978) 365.
23. J.R. Norris, R.A. Uphaus, H.L. Crespi, J.J. Katz, Proc. Natl. Acad. Sci. USA 68 (1971) 625.

24. J.R. Norris, M.E. Druyan, J.J. Katz, *J. Am. Chem. Soc.* 95 (1973) 1680.
25. G. Feher, A.J. Hoff, R.A. Isaacson, L.C. Ackerson, *Ann. New York Acad. Sci.* 244 (1975) 239.
26. R.P.H. Kooyman, T.J. Schaafsma, *J. Mol. Struct.*, in press.
27. C. Weiss, *J. Mol. Spectr.* 44 (1972) 37.
28. G.M. Maggiora, L.J. Weimann, *Int. J. Quantum Chem., Quantum Biology Symp.* 1 (1974) 179.
29. (a) D. Spangler, G.M. Maggiora, L.L. Shipman, R.E. Christoffersen, *J. Am. Chem. Soc.* 99 (1977) 7448.
 (b) J.D. Petke, G.M. Maggiora, L.L. Shipman, R.E. Christoffersen, *J. Am. Chem. Soc.* 99 (1977) 7470.
 (c) J.D. Petke, G.M. Maggiora, L.L. Shipman, R.E. Christoffersen, *J. Am. Chem. Soc.*, in press.
30. H. Beens, Thesis (1970), Free University of Amsterdam.
31. G. Briegleb, "Electronen-Donator-Acceptor-Komplexe" (Springer, Heidelberg, 1961).
32. R.G. Parr, "the Quantum theory of Molecular Electronic Structure", (Benjamin, New York, 1964).
33. D.P. Craig and S.H. Walmsley, "Excitons in molecular crystals" (Benjamin, New York, 1968).
34. S.P. McGlynn, T. Azumi, M. Kinoshita, "Molecular spectroscopy of the triplet state" (Englewood Cliffs, N.J., 1969).
35. M. Kasha, H.R. Rawls, M. Ashraf El-Bayoumi *in* the Proceedings of the VIIIth European congress on Molecular Spectroscopy, Copenhagen 1965 (Butterworths, London).
36. R.S. Mulliken, C.A. Rieke, D. Orloff, H. Orloff, *J. Chem. Phys.* 17 (1949) 1248.
37. H. Sternlicht, H.M. McConnell, *J. Chem. Phys.* 35 (1961) 1793.
38. C.P. Keyzers, D. Haarer, *J. Chem. Phys.* 67 (1977) 925.
39. R.P.H. Kooyman, T.J. Schaafsma, G. Jansen, R.H. Clarke, D.R. Hobart, W.R. Leenstra, *Chem. Phys. Lett.*, in press (Chapter 3 of this Thesis).
40. J.J. Katz, J.R. Norris, L.L. Shipman *in* Brookhaven Symposia in Biology 28 (1976) pp. 16-55.
41. F.K. Fong, *Appl. Phys.* 6 (1975) 151.
42. L.L. Shipman, T.M. Cotton, J.R. Norris, J.J. Katz, *J. Am. Chem. Soc.* 98 (1976) 8222.
43. (a) T. Nakato, T. Chiyoda, H. Tsuboroma, *Bull. Chem. Soc. Japan* 47 (1974) 3001.
 (b) I. Fuijta, M.S. Davis, J. Fajer, *J. Am. Chem. Soc.* 100 (1978) 6280.
 (c) J.C. Goedheer *in* "the Chlorophylls", Eds. L.P. Vernon and G.R. Seely (Acad. Press, New York, 1966) Chapter 6.
 (d) A.A. Krasnovskii jr., N.N. Lebedev, F.F. Litvin, *Dokl. Akad. Nauk SSSR* 216 (1974) 1406.
44. J.R. Harbour, G. Tollin, *Photochem. Photobiol.* 19 (1974) 69.
45. H. Goldstein, "Classical Mechanics" (Addison-Wesley, London, 1964) pp. 107-109.
46. (a) P. Maskov, P.N. Skacke, *Compt. Rend. Acad. bulg. Sci.* 22 (1969) 419.
 (b) P. Maskov, P.M. Skacke, *Compt. Rend. Acad. bulg. Sci.* 22 (1969) 551.
47. R.P.H. Kooyman, T.J. Schaafsma, J.F. Kleibeuker, *Photochem. Photobiol.* 26 (1977) 235.
48. Chapter 4 of this thesis.
49. (a) A.K. Chandra, E.C. Lim, *J. Chem. Phys.* 48 (1968) 2589.
 (b) A.K. Chandra, E.C. Lim, *J. Chem. Phys.* 49 (1968) 5066.
50. L.L. Shipman, *Photochem. Photobiol.* 26 (1977) 287.
51. E. Lippert, *Z. Elektrochem.* 61 (1957) 962.

Summary

Chlorophyll (Chl) molecules can form complexes in two important ways: by ligation at the magnesium atom and/or by hydrogen bonding at the keto-carbonyl group. Under certain conditions these processes may give rise to dimer formation. This thesis describes some properties of complexes and dimers of Chl a, Chl b and pheophytin (Ph) a.

Using optically detected magnetic resonance and fluorescence methods, the positions of the lowest excited singlet state and the zero field splitting parameters D and E of the lowest excited triplet state have been determined for complexes of these molecules. The combination of these parameters opens the possibility to analyze a complicated fluorescence spectrum. Different fluorescence bands were assigned to various complexes, such as singly ligated, doubly ligated, and hydrogen bonded Chl. It is found that for Chl a both the lowest excited singlet state and the D value decreases in energy as the number of molecules bonded to Chl increases, even more in the case of ligation than in the case of hydrogen bonding. Probably, the aldehyde group in Chl b forms hydrogen bonds more easily than the keto group.

For dimers the following was found: two different Chl a dimers could be distinguished, the "pure" dimer (PD) and the "special pair" (SP). In the PD both monomer parts are bonded directly to each other, whereas in the SP two small interstitial "glue" molecules are present. Both the zero field splitting values and the positions of the lowest excited singlet state are different for the two dimers, whereas for the PD a triplet spin polarization pattern was found different from that of the monomer. On the basis of these data we suppose that the SP consists of two approximately plane-parallel monomer parts, as proposed earlier, whereas both monomer parts in the PD are not plane-parallel. For Chl b the dimerization behaviour is much more complicated than for Chl a, due to the presence of an aldehyde group in Chl b. Possibly, Chl b dimers form by interactions of the aldehyde groups, contrarily to those of Chl a, in which keto groups are most important. Ph a dimers form by a different mechanism, due to the absence of a magnesium atom. In this case dimers form by π - π interactions between the monomer parts, the binding energy is smaller than in Chl dimers.

In order to investigate the geometry of these dimers, we also performed

high resolution proton nuclear magnetic resonance measurements. These experiments yielded two sets of mutually independent data, i.e. for each proton a nuclear spin lattice relaxation time and a chemical shift. Both sets can provide geometrical information on the dimers which were studied:

(a) A calculation method was developed to determine the dimer geometry with the help of the experimentally determined spin lattice relaxation times and the monomeric geometry. It is possible to give a quantitative description of spin lattice relaxation times in terms of a rotational diffusion tensor and a geometrical structure. The results of these calculations are:

- the PD consists of two approximately perpendicular molecules;
- for the SP we found a structure corresponding to that previously postulated by Shipman & Katz.

(b) A model previously introduced by others, and describing proton chemical shifts in a porphyrin molecule, has been extended to Chl dimers. Application of this model to the abovementioned Chl a dimers resulted in similar geometries as those found in the spin lattice relaxation calculations.

We also investigated dimer geometries utilizing experimental data on the excited states. To this end we applied a simple model including both "exciton" and "charge resonance" contributions to the excited state singlet and triplet wave functions. Again, the same geometries for the PD and for the SP were found. The Ph a dimer is found to consist of two plane-parallel monomers, somewhat shifted relative to each other.

An additional, more general conclusion is, that ignoring "charge resonance" contributions to the triplet state wave function may result in unreliable geometrical statements, even if these contributions are small ($\sim 5\%$).

Samenvatting

Chlorofyl (Chl) molekulen hebben twee belangrijke complexeringsmogelijkheden: ligandering aan het magnesiumatoom, en/of waterstofbrugvorming aan de keto-carbonylgroep. Onder bepaalde experimentele condities kunnen deze complexeringsmogelijkheden leiden tot de vorming van dimeren. Dit proefschrift beschrijft enige eigenschappen van complexen en dimeren van Chl a, Chl b en feofytine (Ph) a.

Met behulp van optisch gedetecteerde magnetische resonantie en fluorescentie experimenten zijn de ligging van de laagst aangeslagen singlet toestand en de nulveldsplittingsparameters D en E van de laagst aangeslagen triplet toestand bepaald voor complexen van deze molekulen. De combinatie van de zo bepaalde triplet en singlet parameters geeft de mogelijkheid om een ingewikkeld fluorescentiespectrum te ontrafelen. We hebben de verschillende banden in het fluorescentiespectrum toegekend aan verschillende complexen, zoals enkel geligandeerd, dubbel geligandeerd, en waterstofbrug gebonden Chl. Het blijkt dat in Chl a zowel de laagst aangeslagen singlet toestand als de D-waarde van de laagste triplet toestand omlaag gaan in energie naarmate een groter aantal molekulen complexeert met Chl. Dit effect is groter voor ligandering dan voor waterstofbrugvorming. Er zijn aanwijzingen gevonden, dat de aldehyde-groep in Chl b makkelijker een waterstofbrug vormt dan de keto-groep.

Verder zijn dimeren bestudeerd. Hierbij bleek het volgende: voor Chl a konden twee verschillende dimeren worden onderscheiden, het "zuivere dimeer" (ZD) en het "speciale paar" (SP). In het ZD zijn beide monomeren direkt aan elkaar gebonden, in het SP gebeurt dit via twee kleine molekulen, die als "lijm" fungeren. Zowel de D- en E-waarden als de ligging van de laagst aangeslagen singlet toestand zijn voor beide verschillend, terwijl voor het ZD een triplet spinpolarisatiepatroon werd gevonden, dat verschilt van dat van het monomeer. Uit deze gegevens kon voorlopig geconcludeerd worden, dat het SP bestaat uit twee monomeerhelften die ongeveer evenwijdig staan, hetgeen door anderen al eerder was geopperd, en dat de beide helften van het ZD niet evenwijdig staan. Voor Chl b is het dimerisatiegedrag aanzienlijk ingewikkelder dan voor Chl a tengevolge van de aanwezigheid van een aldehyde-groep in Chl b. Mogelijkerwijze worden Chl b dimere gevormd door interacties van de aldehyde-groepen, dit in tegenstelling tot Chl a dimeren, waar de keto-groepen de belangrijkste rol spelen in de binding. De di-

meren van Ph a zijn van een ander type, voornamelijk doordat hier geen magnesium-atoom aanwezig is. Deze dimeren worden gevormd door π - π interacties; vergeleken met Chl a dimeren is de bindingsenergie kleiner.

Om de geometrie van deze dimeren nader te onderzoeken, zijn proton kernspin-resonantiemetingen met hoog oplossend vermogen verricht. Deze metingen leverden ons twee verschillende soorten van wederzijds onafhankelijke gegevens, nl. voor elk proton een kernspinroosterrelaxatietijd en een chemische verschuiving. Beide groepen van gegevens kunnen informatie verschaffen over de geometrie van de bestudeerde dimeren:

(a) Er is een rekenmethode ontwikkeld, waarmee aan de hand van metingen van kernspinroosterrelaxatietijden van een aantal protonen in het dimeer de geometrie van het dimeer bepaald kan worden, indien de geometrische structuur van het monomeer bekend is. Het bleek mogelijk een kwantitatieve beschrijving te geven van kernspinroosterrelaxatietijden in termen van een rotatiediffusietensor en een geometrische structuur. Resultaten van de berekeningen geven het volgende aan:

- het ZD bestaat uit twee molekulen die ongeveer loodrecht op elkaar staan;
- voor het SP vonden we een structuur, overeenkomend met die welke al eerder door Shipman & Katz was gepostuleerd.

(b) Een reeds door anderen opgesteld model dat de chemische verschuivingen van protonen in een porfyriene molekuul beschrijft, is uitgebreid naar Chl dimeren. Met behulp van dit model wordt een geometrie voor het ZD gevonden, die bijna identiek is aan die welke uit de kernspinroosterrelaxatiemetingen werd bepaald, terwijl voor het SP een geometrie wordt gevonden, corresponderend met het Shipman-Katz voorstel.

Ook op andere wijze, gebruikmakend van gegevens met betrekking tot de aangeslagen toestand, zoals die eerder in dit onderzoek werden bepaald, kon de geometrie van dimeren worden onderzocht. Hiertoe is een eenvoudig model opgesteld, waarin zowel "exciton" als "charge resonance" bijdragen tot de golf functies van de aangeslagen singlet en triplet toestand zijn opgenomen. Bij toepassing van dit model op het Chl a ZD en SP worden geometrieën gevonden, in overeenstemming met de resultaten op grond van de kernspinresonantiemetingen. Toepassing van dit model op het Ph a dimeer resulteert in een geometrie, waarbij beide monomeren parallel staan en enigszins verschoven zijn ten opzichte van elkaar.

Een andere, meer algemene conclusie is, dat het verwaarlozen van "charge resonance" bijdragen in de triplet toestand kan leiden tot onbetrouwbare uitspraken over de geometrie, zelfs als deze bijdragen klein ($\sim 5\%$) zijn.

Curriculum vitae

Robertus Petrus Hermanus Kooyman is op 29 april 1950 te Vogelenzang geboren. Na het behalen van het Gymnasium β diploma aan het Triniteitslyceum te Haarlem begon hij in 1968 met de studie Natuurkunde aan de Rijksuniversiteit te Leiden. In juni 1971 werd het kandidaatsexamen Natuurkunde en Wiskunde met Scheikunde (N2) afgelegd. Voor het hoofdstuk Experimentele Natuurkunde werd in de F.O.M.-werkgroep Magnetische Resonantie o.l.v. prof. dr. ir. N.J. Poulis een onderzoek verricht naar domeinwandverschuivingen in een antiferromagnetisch eenkristal. In februari 1975 werd het doktoraal examen Experimentele Natuurkunde met bijvak Wiskunde afgelegd.

In de periode 1 okt. 1974-1 sept. 1975 werd in de werkgroep "Membraanruis" o.l.v. prof. dr. A.A. Verveen een onderzoek verricht naar transportverschijnselen in lipide dubbellagen m.b.v. ruisanalyse.

Van 1 sept. 1975 tot 1 dec. 1979 is hij als gastmedewerker in S.O.N.-verband werkzaam geweest bij de vakgroep Moleculaire Fysica (Landbouwhogeschool, Wageningen), waar o.l.v. prof. dr. T.J. Schaafsma dit proefschrift bewerkt is. Als neventaak had hij het geven van onderwijs aan studenten in de voorkandidaatsfase. Verder heeft hij in deze vakgroep ook de W.U.B. van nabij kunnen meemaken, door enige tijd als sekretaris van de vakgroep op te treden.

Sinds 1 dec. 1979 is hij in dienst van de Rijksuniversiteit te Utrecht en werkzaam in de vakgroep Biofysika o.l.v. prof. dr. Y.K. Levine.